CONTROL OF OOCYTE REAWAKENING BY KIT

APPROVED BY SUPERVISORY COMMITTEE

Diego H. Castrillon, MD, PhD

Rolf Brekken, Phd

Kent Hamra, Phd

James Amatruda, MD, PhD

DEDICATION

Dedicated to my grandparents; Dr. Sami Göl and Güzide Göl

For their unconditional love

CONTROL OF OOCYTE REAWAKENING BY KIT

by

HATICE DUYGU SAATCIOGLU

DISSERTATION /THESIS

Presented to the Faculty of the Graduate School of Biomedical Sciences

The University of Texas Southwestern Medical Center at Dallas

In Partial Fulfillment of the Requirements

For the Degree of

DOCTOR OF PHILOSOPHY

The University of Texas Southwestern Medical Center at Dallas

Dallas, Texas

August, 2016

ACKNOWLEDGEMENTS

First of all, I want to express my gratitude to my mentor Dr. Diego H. Castrillon for his endless encouragement, time, and support during all the stages of this work. I feel very lucky that his passion in science, willingness to share expertise, and humble patience raised me as a member of Castrillon lab. Diego; it has been a pleasure working with you and I'll always be deeply grateful to you for giving me the opportunity to take part in your scientific work.

I want to acknowledge my thesis committee: Drs. Rolf Brekken, Kent Hamra, and James Amatruda; thank you for your constant encouragement, scientific advice and novel perspectives. I also want to thank Drs. Ege Kavalali, Esra Akbay, and Nancy Street for their academic advice when mostly needed. I extend my sincere thanks to Castrillon lab members: Ileana Cuevas for initiating this project; Daryl Harmon for always being helpful, Gina Aloisio for teaching me everything in the lab when I first started; Yuji Nakada for always being very thoughtful and kind; Chris Pena for carefully reading and commenting on my writings; Mohammad Ezatti; Michael Baker; Qing Yun Mai; and Jishnu Mukherjee: thank you all for your support and friendship.

I wouldn't manage to finish this work without all the lifelong friendships Dallas has given to me. Melodi Damla Tastemel, Hunkar Gizem Yesilyurt, Serkan Belkaya, Ayse Ece Ercan, Dicle Berfin Azizoglu, Didem Agac, Yasemin Onder, Xiangyi Li, Hema Manjunath, and Deniz Yorukoglu: thank you for making Dallas feel like home for me.

Ezgi Guner, Canan Candan, Dicle Evliyaoğlu, Idil Findikoğlu, Irem Atay, Sinem Altan, Zeynep Sener, Sermin Tukel, Eylul Harputlugil, Aysu Uygur, Gunes Pekmezciler Hellweger,

Nur Kiziltan: your endless support from all over the world is always tremendous and highly appreciated. Dr. Adil Doğanay Duru, Dr. Tolga Sütlü and Anil Akturk: thanks for being with me during my first scientific journey in Sweden. Drs Batu Erman, Zehra Sayers, Adnane Achour and Selim Cetiner, thanks for your continuous support during my studies.

Last but certainly not least, I have to thank my family for their unconditional love and enormous support. My uncle Kutlu Özgüvenç; my parents; Oya and Ahmet Ayhan Saatçıoğlu; my brother Nevzat Ömer Saatçıoğlu, his wife Melike Uzer Saatçıoğlu, and his adorable son Sami Sinan Saatcıoğlu: your smiling faces and true support always give me the strength to achieve whatever I want.

CONTROL OF OOCYTE REAWAKENING BY KIT

HATICE DUYGU SAATCIOGLU

The University of Texas Southwestern Medical Center at Dallas, 2016

DIEGO H. CASTRILLON, M.D, Ph.D.

In mammals, oocyte reawakening is a fundamental biological process controlling follicle maturation, female fertility, the onset of the menopause, and thus, overall aging. We demonstrate through complementary genetic experiments that Kit is the upstream receptor regulating reawakening within oocytes. Although many factors have been proposed as candidates, the data have remained contradictory, and definitive genetic evidence in support of any factor has been lacking. We engineered two novel *Kit* alleles in mice, one a dominant gain-of-function point mutation active in the germline, the other a floxed allele for conditional inactivation. These

alleles permitted us to conduct elegant genetic experiments whereby Kit was activated or inactivated in primordial oocytes. The results were complementary and striking. Oocyte-specific Kit activation resulted in a syndrome of female sterility due to global and premature reawakening leading to ovarian failure. In contrast, Kit inactivation also led to female sterility, albeit via a contrasting and opposite phenotype: a complete failure of primordial follicles to reawaken. Additional studies demonstrated that Foxo3 was the mediator of both phenotypes, linking our findings to prior discoveries. These complementary genetic experiments thus definitively incriminate Kit as the upstream receptor regulating reawakening. We believe our study will be of interest to general scientific and lay audiences as well as geneticists, given the importance of oocyte maintenance in the menopause, overall female aging, and reproduction.

TABLE OF CONTENTS

ABSTRACT vi

TABLE OF CONTENTS viii

PRIOR PUBLICATIONS xii

LIST OF FIGURES xiii

LIST OF ABBREVIATIONS xvi

CHAPTER 1 1

ARRANGEMENT AND SOME GENERAL BUT UNDERAPPRECIATED ASPECTS OF OOGENESIS 1

PREMATURE OVARIAN INSUFFICIENCY (POI) 3

PI3K-PTEN-FOXO3 AXIS IN OOCYTE REAWAKENING 4

PI3K- TSC(1,2)-MTOR AXIS IN OOCYTE REAWAKENING 6

UPSTREAM ACTIVATORS CONTROLLING OOCYTE REAWAKENING 7

RECEPTOR TYROSINE KINASE KIT 8

DISSERTATION OBJECTIVES 12

CHAPTER 2 20

MOUSE STRAINS, BREEDING AND ANALYSIS 22

GENOTYPING 22

TISSUE-PROCESSING AND HISTOMORPHOLOGIC ANALYSIS OF OVARIES 23

IMMUNOHISTOCHEMISTRY (IHC) AND IMMUNOFLUORESCENCE (IF) 23

ANTIBODIES FOR IF AND IHC 24

RNA ISOLATION AND SANGER SEQUENCING 25

TOLUIDINE BLUE STAINING AND ELECTRON MICROSCOPY. 25

WESTERN BLOT 26

FSH AND LH ANALYSES 26

NORTHERN ANALYSIS 27

RADIATION TREATMENT OF LIVE MICE 27

STATISTICAL ANALYSIS 27

CHAPTER 3 28

INTRODUCTION 28

RESULTS 32

SINGLE CELLS OF SSC CULTURES ARE CAPTURED WITH HIGH EFFICIENCY BY THE C1 FLUIDIGM SYSTEM 32

DIFFERENTIALLY EXPRESSED GENES IN THE SSC CULTURES ARE IDENTIFIED BY SINGLE-CELL QPCR. 32

PRINCIPAL COMPONENT ANALYSIS (PCA) REVEALED NO DISTINCTIVE WELL-DEFINED CELLULAR SUBTYPE IN THE SSC CULTURE CELLS USING THE THE 96 GENE PANEL. 33

DISCUSSION 34

CHAPTER 4 40

INTRODUCTION 40

RESULTS 41

GENERATION AND VALIDATION OF THE CONDITIONAL DOMINANT GAIN-OF-FUNCTION ALLELE *KIT*$^{D818V(L)}$ 41

CONSTITUTIVE KIT ACTIVATION IN TRANSIT-AMPLIFYING SPERMATOGONIA NOT AFFECT SPERMATOGENESIS 42

KITD818V MUTATION IS EMBRYONIC LETHAL IN THE HEMIZYGOUS STATE AND HYPERACTIVE KIT MIGHT CAUSE DEFECTIVE GERM-CELL MIGRATION IN MALES 45

KIT MIGHT BE DOWN-REGULATED IN D818V EMBRYOS 46

BLIMP-1-CRE; KIT$^{D818V(L)/+}$ MICE ARE EMBRYONIC LETHAL 47

SOME OF THE *VC;KIT*$^{D818V(L)/+}$ MALES GET KIT OVEREXPRESSING TUMORS BY ONE YEAR OF AGE 48

A RADIATION DOSING REGIMEN DOES NOT LEAD TO MALIGNANT TRANSFORMATION OF GERM CELLS FROM *VC; KIT*$^{D818V(L)/+}$ MALES BUT DOES LEAD TO LYMPHOMAS IN CONTROL AS WELL AS EXPERIMENTAL ANIMALS. 49

GENERATION AND VALIDATION OF CONDITIONAL FLOXED ALLELE *KIT*^{L} 50

KIT INACTIVATION LEADS TO INFERTILITY DUE TO A DEFECT IN TRANSIT AMPLIFYING SPERMATOGONIA 51

VC; KITD818V$^{(L)/-}$ DO NOT HAVE A MALIGNANT PHENOTYPE BUT DO HAVE A SEVERE DEFECT IN SPERMATOGENESIS 52

KIT$^{D818V(L)}$ HOMOZYGOUS MALES ARE INFERTILE AND THEY MAY HARBOR NON-GERM CELL RELATED TUMORS AT LATER AGES 53

DISCUSSION 54

CHAPTER 5 73

INTRODUCTION 73

RESULTS 74

KIT ACTIVATION IN PRIMORDIAL OOCYTES RESULTS IN A GLOBAL PRIMORDIAL FOLLICLE REAWAKENING PHENOTYPE 74

KIT ACTIVATION RESULTS IN GLOBAL PRIMORDIAL OOCYTE REAWAKENING VIA AKT-FOXO3 76

ANALYSIS OF CONDITIONAL FLOXED ALLELE *KIT*^{L} IN FEMALES 77

CONDITIONAL INACTIVATION OF KIT WITHIN PRIMORDIAL OOCYTES RESULTS IN A COMPLETE FAILURE OF OOCYTE REAWAKENING WITH PERSISTENCE OF QUIESCENT PRIMORDIAL FOLLICLES 78

DISCUSSION 80

REFERENCES 97

PRIOR PUBLICATIONS

Aloisio GM, Nakada Y, **Saatcioglu HD,** Peña CG, Baker MD, Tarnawa ED, Mukherjee J, Manjunath H, Bugde A, Sengupta AL, Amatruda JF, Cuevas I, Hamra FK, Castrillon DH. 2014. PAX7 expression defines germline stem cells in the adult testis. 2015. J Clin Invest. 124(9):3929-44. doi: 10.1172/JCI75943

Peña CG, Nakada Y, **Saatcioglu HD,** Aloisio GM, Cuevas I, Zhang S, Miller DS, Lea JS, Wong KK, DeBerardinis RJ, Amelio AL, Brekken RA, Castrillon DH. 2015. LKB1 loss promotes endometrial cancer progression via CCL2-dependent macrophage recruitment. J Clin Invest. doi: 10.1172/JCI82152.

Ezzati MM, Baker MD, **Saatcioglu HD**, Aloisio GM, Pena CG, Nakada Y, Cuevas I, Carr BR, Castrillon DH. Regulation of FOXO3 subcellular localization by Kit ligand in the neonatal mouse ovary. J Assist Reprod Genet. 2015 Dec;32(12):1741-7. doi: 10.1007/s10815-015-0589-9.

Saatcioglu HD, **Cuevas I**, Castrillon HD. 2015. Control of primordial oocyte reawakening by Kit. PLOS genetics, *Accepted: July 2nd, 2016*

LIST OF FIGURES

FIGURE 1.1: Stages of follicular maturation ..... .16

FIGURE 1.2: Global oocyte reawakening phenotype and unknown control of upstream signaling..... 17

FIGURE 1.3: Receptor tyrosine kinase Kit 18

FIGURE 1.4: Expression of Kit in male and female germ cells..... 19

FIGURE 3.1: SSC cultures have 99% capturing efficiency by the C1-Fluidigm assay..... 36

FIGURE 3.2A: mRNA abundance patterns of 95 single SSCs are identified by violin plots.....37

FIGURE 3.2B: mRNA abundance patterns of 95 single SSCs are identified by violin plots.....38

FIGURE 3.3: Principal Component Analysis (PCA) of SSC cultures revealed no distinctive heterogeneity. 39

FIGURE 4.1: Map of the $Kit^{D818V(L)}$ allele 59

FIGURE 4.2: Generation of germline specific Kit^{D818V} 60

FIGURE 4.3: Germ-line specific Kit^{D818V} mutation does not affect spermatogenesis 61

FIGURE 4.4: Marker analysis of control and $VC;Kit^{D818V(L)/+}$ testes 62

FIGURE 4.5: $Kit^{D818V/+}$ embryos are embryonic lethal and they have congested blood vessels with abnormal white-blood cell clusters. 63

FIGURE 4.6: *Kit*^{D818V} mutation leads to fewer germ cells migrated into the primitive cords with down-regulated Kit expression and predominantly nuclear Foxo1. 64

FIGURE 4.7: *Blimp1-cre (BC);Kit*$^{D818V(L)/+}$ embryos are lethal. 65

FIGURE 4.8: Spermatogenesis is normal but Kit expressing tumors can occur in *VC; Kit*$^{D8181V(L)/+}$ mice due to rare ectopic expression. 66

FIGURE 4.9: *VC; Kit*$^{D818V(L)/}$+ testes are smaller 6 months after low-dose radiation 67

FIGURE 4.10: Maps of *Kit* locus (exons 14-21) and targeting construct……....68

FIGURE 4.11: Generation of *Kit*^{L} allele (exon 17 floxed). ..... …. 69

FIGURE 4.12: Infertility due to Kit loss of function mutation in males 70

FIGURE 4.13: Germ-cell specific *Kit*$^{D818V/-}$ mice have smaller testes and lack undifferentiated spermatogonia 71

FIGURE 4.14: Heterozygous *Kit*$^{D818V(L)}$ mice are normal but homozygous *Kit*$^{D818V(L)}$ males are infertile and they form tumors by 1 years of age 72

FIGURE 5.1: Global oocyte reawakening phenotype following conditional Kit activation within oocytes 86

FIGURE 5.2: Quantitative analyses of oocyte phenotypes following conditional Kit activation within oocytes 87

FIGURE 5.3: Kit activation promotes oocyte reawakening through AKT-Foxo3 axis. 88

FIGURE 5.4: Analysis of Kit expression in *VC; Kit*$^{D818V(L)/+}$ ovaries. 89

FIGURE 5.5: Reawakened oocytes differentiate normally in *VC; Kit*$^{D818V(L)/+}$ ovaries (PD14). 90

FIGURE 5.6: Loss of the primordial follicle pool due to oocyte reawakening. 91

FIGURE 5.7: Primordial follicle arrest phenotype following Kit inactivation in oocytes……..92

FIGURE 5.8: Quantitative analyses of oocyte phenotypes following Kit inactivation in oocytes. 93

FIGURE 5.9: Ultrastructural analysis and absence of zona pellucida in *VC; Kit* $^{L/-}$ follicles…. 94

FIGURE 5.10: *VC;Kit*$^{L/-}$ oocytes die by 6 months of age. 95

FIGURE 5.11: Marker studies of Kit-deficient oocytes are consistent with specific defect in oocyte reawakening via Foxo3. 96

LIST OF ABBREVIATIONS

AMH: anti-mullerian hormone

Abcb1b: ATP-binding cassette, sub-family B (MDR/TAP), member 1B

BMP15: bone morphogenetic protein 15

Ccnd1: cyclin d1

cDNA: complementary deoxyribonucleic acid

DMEM: Dulbecco's modified eagle's medium

DNA: deoxyribonucleic acid

E: embryonic day

FSP1: Fibroblast specific protein 1

FSH: follicle-stimulating hormone

GCNA: germ cell nuclear antigen

GDF9: growth differentiation factor 9

GDNF: glial cell derived neurotrophic factor

GIST: gastrointestinal stromal tumor

GPCRs: G protein–coupled receptors

H&E: hematoxylin & eosin

IF: immunofluorescence

IGF1R: insulin-like growth factor 1 receptor

Insr: insulin receptor

IHC: immunohistochemistry

ITGCN: intratubular germ cell neoplasia

LH: luteinizing hormone

Lhx8: lim homeobox protein

MEF: mouse embryonic fibroblast

mTOR: mammalian target of rapamycin

MDR1: multi-drug resistance 1

PAS: periodic acid schiff

PBS: phosphate buffered saline

PCNA: proliferating cell nuclear antigen

PD: post-natal day

PI3K: phosphoinositide 3-kinase

PIP2: phosphatidylinositol 4,5-biphosphate

PIP3: phosphatidylinositol 3,4,5-triphosphate

Pou5f1: pou domain, class 5, transcription factor

Plzf: promyelocytic leukemia zinc finger protein

PTEN: phosphatase and tensin homologue deleted on chromosome 10

PKB: protein kinase B (also known as AKT)

QPCR: quantitative polymerase chain reaction

RTK: receptor tyrosine kinase

Sohlh1: spermatogenesis and oogenesis specific basic helix-loop-helix 1

SSC: spermatogonial stem cell

SCF: stem cell factor

WT: wild-type

Zbtb16: zinc finger and BTB domain containing 16

Zp: zona pellucida

CHAPTER 1
Introduction

OOCYTE REAWAKENING AND KIT SIGNALLING

Arrangement and some general but underappreciated aspects of oogenesis

Oogenesis is the process in which ova are generated from individual oocytes after multiple stages of follicular maturation. Ovulation occurs every 5 days in mice and every 28 days in humans (Sullivan and Castrillon, 2011). Follicles are individual oocytes surrounded by nursery cells—granulosa cells—that nourish the oocyte and support its development. The primordial follicles, assembled in the perinatal period, are the minute long-lived follicles that make up the females' reserve source of reproduction providing the oocytes for each cycle to be developed for maturation. Since there is no neo-oogenesis postnatally, the primordial oocytes represent a finite pool that must be carefully utilized, particularly in long-lived mammals. Most of the primordial oocytes stay dormant for prolonged intervals, but are individually activated via poorly-understood, ovarian-intrinsic mechanism known as primordial follicle activation, initiation, or reawakening. (**Figure 1.1**). Although much is known about ovulation and the later stages of follicle maturation, relatively little is known about the biology of primordial oocytes or how they are reawakened; for example how the balance of maturation, quiescence/reawakening or cell death is regulated, or even how these decisions are generally controlled (Edson et al., 2009). Conceptually, these processes might be regulated stochastically, or perhaps more likely, via the complex integration of multiple follicle-intrinsic and follicle-extrinsic mechanisms, as well as ovarian and extra-ovarian influences. However, if a primordial oocyte begins to grow; i.e., is activated or reawakened, this growing oocyte ultimately either dies at some step of its

maturation or completes eventually all stages of follicle maturation, culminating in ovulation (i.e. the release of the mature egg). Of note, all stages of follicle maturation including reawakening appear to be irreversible, and thus, a primordial oocyte that has reawakened decreases the primordial reserve, and will soon (within a few weeks) undergo death or ovulation (Edson et al., 2009; Sullivan and Castrillon, 2011).

Follicular maturation is a highly dynamic process with complex morphological changes, beginning from a primordial follicle, turning into a primary, secondary, early antral and preovulatory follicle (**Figure 1.1**). Many follicles die from atresia (programmed cell death) during each different maturation step, selecting the "best" oocyte for ova formation (Kaipia and Hsueh, 1997). Primordial follicles contain a small oocyte (~17 μm), arrested in prophase stage of meiosis I, and which is surrounded by flattened granulosa cells known as pregranulosa cells at this stage; i.e. prior to reawakening of the primordial follicle. Once an oocyte begins to grow actively, its granulosa cells differentiate and turn into proliferative, cuboidal-shaped cells. The follicle is called a primary follicle once its diameter grows up to 28 μm and it becomes surrounded with one layer of cuboidal granulosa cells (Kim, 2012; Sullivan and Castrillon, 2011). This rapid growth in oocyte diameter correlates with an approximately 300 fold increase in RNA synthesis, an increase in the rate of protein synthesis, as well as a significant increase in the volume content of the oocyte (Liu et al., 2006). This irreversible initiation of oocyte growth (reawakening) is clearly to be gonadotropin-independent; for example, the granulosa cells do not express functional gonadotropin receptors at early stages of follicle maturation, and injections of gonadotropins do not alter the reawakening follicle numbers in neonatal mice. (Peters et al., 1973). Also, oocyte reawakening begins before birth independent of the reproductive cycles (John et al., 2007). Furthermore, mutations in the loci encoding the gonadotropins or their

receptors (i.e. FH, LH, FHR, and LHR) do not affect the dynamics of reawakening of early stages of ovarian follicle maturation, although the female mice are sterile due to the failure of ovulation (Edson et al., 2009).

When the first meiotic division is completed in the oocyte, the activated follicle becomes a secondary follicle with two layers of granulosa cells that acquire additional functional importance in controlling oogenesis. After the secondary follicle stage, the granulosa cells begin to express follicle stimulating hormone (FSH) and luteinizing hormone (LH) receptors (FSHR and LHR), which make these more advanced follicles responsive to gonadotropins (Sanchez and Smitz, 2012). After the onset of puberty, FSH and LH levels control ovulation from the mature follicles under the control of the hypothalamic-pituitary-ovarian axis.

Premature Ovarian Insufficiency (POI)

Premature ovarian insufficiency (POI) affects 1% of women who are older than 40 years of age. This condition is characterized by the absence, non-functionality, or early depletion of the ovarian reserve (Fortuno and Labarta, 2014; Sullivan and Castrillon, 2011). The patients generally have at least a four months of absence of a menstrual period, as well as high (menopausal-like) levels of FSH and LH, and Anti-mullerian hormone (AMH) (Fortuno and Labarta, 2014). As none of those criteria is enough by itself to prove complete depletion of the ovarian reserve (i.e. the presence of primordial follicles), there is a great need for biomarkers of the follicle reserve. Growing follicles begin secreting AMH at the primary follicle stage, and there has been considerable interest and utility in measuring serum AMH as an indirect marker of the follicular reserve. Unfortunately, its utility is limited by the fact that primordial follicles do not produce AMH, and furthermore, ultrasonography is capable of visualizing large growing follicles, but not primordial follicles, which are minute. In some women diagnosed with POI (in

the range of 5-10%), spontaneous pregnancy may still occur due to sporadic ovulation and the persistence of a small number of follicles.

Environmental and iatrogenic factors such as use of oral contraceptives, smoking, other health problems such as viral infections, metabolic and autoimmune diseases, and treatment with chemotherapeutic agents that damage or kill oocytes have been correlated with POI (Fortuno and Labarta, 2014; Luisi et al., 2015). However, 10-15% of the cases have family histories suggesting the condition might have some genetic predisposition (Sullivan and Castrillon, 2011). Characterization of the disease using clinical material alone has been difficult as biopsies from ovaries of young patients are rare, if ever obtained in the clinical workup of this condition. Such a procedure is invasive with attendant medical risks, and for the time being, the results of ovarian histopathologic analysis would not alter prognosis, since there is no effective treatment strategy to reverse POI or preserve the primordial follicle reserve (although hormone replacement therapy can alleviate symptoms due to hormone withdrawal, and reduce the general medical risks associated with early menopause, such as osteoporosis and heart disease) Therefore, studies of mouse models are invaluable to understand and provide new insights about this condition (Jagarlamudi and Rajkovic, 2012) .

PI3K-PTEN-FOXO3 axis in oocyte reawakening

The phosphoinositide 3-kinase (PI3K) pathway is a crucial cell-intrinsic signaling pathway controlling cell proliferation and other cellular processes. PI3K catalyzes the formation of a lipid second messenger, phosphatidylinositol 3,4,5-trisphosphate (PIP3), from phosphatidylinositol 4,5-bisphosphate (PIP2). PIP3 in turn leads to the phosphorylation and activation of AKT. Pten, a lipid phosphatase that converts PIP3 back to PIP2, potently suppresses AKT activation (Vanhaesebroeck et al., 2010). The PI3K signaling pathway is

reported to be active in primordial and primary oocytes, as evidenced by diverse genetic studies conducted in several laboratories (John et al., 2008; Liu et al., 2006).

As vital effectors of PI3K-AKT signaling, the Foxos serve fundamental biological roles in aging, cancer, and stem cell maintenance (Goertz et al., 2011; Martins et al., 2015; Paik et al., 2007). The three canonical Foxos—Foxo1, Foxo3, and Foxo4—are coexpressed and exhibit genetic and functional redundancy in most cell types (Goertz et al., 2011; Paik et al., 2007; Tothova et al., 2007). In contrast, in the mouse germline, Foxo1 and Foxo3 have diverged to serve complementary roles in the maintenance of the male and female germline, respectively. Whereas Foxo3 is the principal Foxo protein in the oocyte, Foxo1 is the principal Foxo within undifferentiated spermatogonia, and is the only Foxo required for the maintenance of spermatogonial stem cells (Goertz et al., 2011; Tarnawa et al., 2013). In both the female and male germline, genetic experiments conducted in our laboratory and others have shown that Foxo activity is regulated by its subcellular (nuclear vs. cytoplasmic) localization via its AKT-dependent phosphorylation. When phosphorylated, Foxo proteins are functionally inhibited by their retention in the cytoplasm via interactions with 14-3-3 proteins (Brunet et al., 1999).

The forkhead transcription factor Foxo3 functions as a switch that controls (suppresses) primordial oocyte reawakening. Foxo3 undergoes a cytoplasmic (inactive) to nuclear (active) translocation after primordial follicles are assembled (John et al., 2007). In nullizygous or oocyte-conditional *Foxo3* knockout mice, primordial follicles are assembled normally (John et al., 2007), but undergo global reawakening at birth (**Figure 1.2A**). This leads to a characteristic sequential syndrome of ovarian hyperplasia, follicle depletion, and primary ovarian insufficiency (Castrillon et al., 2003). In the adult ovary, Foxo3 protein localizes to the primordial oocyte nucleus, where it restrains reawakening in a PI3K-AKT dependent manner. Oocyte-specific

deletion of *Pten* hyperactivates AKT, resulting in Foxo3 nuclear export and global reawakening (John et al., 2008; Reddy et al., 2008). Foxo3 normally undergoes nuclear export during the primordial to primary follicle transition (followed by its degradation within the cytoplasm via unknown mechanisms), suggesting that *Pten* inactivation mimics a naturally-occurring PI3K-dependent signal that regulates Foxo3 localization and hence reawakening (John et al., 2008).

John *et al.* showed that PI3K-AKT-Foxo3 pathway is a bona-fide switch, active throughout life, by temporal genetic ablation of Foxo3 in adult mice, which resulted in global oocyte activation (John et al., 2008). Other studies have confirmed Foxo3's role as the molecular switch controlling reawakening in a PI3K-AKT dependent manner, and the utility of Foxo3 nuclear vs. cytoplasmic localization as a marker of oocyte maturation (Cheng et al., 2015; Li et al., 2010; Pelosi et al., 2013; Ren et al., 2015; Zheng et al., 2012). Among these, a mouse model of constitutive Foxo3 has been generated and reported to have increased number of dormant oocytes as well as reproductive capacity (Pelosi et al., 2013).

PI3K- TSC(1,2)-mTOR axis in oocyte reawakening

The mammalian target of rapamycin *(*mTOR) pathway is also another crucial related signaling pathway controlling cell growth and survival; by regulating mRNA translation, metabolism and autophagy (Guertin and Sabatini, 2007). mTOR itself is a member of PI3K family and there is extensively complex crosstalk between PI3K and the mTOR pathway. mTOR controls mTORC1 and mTORC2, which act through different signaling pathways. mTORC2 components are not as well-characterized but they control AKT kinase downstream of PI3K, regulating cell growth and other cellular processes (Guertin and Sabatini, 2007). mTORC1 acts

on to phosphorylate the downstream factors, S6K and 4EBP, which in turn regulate mRNA translation into protein to control cell growth, proliferation and survival (Guertin and Sabatini, 2007; Sarbassov et al., 2005). The Tsc1-Tsc2 complex is well-characterized to negatively regulate mTORC1. Such that, Tsc1 functions through stabilizing Tsc2, and Tsc1 nullizygous mice are embryonic lethal due to persistent phosphorylation of S6K (Adhikari et al., 2010; Kwiatkowski et al., 2002).

Oocyte-specific inactivation of Tsc1 also resulted in a global oocyte reawakening phenotype, establishing an important but incompletely understood role of mTOR signaling in this process (**Fig. 1.2A**) (Adhikari et al., 2009; Adhikari et al., 2010; Sullivan and Castrillon, 2011). Further analysis showed that the global oocyte reawakening phenotype was due to extensive phospohorylation of S6K and 4EBP1, but not due to Akt phosphorylation or Foxo3 inactivation (Adhikari et al., 2010). Interestingly, inactivation of both Tsc1 and PTEN resulted in a more severe oocyte reawakening phenotype (i.e. faster depletion of the oocytes and larger oocyte diameter) suggesting that PTEN and Tsc1 controls oocyte reawakening in a synergistic way but via different signaling components (Adhikari et al., 2010; Sullivan and Castrillon, 2011).

Upstream activators controlling oocyte reawakening

In many physiological processes, the upstream activators of class I PI3Ks are transmembrane receptor tyrosine kinases (RTKs) such as insulin-like growth factor 2 (Igfr1), insulin receptor (Insr), Ret, Pdgfr, or Kit (Vanhaesebroeck et al., 2010). Ligand binding activates PI3K by phosphotyrosine-mediated binding through an SH2 domain on the p85 subunit of PI3K. G protein–coupled receptors (GPCRs) can also activate PI3K through the p110γ catalytic subunit

isoform. However, p110$\gamma^{-/-}$ mice are viable and fertile (but display various GPCR-mediated immunological defects), suggesting that GPCRs may not play essential roles in the regulation of the PI3K pathway during oocyte reawakening (Hirsch et al., 2000). The identification of a presumptive oocyte surface RTK that acts through PI3K-AKT-Foxo3 to regulate reawakening has remained an outstanding question in reproductive biology (Da Silva-Buttkus et al., 2009), and this question was the central focus of my dissertation research. Several candidates including Kit have been proposed over the years, but definitive (i.e. genetic) evidence about which is the *bona fide* receptor has been lacking (**Fig. 1.2B**) (Ezzati et al., 2015; Gallardo et al., 2007b; John et al., 2009; Skinner, 2005; Sullivan and Castrillon, 2011). The unique biological features of primordial follicle reawakening, some of which are not readily modeled *in vitro*, prompted me to apply rigorous genetic approaches to identify and validate this factor.

Receptor tyrosine kinase Kit

Highly conserved among mammalian species, the *Kit* gene encodes a type III receptor tyrosine kinase. The gene is located on chromosome 5 in mice, and chromosome 4 in humans (Yarden et al., 1987). It has 21 exons and a relatively large 3'UTR in both species (2158 nt in humans), suggesting that the gene is being extensively regulated by post-transcriptional mechanisms, an idea borne out by many studies and led to the identification of miRNA target sites in the 3'UTR (Godshalk et al., 2011). The main gene product is a 5.5 kb mRNA transcript that yields a main protein product of 145 kDa (Mithraprabhu and Loveland, 2009; Yarden et al., 1987). The receptor tyrosine kinase Kit has four main domains: 1) an extracellular domain with five immunoglobulin-like repeats, 2) a transmembrane domain that anchors the receptor to the

cell membrane; 3) an intracellular domain with proximal kinase region (required for ATP binding); and 4) a phosphotransferase kinase region (Mithraprabhu and Loveland, 2009).

Early genetic experiments showed that random, naturally-occurring mutations at the murine dominant *white spotting locus* (*W)* affect various aspects of sterility, coat color abnormalities, severe macrocytic anemia and mast cell deficiency. Interestingly, all phenotypes are cell intrinsic (i.e hematopoietic phenotypes being the same also *in vitro* conditions), which suggests a correlation of this locus with a gene controlling cell (possibly stem-cell) development (Dexter and Moore, 1977). Later on it was discovered that *W* mutations occur in the transmembrane or kinase domain of the *Kit* gene, establishing that Kit is encoded by the *W* locus (Chabot et al., 1988; Geissler et al., 1988). Depending on the specific region of mutation that affects the nature and the function of the receptor tyrosine kinase Kit, different types of mutations affect development of diverse cell types. Homozygous *W/W* mice are found to be embryonic lethal, whereas *W/+* mice are fertile with no anemia but spotting, and W^{37}/+ mice are fertile with mottled coat, and mast cell deficiency. W^{v}/W^{v} mice are sterile, black-eyed, white colored and mast cell deficient (Nocka et al., 1990). Many other *W* alleles have been described, with highly pleiotropic phenotypes.

Recalling in several respects the *W* phenotypes including their diverse phenotypic manifestations, mutations on the *Steel* (*Sl) locus* are also characterized with aberrant germ cells, melanocytes, hematopoietic stem cells, and mast cells (Nocka et al., 1990). In the hematopoietic system, using transplantation and *in vitro* culture experiments, the *Sl locus* has been identified to act on the stromal cells (Dexter and Moore, 1977). Later investigations by various groups showed that the mutations affecting the *Sl locus* altered the amino acid sequence of the Kit ligand, also known as stem cell factor (SCF) (Ashman, 1999; Dexter and Moore, 1977; Witte,

1990). Concordantly, various *Sl* mutations have been shown to occur within the Kit ligand gene, establishing that the *Sl* locus encodes Kit ligand. The *Sl* (Kit ligand, or KL) locus is on chromosome 10 in mice, and the Kit ligand locus is located on chromosome 12 in humans. There are two different isoforms of Kit ligand, due to differential splicing and proteolytic cleavage: these two isoforms are known as membrane bound and soluble (Huang et al., 1992). Experiments on myeloid cell lines showed that membrane bound form is more potent and leads to higher Kit activity (Miyazawa et al., 1995).

Upon ligand binding, the Kit receptor dimerizes, resulting in dramatic increases in its autophosphorylation activity, which in turn can act through various downstream signalling pathways including the PI3K/AKT, JAK/STAT, and RAS/MAPK pathways (**Figure 1.3**). The type of pathway or combination thereof activated depends on the cell type as well as the developmental stage (Mithraprabhu and Loveland, 2009).

Kit signaling controls the normal development of mast cells, interstitial cells of Cajal, melanocytes and germ cells. The specific functional and genetic requirements of Kit in these restricted cellular subsets is entirely rationalized by the high levels of Kit expressed in these cells (i.e. presence of Kit on the cell membrane). In other words, these cell types normally express high levels of Kit, whereas most cell types do not express Kit to a significant or detectable degree. Aberrant Kit signaling in diverse cancers that arise from these cell types are due to point mutations in the Kinase domain or juxta-membrane domain of Kit, resulting in constitutive Kit hyperactivity; i.e. in the absence of Kit ligand. Such mutations are commonly present in mast cell lymphomas, gastrointestinal stromal tumors (GISTs), melonomas, acute myeloid leukemia, and germ cell tumors, most notably seminomas. The most common oncogenic mutation seen in seminomas and mast cell neoplasms (mastocytomas) is D816V in human, corresponding to

D818V in mice (Liang et al., 2013). This point mutation has been reported to lead to constitutive activation of Kit, by activation of the PI3K/AKT and RAS/MAPK signaling pathways with a significant role in malignant transformation through these downstream pathways (Chian et al., 2001; Kosmider et al., 2005).

Kit and SCF serve numerous roles in the germ cell lineage, particularly in primordial germ cell migration/survival, primordial follicle assembly, and spermatogenesis (Jones and Pepling, 2013). In normal spermatogenesis, Kit is highly expressed in transit amplifying spermatogonia (**Figure 2.2**) and Leydig cells —somatic cells adjacent to the seminiferous tubules that are viewed as homologous to granulosa cells (Sandlow et al., 1996; Unni et al., 2009). Acrosomal granules of spermatids also express Kit but they synthesize truncated forms of Kit (3.5 and 2.3 kb), which lack either the transmembrane domain or the extracellular domain, making them irresponsive to SCF-Kit signalling (Mithraprabhu and Loveland, 2009; Sorrentino et al., 1991). SCF is also highly expressed in the Leydig cells (Sandlow et al., 1996). *W* and *Sl* homozygous males are sterile with a very similar phenotype: seminiferous tubules depleted of spermatogenesis and with very small numbers of spermatogonia (Ogawa et al., 2000). Interestingly, when the germ cells from homozygous *Sl* mice are transplanted to homozygous *W/W* mice, the transplanted cells can regenerate spermatogenesis, suggesting that Kit signalling is important in regulation of spermatogonia, and that its interaction with SCF drives spermatogenesis in a non-cell autonomous manner (i.e. Kit ligand is produced in Leydig cells and diffuses into the seminiferous tubule to bind to the Kit receptor expressed on spermatogonia) (Ogawa et al, 2000).

In females, SCF is produced by granulosa cells in primordial follicles (Manova et al., 1990) and Kit is highly expressed on the primordial oocyte membrane (Figure 2.2). Thus,

patterns of Kit and KL expression within the ovary do make them plausible candidates as factors regulating reawakening. *In vivo* female mouse models of Kit-KitL also suggest that this pathway is functional during follicular maturation (Huang et al., 1993; John et al., 2009). *Steel*^{panda} females (which harbor a complex chromosome rearrangement of the Steel locus and resemble minute panda bears due to pigmentation defects) are infertile due to an arrest in the primordial follicle stage. In *Kit*^{Y719F} females, where Kit signaling via PI3K-Akt pathway is non-functional due to a mutation abrogating binding to PI3K, there are defects in the primary to secondary follicle transition (John et al., 2009; Serve et al., 1994). *In vitro* studies conducted with explanted ovaries treated with KL or Kit inhibitors also have been interpreted as supportive of this hypothesis (Thomas et al., 2008; Thomas and Vanderhyden, 2006). On the other hand, some of the above mutant phenotypes have proven difficult to interpret due to their pleiotropic nature. For example, *Steel*^{panda} ovaries have very few primordial follicles, obscuring interpretation of phenotypes.

Dissertation objectives

Earlier studies in our laboratory have defined a new marker (Pax7) restricted to a very small subset of stem cell population in testis, which is functional in normal spermatogenesis as well as after radiation and chemotherapy treatments (Aloisio et al., 2014). These results and other studies (see **Chapter 3**), lead to very interesting questions in the male-germ line stem cell field: (1) Are there other unique population of germ cells that are responsible for continuous spermatogenesis? (2) What genes are responsible for stemness characteristics of spermatogonia? Such a gene signature defining a spermatogonial stem cell population would allow us to understand the mechanisms of stem cell self renewal and maintenance in spermatogenesis. As

conventional RNA methods use genetic information from bulk cells, single cell gene analysis approach was needed to analyze heterogeneity among germ cells. To address the heterogeneity question in male stem cells, I performed experiments with single cell quantitative polymerase chain reaction (QPCR) from a well-established spermatogonial stem cell culture system, defined some differentially expressed genes and analyzed their hierarchal classification (**Chapter 3**). While these studies proved insightful, I became more interested in the potential to better understand the role of Kit in germ cell biology through genetic methods employing two novel alleles generated in our laboratory (**Chapters 4** and **Chapter 5**).

The primary focus of this dissertation was to develop an experimental mouse model for Kit hypoactivation and hyperactivation via genetic means. Kit is expressed in male and female germ cells, where it has a vast array of biological functions, as heretofore explained. We generated a mouse model that recapitulates the most common oncogenic mutation seen in testicular cancers. This point mutation (D818V) of the receptor tyrosine kinase Kit leads to constitutive activation of PI3K—a crucial signaling pathway controlling germ cell migration, proliferation and survival. We also generated a floxed allele of Kit for loss-of-function studies. Then, I activated or inactivated Kit specifically in the germline. My extensive histologic and immunohistochemistry analyses on normal and experimental males revealed that germline specific Kit hyperactivity, surprisingly, does not affect spermatogenesis, likely because of compensatory biological mechanisms operating within male germ cells. This unexpected result led me to further analyze and characterize the phenotypes of Kit hyperactivity during male-germ cell migration during embryogenesis, Kit inactivity in spermatogenesis, and effect of Kit hyperactivity on other cells types, (presented in **Chapter 4**).

In females, the molecular control of late follicle maturation and ovulation are well understood in terms of the hypothalamic/pituitary/ovarian axis. However, ovarian follicle maturation, female fertility, and reproductive aging are ultimately governed by the more obscure process of reawakening. Females are born with a finite endowment of oocytes stored for prolonged intervals (decades in humans) as minute and long-lived primordial follicles. Reawakening depends upon the forkhead transcription Foxo3, which acts as a molecular switch under the control of the PI3K pathway. However, the presumptive upstream receptor (predicted to be a tyrosine kinase) controlling reawakening has remained elusive prior to studies described in this chapter. Because of the complexity of this biological process and the lack of *in vitro* model systems, genetic approaches were essential for discovery and authentication of any regulator of reawakening.

Utilizing conditional genetic approaches, I analyzed the ovarian-associated phenotypes of the aforementioned genetic mouse models of Kit hypoactivation and hyperactivation. The results with these two novel alleles were complementary and striking. Oocyte-specific Kit activation led to larger ovaries due to reawakening of every single oocyte, phenocopying *Foxo3* knockout mice. On the other hand, oocyte specific Kit inactivation within oocytes, led to smaller ovaries due to complete failure of oocyte reawakening. Both phenotypes resulted in female infertility, but via opposite ovarian defects: too much reawakening, or none at all. Analysis of our novel mouse models of Kit hyperactivity as well as Kit inactivity in females thus permitted me to more fully characterize the role of Kit in oocyte reawakening than previously possible (**Chapter 5, the central chapter of this dissertation**). We believe these genetic studies strongly implicate Kit as the key upstream receptor controlling reawakening through the PI3K/AKT/Foxo3 pathway. This discovery could lead to insights into ovarian aging or infertility syndromes associated with

follicle depletion. Control of oocyte reawakening by pharmacologic manipulation of Kit might someday prove useful to control follicle maturation *in vitro* or perhaps even *in vivo*

.

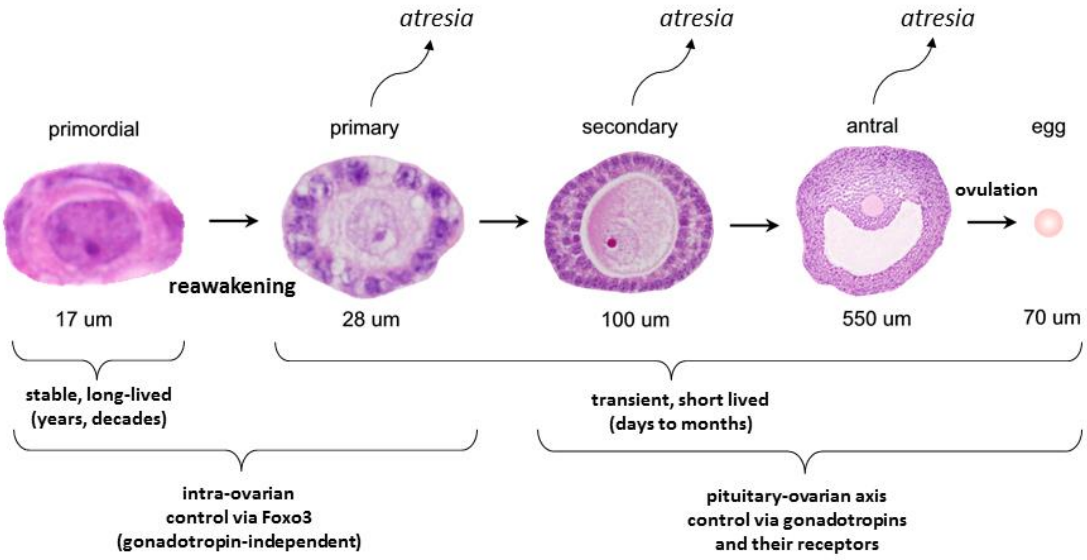

Figure 1.1: Stages of follicular maturation. Mouse follicles are depicted (not to scale: approximate follicle sizes including granulosa cells are shown below each follicle). Follicle growth is normally asynchronous, such that the adult ovary contains follicles at all stages of development. However, the vast majority of follicles at any time are primordial, with only a very small percentage of follicles actively growing. Follicle reawakening, sometimes called initiation or activation is the regular, metered process by which individual primordial follicles are continually selected to begin the elaborate program of follicle maturation that culminates in ovulation. The earliest morphologic hallmark of reawakening is increased oocyte size followed by a change in granulosa cells from a flattened to a cuboidal shape, and then by granulosa cell proliferation. Whereas primordial follicles are long-lived, growing follicles are transient and short-lived, because growing follicles that do not progress to the next stage undergo atresia. Primary follicles are defined as follicles that have initiated oocyte growth and undergone a transition from flattened to cuboidal granulosa cells but have only one layer of granulosa cells. Secondary follicles have two layers of granulosa cells, and antral follicles are large follicles with a chamber (antrum) in preparation for ovulation.

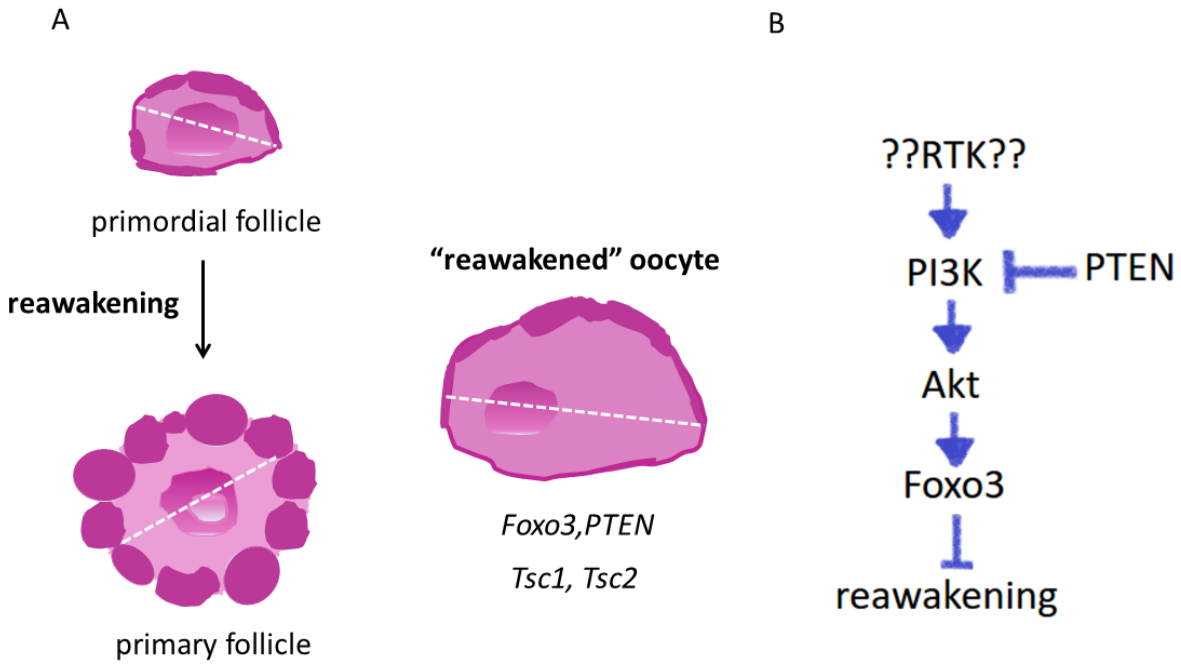

Figure 1.2. Global oocyte reawakening phenotype and unknown control of upstream signaling. (A) Representative drawings of a primordial and a primary follicle. White dashed lines demarcate the diameter of an oocyte—increase in oocyte diameter is a hallmark of oocyte reawakening. A primordial follicle is an individual oocyte surrounded by flattened shaped granulosa cells. A primary follicle is an activated oocyte surrounded by one layer of cuboidal and differentiated granulosa cells. Two main pathways are reported to control oocyte reawakening. 1) PI3K-AKT; which in turn inactivates Foxo3 2) mTOR-Tsc1,Tsc2, which in turn activates S6 and 4EB2. "Reawakened oocyte" drawing represents the aberrant and activated oocyte in the mutant females. In *Foxo3, PTEN, Tsc1* and *Tsc2* knockout females, every single oocyte grows in size irreversibly after birth and, in most cases, the granulosa cells stay flattened and undifferentiated. Early and global reawakening of oocytes leads to female infertility due to primary ovarian insufficiency. **(B)** PI3K is typically regulated by upstream cell surface receptors such as receptor tyrosine kinases. However which many candidates have been considered as the upstream cell surface receptor controlling oocyte reawakening, its elusive identity is not known.

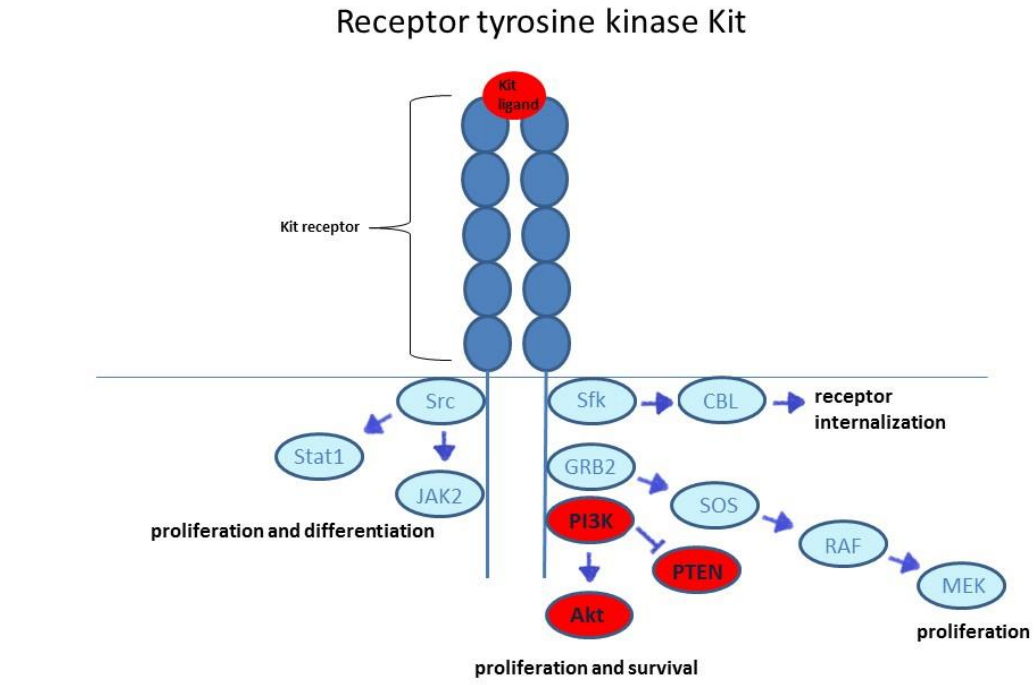

Figure 1.3. Receptor tyrosine kinase Kit: Kit is a type III receptor tyrosine Kinase. Stem cell factor (SCF) is the ligand for Kit and Kit signaling pathways are activated upon ligand binding, which leads to dimerization of the extracellular domain. JAK-STAT; PI3K-AKT; RAF-MEK are among the signaling pathways that are the main pathways through which Kit acts SCF binding.

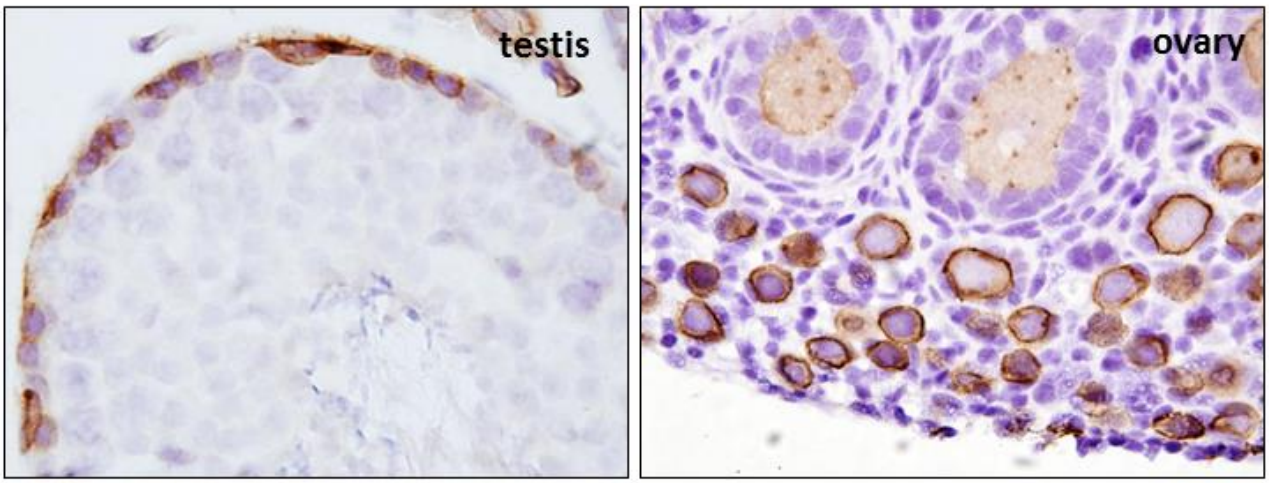

Figure 1.4. Expression of Kit in male and female germ cells. Kit immunohistochemistry on mouse testis and ovary. In males, Kit is expressed in transit amplifying germ cells known as differentiating spermatogonia. *Kit* mutations are the most common oncogenic mutations in testicular cancers (seminomas). In females, Kit is highly expressed in oocyte membrane. Its function on the oocyte membrane has not been fully characterized but is the subject of this dissertation.

CHAPTER 2

METHODOLOGY

Establishment and propagation of spermatogonial stem cells (SSCs)

SSC cultures were derived from PD7-PD10 DBA2 mouse testes as previously described on irradiated MEF feeder cells (Aloisio, 2015; Falciatori et al., 2008) At least 4 neonatal testes were digested with dispase (BD Biosciences, #354235) at 37°C for 28 minutes until the seminiferous tubules were visibly disassociated. The cells were centrifuged and washed with Dulbecco's modified eagle's medium (DMEM)/F12; resuspended in SF medium; and plated onto irradiated MEF feeder cells. It took approximately ten days for SSCs to start proliferating in clumps. Established cell cultures were fed with supplemented SF medium every two days and plated onto irradiated feeder layer of MEFs, and passaged at a 1:5-7 dilutions. Components of the SF medium are described in an earlier publication in our laboratory (Aloisio, 2015) and based on previous protocols (Falciatori et al., 2008; Hamra et al., 2008)

Capturing and quantitative PCR analysis from SSCs

SSCs were harvested from the feeder layer, and the cells were detached with gently shaking (1400 rpm) at 37^0 in trypsin (0.05%) and DNAse (1µg) for ten minutes. Cell viability and diameter were automatically calculated with the Countess Automated Cell Counter (Invitrogen) after trypan-blue staining. Approximate cell diameters in the SSC cultures were 10

μm, and cell viability was 98%. Individual cells from the suspension were captured by the C1-STA integrated fluidic circuit (IFC) chip (Fluidigm), which is designed for capturing cells that are 10-17 μm. 1300 SSCs were loaded onto the IFC chip and captured cells were analyzed under the microscope. Wells in the chip with captured cells were counted manually and capturing efficiency was calculated. Ninety-five out of 96 wells contained a single SSC as desired, and then subjected to further manipulations as described below prior to analysis. After manual visualization, the IFC was inserted in the automated C1 machine to lyse each cell for RNA isolation, complementary deoxyribonucleic acid (cDNA) synthesis and amplification per the manufacturer's protocols. Total time between addition of the cell suspension to the chip and to cell lysis was less than 60 minutes.

Amplified cDNAs, Fluidigm STA reagents, Evagreen QPCR reagents, and pooled PCR primers which were 1:10 diluted and were individually pipetted onto assay insets of the 96.96 dynamic array IFC chip (Fluidigm) by manufacturer's instructions. The 96 pooled primers were designed by Fluidigm Assay Design group (please see **Chapter 3** introduction for details of gene selection for the 96 gene panel and the underlying rationale for the selected genes). QPCR was performed by the automated BioMark HD real-time PCR (Fluidigm) using standard fast-cycling and melt-curve analysis. The PCR results were then analyzed by Fluidigm Real-time PCR software as provided by the manufacturer, with advice and support provided by Fluidigm technical support. R-script packages and SINGular analysis toolset, 2.1 (Fluidigm) were used to generate outlier exclusion, hierarchical clustering heatmap, violin plots, and principal component anlaysis (PCA).

Mouse strains, breeding and analysis

All live animal experiments were approved by the UTSW Animal Care and Use Committee. Mice were housed in a pathogen-free animal facility in microisolator cages and fed ad libitum on standard chow under standard lighting conditions. Generation of the Vasa-cre mice were described previously (John, Gallardo et al. 2008, Gallardo, Shirley et al. 2007).

D818V(L) and Kit floxed alleles were generated in the Castrillon lab by Dr. Ileana Cuevas. The D818V(L) allele was designed to provide wild-type *Kit* function prior to Cre-mediated recombination and activation of the allele ($Kit^{D818V(L)} \rightarrow Kit^{D818V}$), a strategy similar to the well-known $Braf^{V600E}$ conditional allele (Dankort et al., 2007). In the latent $Kit^{D818V(L)}$ allele, the C-terminal *Kit* sequences are encoded by an exon 17-21 cDNA/polyadenylation site cassette (shown in green in **Chapter 4, Fig. 4.1**). For the Kit floxed alles, *loxP* site was integrated within the intron following exon 17 (**Chapter 4, Fig.4.10**). Electroporation into SM-1 ES cells and subsequent "plus/minus" selection was conducted by standard methods.

The mice were of mixed background including B6(C3)-Tg(Pgk1-FLPo)10Sykr/J transgenic mice (Jackson Laboratory, Bar Harbor, Maine) and FVB. For analysis of the germ-cell specific Kit hyperactivity and inactivation, different time points were analyzed from at least from 3 different experimental and sibling controls. Time points were PD7, PD28, 6 weeks, 12 weeks, 16 weeks, and 6 months.

Genotyping

Mice were routinely genotyped from tail DNA by PCR with Promega GoTaq in 1.6 mM $MgCl_2$ with custom oligonucleotide primers. Genotyping primers for the *KitD818V* allele are as

follows: (a1) 5'-ATTAGAGCCCCGATCCTGTG-3' and (b1) 5'-GCAACAGCCATTCATTTCAGC-3' (see Figure S1 for positions of a1/b1 primers), under the following cycling conditions: 95^{o} x 2 min; 94^{o} x 30 sec, 60^{o} x 30 sec, 72^{o} x 30 sec (35 cycles); 72^{o} x 7 min. The product sizes are 219 bp for the floxed allele $Kit^{D818V(L)}$ and 171 bp for the wild type *Kit* allele. Genotyping primers for Kit^{L} allele are as follows: (a1) 5'-AGTTCTGAAGAGACTGTCAAGGT-3' and (b2) 5'-ACACCCCATTTCCTTATTTTTGCT -3'(see Figure S3 for positions of a1/b1 primers), under the following cycling conditions: 95^{o} x 2 min; 94^{o} x 30 sec, 60^{o} x 30 sec, 72^{o} x 30 sec (35 cycles); 72^{o} x 7 min. The product sizes are 174 bp for the floxed Kit^{L} allele and 126 bp for the wild type *Kit* allele

Tissue-processing and histomorphologic analysis of ovaries

Ovaries were fixed in 10% formalin overnight, embedded in paraffin and serially sectioned (5 μm). Every fifth section was H&E stained and analyzed. For *VC*; $Kit^{D818V(L)}$/+ and control ovaries, the middle section of the series was used for relative follicle counts and diameter measurements as described in the text. For *VC*; $Kit^{L/-}$ and control ovaries, all the primordial and primary oocytes were counted in every fifth section. The longest diameter of 50 oocytes for which nuclei were in the plane of section was determined with ImageJ.

Immunohistochemistry (IHC) and Immunofluorescence (IF)

For immunohistochemistry (IHC) and immunoflouresence (IF), tissues were fixed in 10% formalin overnight, embedded in paraffin, and cut into 5 μm sections. Sections were rehydrated in EtOH series after deparaffinization in xylene. For IHC, antigen retrieval was performed in

parboiling 10 mM sodium citrate (pH 6.0) x 20 min, cooled at RT, followed by peroxidase blocking (3% H_20_2) and blocking in 0.5-1% BSA in phosphate buffered saline (PBS). ImmPRESS (Vector Laboratories) was used for detection. For IF, sections were rehydrated in an EtOH series after deparaffinization in xylene. Antigen retrieval was performed in parboiling 10 mM sodium citrate (pH 6.0) x 20 min, cooled at RT, followed by PBS washes, 10 minutes of autofluorescence blocking (100 nm Tris Glycine), and blocking in 2.5% BSA+5% goat serum (Vector Laboratories) in PBS. Fluorophore conjugated secondary mouse (Alexa Fluor 555) or rabbit (Alexa Fluor 488) IgGs at 1:500 (Invitrogen #A21429 and #A11029) were used for detection. DAPI (1:1000; for ten minutes) was used for nuclear staining. For double labeling, the slights were blocked with 2.5% BSA+5% goat serum (Vector Laboratories) in PBS after 3x10 mins of PBS washes; stained with a second primary antibody, and a different Fluorophore conjugated secondary antibody in the blocking buffer for an hour, washed in PBS (3X10 minutes) and stained with DAP. Zeiss LSM 510 confocal microscopy was used for fluorescence imaging.

Antibodies for IF and IHC

Antibodies and titers were: Kit 1:750 for IHC; 1:50 for IF (Cell Signaling #3074S); Foxo3 1:50 for IHC and IF (Santa Cruz #sc-11351); Other antibodies and titers for IHC were: Vasa 1:200 (Abcam #27591); P-AKT 1:75 (Cell Signalling #S473); Sall4 1:1000 for IHC (Abcam #57577); AMH 1:500 (Serotec #MCA2246); P63 1:500 (Thermo Fisher #MS-1081); Inhibin (Biorad #MCA951ST); Gata-1 (Santa Cruz #sc-265); Zp1 (Santa Cruz #sc-23708); Gdf9 (Santa Cruz #sc-12244); Ki67 (Abcam #15580); Sohlh1 and Nobox (provided by Dr. Aleksandar Rajkovic (Magee-Womens Research Institute). Foxo1 (Cell Signalling #2808),

GCNA **(**provided by G.C. Enders, University of Kansas, Kansas City, Kansas)**,** Cbl (BD Biosciences, #610442) PCNA (Cell Signalling #2586),

RNA isolation and Sanger sequencing

Total RNA was prepared from ovaries with the Tripure isolation reagent (Roche #93876820) per manufacturer's instructions. To validate the Kit^{D818VL} allele, Exon 17 was amplified by one step RT-PCR (Qiagen #210210) using the primers: AGATTTGGCAGCCAGGAATA(forward) and ATTTCCTTTGACCACGTAATTC (reverse). For validation experiments of the *Kit*$^{-}$ allele, cDNA was synthesized with the M-MuLV Reverse Transcriptase (New England BioLabs #28025-013). Kit cDNA sequences, spanning exons 14 to 18 were amplified by Phusion High-Fidelity DNA Polymerase (New England BioLabs #M0530S). Forward primers close to exon 14 were GAGAAGGAAGCGTGACTC; reverse primers close to exon 18 were AGGAGAAGAGCTCCCAGA. PCR conditions were: 98°C x 3 min; 34 cycles of 98°C x 60 sec, 60°C x 60 sec, 72°C x 120 sec; then 72°C x 5 min. RT-PCR products were analyzed by gel electrophoresis and bands were purified with the QIAquick gel extraction kit (Qiagen #28704). The *KitD818V* mutation or exon 17 deletion were confirmed by Sanger sequencing (UTSW sequencing core).

Toluidine blue staining and Electron microscopy.

Two ovaries per genotype were fixed, embedded in Embed 812 resin (Electron Microscopy Sciences) and prepared for negative staining as described (John et al., 2007). Images

were acquired using a FEI Tecnai G2 Spirit electron microscope. Thin sections were also stained with Toluidine blue and analyzed with light microscope.

Western Blot

Ovaries (two/genotype) were homogenized in RIPA buffer supplemented with Complete Proteinase inhibitor cocktail (Roche) and Phosphatase Inhibitor cocktail 2 (Sigma). Following homogenization, extracts were centrifuged at 10000 rpm for 7 min. Supernatants were collected, mixed with 4x Laemmli Sample Buffer (BioRad) and boiled for 10 min. Equal amounts were loaded in a 10% SDS PAGE and run at 100V. Gel was transferred to Immobilon P membrane (Millipore). The membrane was blotted with 5% dry milk in TBS-T (BB), and probed with 1:1000 dilution of Kit antibody in BB overnight at 4^0C (Cell Signaling, #3074). The membrane was stripped with Restore Stripping Buffer (Thermo Scientific), blotted and probed with 1:5000 α-tubulin in BB for 1hr at room temperature (Sigma, T9026). Blots were developed with SuperSignal West Dura Extended Duration Substrate (Thermo Scientific) and digital images acquired with a ChemiDoc system (BioRad).

FSH and LH analyses

Serum FSH/LH levels were measured by the Ligand Assay Core at the University of Virginia. Serum was diluted 1:10 prior to analysis.

Northern analysis

Total RNA was prepared from adult testes with the Tripure isolation reagent (Roche #93876820) 10 µg RNA was electrophoresed on a 1% formaldehyde gel. RNA, transferred to Hybond N+, probed with *Kit* spanning exon 5 to exon 11(primers used were gccaggagacgctgactatc and ttctgggaaactcccatttg) and reprobed with *Gapdh* as a loading control.

Radiation treatment of live mice

The mice were restrained in acrylic boxes and whole-body radiation was administered in three fractionated doses with two 24 hour intervals (2 Gray) by XRAD 320 irradiator. No specific method was used for randomization of experimental (treated) and control (untreated) animals and the investigators were not blinded.

Statistical analysis

P values and means +/- S.E.M. were calculated by two-tailed unpaired Student's t test with GraphPad Prism 6.

CHAPTER 3

Results

SINGLE CELL RT-QPCR ANALYSIS OF SPERMATOGONIAL STEM CELLS (SSCs)

Introduction

Spermatogenesis generates more than 100,000 sperm in the adult mouse testis per day to maintain male fertility throughout life (Singh et al., 2011). A_{single} spermatogonia, believed to represent or contain the true stem cells that ultimately sustain spermatogenesis, sometimes mitotically divide with incomplete cytokinesis to form $A_{alligned}$ cells (initially a pair of cells known as A_{pair}) With the help of a few well-known spermatogonial markers, such as lin28 or Foxo1, undifferentiated or chained cells of spermatogonia can be visualized by whole mount staining of seminiferous tubules in mice or rats (Abid et al., 2014; Aloisio et al., 2014; Gassei et al., 2014; Nakagawa et al., 2010). However, characteristics of the spermatogonia are poorly understood. Questions such as, what type(s) or subset(s) of spermatogonia are ultimately responsible for self-renewal, quiescence and differentiation to maintain continuous spermatogenesis, and what are the molecular mechanisms regulating spermatogonial self-renewal and maintenance are still being investigated with different methodologies; results and interpretations remain hotly contested, with no consensus as of yet as to the answers to these questions (Kanatsu-Shinohara and Shinohara, 2013).

The A_{single} theory posits that all the A_{single} cells are capable of self-renewing or differentiating into A_{paired} and then more advanced $A_{alligned}$ spermatogonia which then become differentiating spermatogonia that ultimately undergo meiosis to form the mature sperm

(Huckins, 1971). However, more recent studies have suggested that A_{paired}, $A_{aligned}$, or fragmented spermatogonia also have stemness characteristics of self-renewal and regenerating spermatogenesis by multiple, complex, and reversible pathways (Nakagawa et al., 2010). Transplantation, lineage tracing, and immunolabeling experiments in several laboratories have suggested that only a subset of cells in the A_{single} spermatogonia population such as those expressing Pax7, ID4, and Erbb3 are capable of replenishing spermatogenesis, which suggests that A_{single} spermatogonia are more heterogeneous than previously believed and may include both true stem and transit amplifying subsets that remain poorly characterized (Abid et al., 2014; Aloisio et al., 2014; Chan et al., 2014; Sun et al., 2015). However, it is challenging to explore heterogeneity of spermatogonia *in vivo* as only 0.02% to 0.03% percent of cells are reported to be A_{single} and only 12% of the A_{single} population are thought to have stemness characteristics although their molecular markers and guiding mechanisms and gene signatures remain obscure (Kanatsu-Shinohara and Shinohara, 2013; Nagano, 2003).

SSCs can be cultured and enriched at least for two years (and likely indefinitely, as these cells appear to be truly immortal) on top of feeder cells in the presence of glial cell derived neurotrophic factor (GDNF) and other growth factors (Kanatsu-Shinohara et al., 2005; Singh et al., 2011). More importantly, cultured SSCs can reinitiate spermatogenesis when transplanted into the testes of immunocompromised/infertile mice, retain their epigenetic characteristics and are capable of generating offspring (Kanatsu-Shinohara et al., 2005; Oatley et al., 2006). Interestingly, well-known markers of spermatogonia such as promyelocytic leukemia zinc finger protein (PLZF), Foxo1, and GFRα are expressed uniformly in all the cells of the SSC cultures (Aloisio, 2015; Dann et al., 2008; Ryu et al., 2005). However, some specific A_{single} markers, such as Oct4, Pax7, ID4 and Sohlh1 have been shown to be expressed only in a small subset of cells

in SSC cultures suggesting that SSC cultures might have distinctive gene signatures, which may reveal their stemness characteristics (Aloisio, 2015; Chan et al., 2014; Dann et al., 2008). SSCs cultured in different conditions can also have the capacity to acquire pluripotency (i.e they can differentiate into derivatives of three embryonic germ layers *in vitro*) and to generate teratomas when transplanted in immunodeficient mice. (Guan et al., 2006). Therefore, The SSC culture system serves as an important read-out to study stem cell characteristics and cell functionality *in vitro*. As in the testes, it is believed that only a subset of the cells in SSC cultures are true stem cells capable of long-term renewal; however, the fraction of such cells is several orders of magnitude higher than in the adult testis.

Single cell analysis methods can be used to reveal heterogeneity in different cell populations. Single-cell mRNA analysis by the Fluidigm system uses an integrated fluidic circuit to capture 96 individual cells within microcompartments within a special chip, followed by an automated system and experimental workflow to do cDNA synthesis, amplification and QPCR analysis. For example, recent studies revealed molecular signatures and characterized subpopulations of acute myeloid leukemia cells within a transcriptional profile of 175 genes by principal component analysis (PCA) (Saadatpour et al., 2014). There have been numerous studies of various tissues using single cell analysis, which have revealed previously unsuspected molecular subsets of cells expressing particular markers or combinations thereof. PCA is a computational technique for dimensionality reduction, which can identify the subpopulation of cells with the highest degree of variation (i.e. gene signatures analyzed).

In this study, we aimed to understand the heterogeneity in SSC cultures, with the ultimate goal of revealing specific and heretofore unknown cellular subsets, some or one of which would be expected to represent the bona fide stem cell population. Characterization of the specific

genes defining such subsets would in turn lead to insights into the molecular pathways controlling stemness vs. differentiation. For preliminary characterization and PCA, we selected a panel of 96 different genes selected on the basis of being highly expressed in either differentiated spermatogonia (e.g. Kit), or undifferentiated spermatogonia (e.g. Foxo1), genes specifically expressed in germ cells (e.g. Vasa) or which represent pluripotency genes (e.g. lin28, Oct4), cell-cycle related genes (e.g. cyclin D1 (Ccdn1)), house-keeping genes (e.g. GAPDH), oocyte-related genes and MEF specific genes (our feeder layer was MEFs, so this class of genes was selected to permit identification of contaminating MEFs, should this ever occur) to analyze in SSC cultures **(see Chapter 2, methodology for details).** Other genes were selected on the basis of their being believed to be differentially expressed in undiferentiated spermatogonia (i.e. GFRα, Pax8, ID4, and ERBB3); the latter being a particularly important class as they are perhaps the most likely to be discriminant. We hypothesized that PCA analysis conducted with the 96 different gene expression patterns from 96 different cells (the maximum that can be analyzed in a single experiment in the Fluidigm platform) could reveal subpopulations of SSC cultures with discrete mRNA expression patterns that would let us identify some signatures of "undifferentiation" or "differentiation" in this unique culture system to characterize the "stemness identity" of SSC cultures. Additional studies would then be required to determine the significance of these gene expression patterns, or the functional significance of individual factors.

Results

Single cells of SSC cultures are captured with high efficiency by the C1 fluidigm system

The C1-STA integrated fluidic circuit (IFC) chip is designed to capture cells with homogenous sizes (i.e. in the range of 10-17 µm). SSC cultures grow by forming grape-like clumps on top of MEF layers and their average sizes have not been reported elsewhere (**Fig 3.1A**). Here, I optimized the SSC cultures to permit detachment from each other with excellent viability so that they can be captured by the IFC system individually (**Figure 3.1B-C**). The average size of a detached SSC was 10 µm (determined with the Countess system), which permitted us to achieve an outstanding 99% capturing efficiency with the IFC chip designed for 10-17 µm cell sizes (**Fig 3.1C-D**). My results showed that the IFC chip is well-suited for single cell analysis from the SSC cultures. We then proceeded with the cell lysis, and cDNA synthesis, and then proceeded to analyze and characterize single cell expression levels of 96 different genes from the 95 different cells. In order to make sure that the captured cells were SSCs, and not the feeder layer (MEFs), we also included two fibroblast specific genes (Col5a2, Fibroblast specific protein 1 (Fsp1)) in the panel to be analyzed among the 96 genes as well as positive (Hprt, Actinb, GAPDH and a negative control (cre).

Differentially expressed genes in the SSC cultures are identified by single-cell qPCR.

Violin plots, which are mirror histograms, can compare gene expression levels from multiple cells. The Y axis shows the distribution of Log2(Ct) values of gene expression from individual cells. For example, among the 96 genes analyzed, Gapdh is expressed at highest levels (Log2(Ct)>10), while the negative control, cre, is expressed at the lowest levels in every single cell analyzed, as expected (**Fig 3.2A-B**).

Variation of width from the violin graphs represents distribution of gene expression levels among the different cells analyzed such that Gapdh has a much narrower distribution or less variation in terms of gene expression (**Fig 3.2**). However, bimodal distribution of the violin plots indicates that the genes are differentially expressed in at least two distinct subpopulations. Depending on our violin plot analysis, the A_{single} marker Pax7, is differentially expressed in SSC cultures. Interestingly, other potential stem-cell related markers such as Nobox, lim homeobox protein 8 (Lhx8), ATP-binding cassette, sub-family B, member 1BMDR1 (Abcb1b) (also known as Multi-Drug Resistance (MDR1)) are differentially expressed among the SSCs analyzed. Those genes might have novel functions in SSC cultures. Consistently, the genes which are potentially implicated in SSC differentiation, such as Kit, KitL and spermatogenesis and oogenesis specific basic helix-loop-helix (Solhl1) also revealed bimodal distributions (**Fig 3.2A-B**). Our analysis showed that a few genes were differentially expressed in SSC cultures. These differentially expressed genes may be functional in terms of providing stemness characteristics to the SSCs. Additionally, some genes were expressed at higher levels from every single cell analyzed. The expression of Dmrt1 ,2, and 3 in every SSC might suggest novel roles in SSCs and interestingly these genes are also implicated as candidate genes involved in seminomas (Waheeb and Hofmann, 2011).

Principal component analysis (PCA) revealed no distinctive well-defined cellular subtype in the SSC culture cells using the 96 gene panel.

I analyzed the single cell gene expression data from 95 different cells by principal component analysis (PCA) to see if SSCs might be clustered depending on their gene signatures (**Fig.3.3**). The PCA analysis revealed random distribution of 5 cells, which have been

characterized as outliers depending on the aberrant Ct values they have. Depending on our results, 90 cells were clustered together by PCA analysis suggesting that the SSC cultures were not significantly heterogeneous within the 96 genes analyzed **(Fig.3.3)**.

Discussion

Pax7 has been reported to be a marker for a subset of A_{single} spermatogonia by a former graduate student in Castrillon lab (Aloisio et al., 2014). Aloisio's preliminary data also showed that Pax7 is heterogeneously expressed in SSC cultures by immunofluorescence (Aloisio, 2015). Here, I also showed Pax7 mRNA do differ in individual cells within SSC cultures by single cell qPCR. Our results are highly suggestive that Pax7 positive cells in SSC cultures may be a subset of spermatogonial stem cell cultures that may have special renewal capabilities. Additional experiments such as transplantation experiments would be required to explore this possibility. Single cell RNA-sequencing experiments of genetically labeled Pax7 spermatogonia (i.e. fluorescent reporter knockin) could be employed to reveal some other genes controlling stem cell characteristics of spermatogonia *in vitro*. Our results showed that C1 Fluidigm is technically capable of single cell capture and then subject the single cells to a molecular workflow to analyze single cell spermatogonia from cultures.

As a result of our violin plot analysis, we have analyzed and determined differentially expressed genes from SSC cultures. These novel data may provide a basis for single cell analysis of SSC cultures. Recently, Hermann *et al.* showed that THY1 sorted spermatogonia, isolated from six days of mouse testes were heterogeneous by analyzing 172 different genes by the C1 fluidigm system. Considering different types of spermatogonia (i.e A_{single}, A_{paired}, $A_{alligned}$) present

in vivo, their PCA analysis revealed three putative clusters with reportedly 1) stem, 2) progenitor, and 3) differentiating gene signatures. However, they reported that ID4 positive spermatogonia were homogeneous (Hermann et al., 2015). Our analyses of SSC cultures, which may be enriched A_{single} spermatogonia, were also homogeneous among the 96 genes we analyzed. Comparing our data with this study, we opted not to repeat the qPCR experiment since our PCA analysis did not lead us to discover any statistically significant hierarchical clusters which may indicate that the SSC cultures do not have heterogeneous gene signatures. We also considered the possibility that subsets of the 96 gene panel might prove superior in PCA component analysis; however, no subset was identified that proved more effective in PCA analysis. Also discouraging was the fact that while some genes did show some variation (such as Pax7, as discussed above), when two or more genes were analyzed together, there appeared to be no consistent logical pattern; i.e. correlation of Pax7 or Id4 levels, or other genes that may or should be co-expressed or be mutually expressive. All in all, the single cell analysis platform did not prove successful in identifying novel subset of cultured SSCs. It is possible that the artificial conditions of the SSC culture system, which include very high levels of growth factors including GDNF, force the cells in the culture system to adopt a rather monomorphic pattern of differentiation.

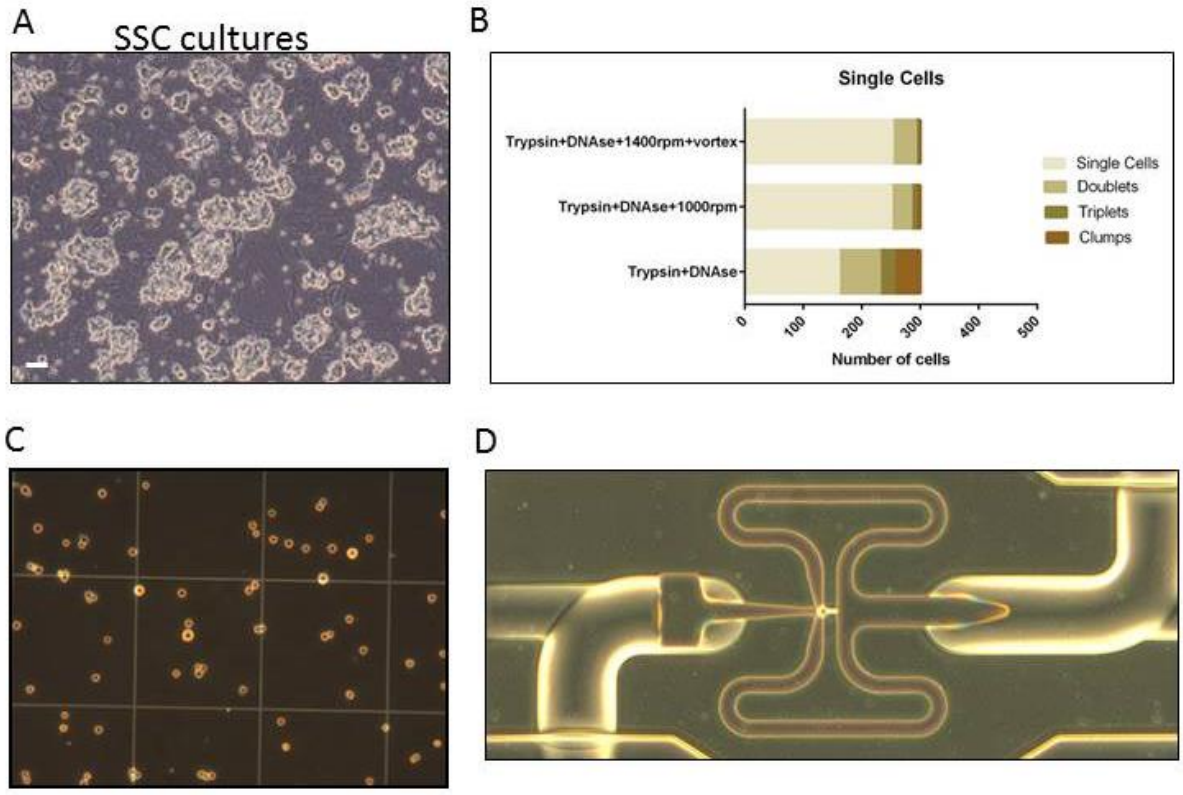

Figure 3.1. SSC cultures have %99 capturing efficiency by the C1-Fluidigm assay: (A) Clump-forming SSC cultures on top of MEF feeder layers. Scale bar is 60µm. **(B)** Quatification of single, double, triplet and clumps from the SSC cultures after different types of treatments. 300 cells are count after different types of treatments. Note that trypsin, DNAse and 10 mins of vortexing with 1400 rmp at 37^0 was the optimal condition to detach the SSCs for capturing by C1-STA integrated fluidic circuit (IFC) chip **(C)** Analysis of the single cell viability before loading into the IFC chip. Detached SSCs were 98% viable. Average cell size of single SSCs was 10µM. **(D)** The chip was analyzed under light microscope to calculate capturing efficiency. The image shows higher magnification of one nest capturing a single cell. 95 nests out of 96 captured a single SSC. Capturing efficiency was 99% percent for SSC cultures under this conditions.

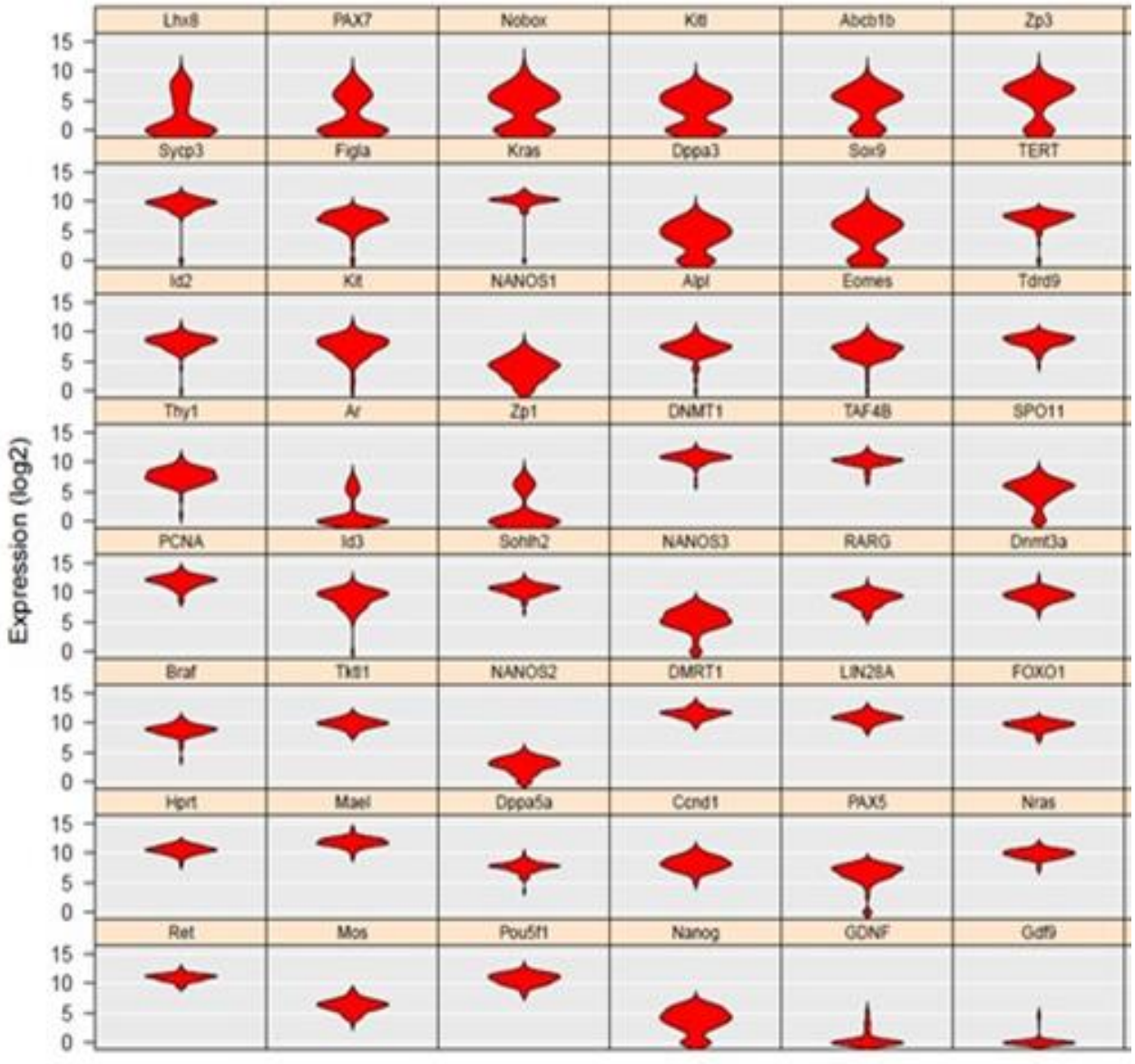

Figure 3.2.A. mRNA abundance patterns of 95 single SSCs are identified by violin plots: Violin plot analysis from 95 SSCs captured. Five cells were excluded from the analysis after outlier identification. The violin plots were generated with SINGuLar Analysis Toolset 2.1 in R. Y axis shows the Log2 transformed Ct values for each gene of interest from single cells. The higher the Log2 transformed Ct values are the higher the expression levels are. The X axis of the violin plot indicates distribution of variation among the 95 cells. Note that the house keeping genes were expressed at high levels (Log2>10) from every cell (Gapdh, Actb and Hprt), while the negative control cre was not expressed in any of the cells.

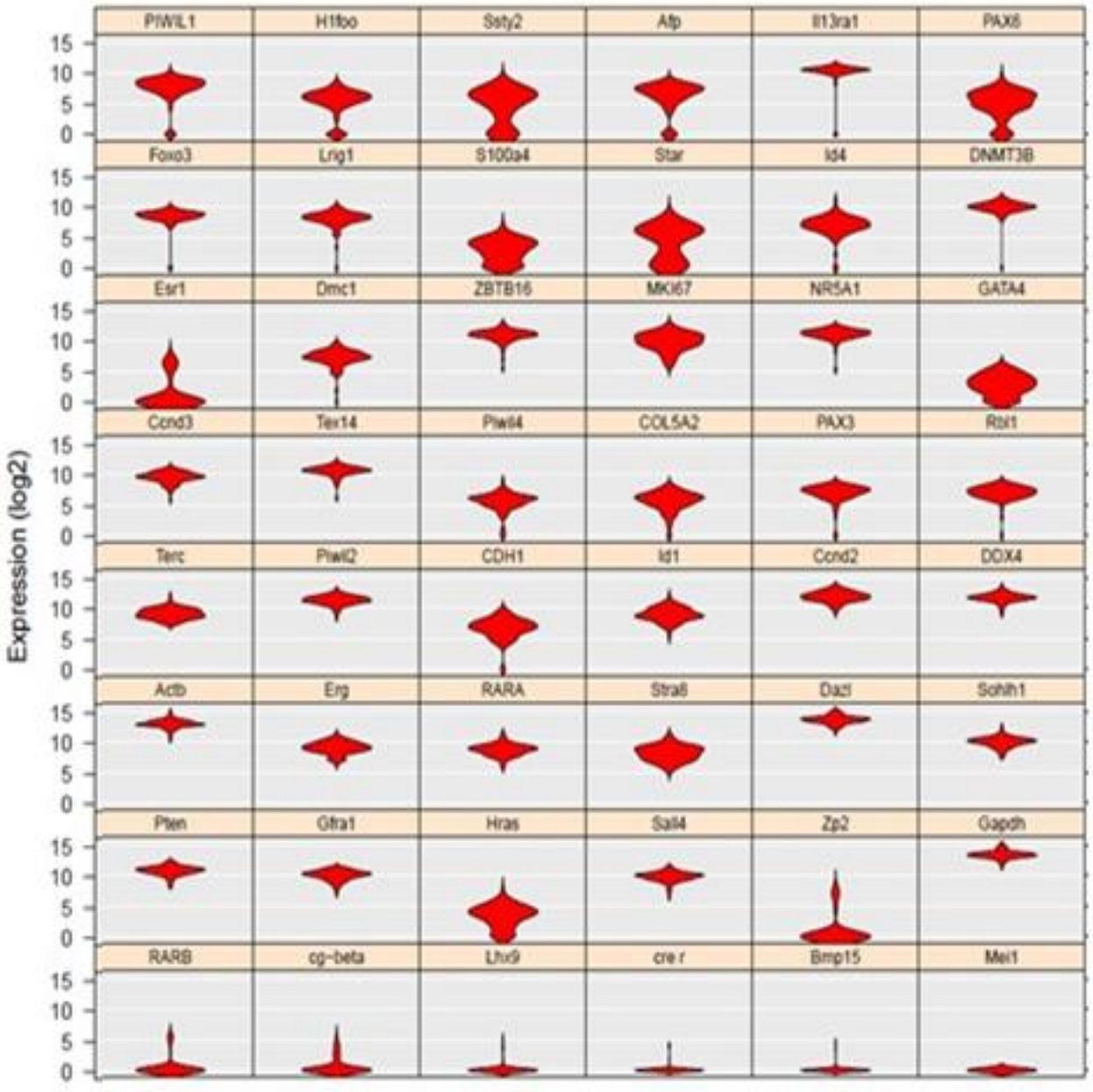

Figure 3.2B. Distinct mRNA abundance patterns of 95 single SSCs are identified by violin plots. (The figure is spitted into two pages for representative purposes, see Figure 3.2A)

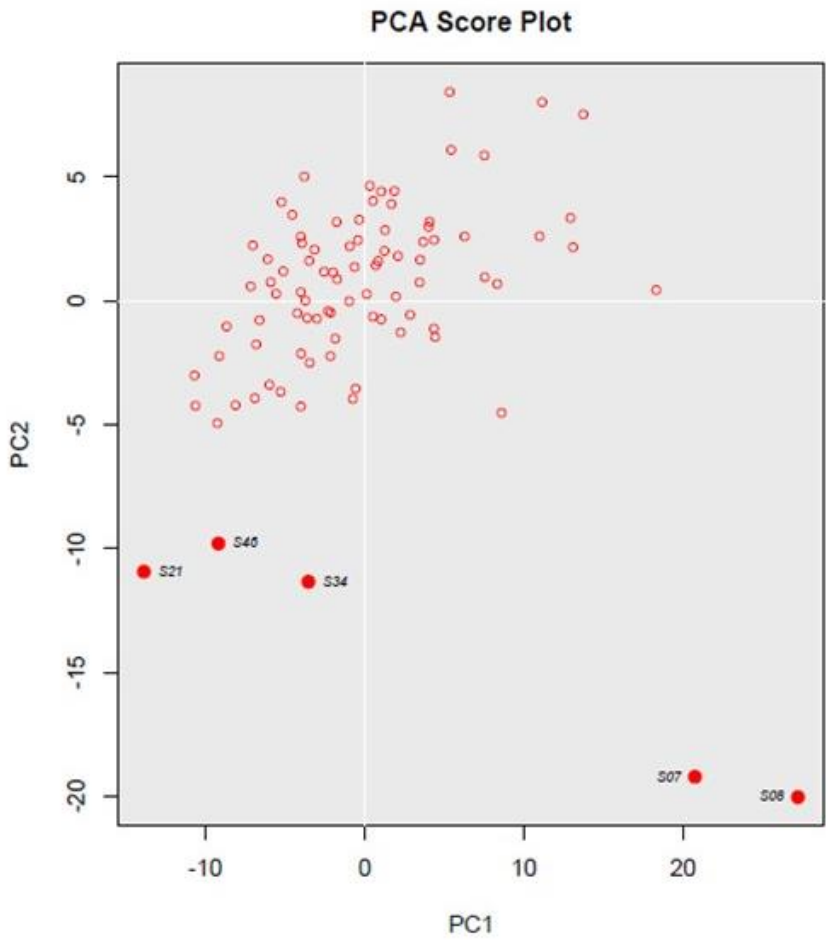

Figure 3.3. Principal Component Analysis (PCA) of SSC cultures revealed no distinctive heterogeneity. PCA was used to compare the similarity of mRNA levels in 96 individual cells. Each individual point is an individual cell. The 5 cells that are located outside of the cluster (red cells) are technical outliers depending on the high or low Ct values they revealed for every 96 gene analyzed.

CHAPTER 4

Results

ROLE OF KIT IN SPERMATOGENESIS

Introduction

Spermatogenesis is a continuous process, where male germ cells are first mitotically amplified to produce high number of primary spermatocytes which then form the mature sperm following meiosis (de Rooij, 2001; Mauduit et al., 1999). The receptor tyrosine kinase Kit (corresponding to the classical murine allele, *Dominant White Spotting* (*W*), is expressed in the mitotically-proliferative spermatogonia that will form the spermatids, while Kit ligand, a.k.a. stem cell factor (SCF) (corresponding to the classical murine allele, *Steel* [*Sl*]), is expressed in sertoli cells (Schrans-Stassen et al., 1999) Among the many other functions of Kit in male germ-cell development, it has been shown that Kit regulates the mitotic proliferation of the spermatogonia at early stages of spermatogenesis, where Kit is highly expressed (Ohta et al., 2000). Understanding the molecular details underlying this transit-amplifying stage of spermatogenesis is important as continuous spermatogenesis depends on this unique population.

Seminomas, germ cell tumors of the testes, are the most common malignancies affecting male adults from age 35 to 45 (Browne et al., 2005). Main characteristics of seminomas are high expression levels of specific markers such as alkaline phosphatase, Oct4 and Kit (Browne et al., 2005). Kit is the most commonly mutated gene in seminomas and it is highly expressed by 77-100% of the primary tumors (Cardoso et al., 2014; Kemmer et al., 2004; Nikolaou et al., 2007). Loss of function mutations in the human loci corresponding SCF/Kit system have been linked to infertility, while over-activation mutations have been linked to seminomas and teratomas (Cardoso et al., 2014). Considering the diverse functions of Kit in the proliferation, differentiation and survival of normal spermatogonia, it has been suggested that malignant

transformation of Kit-positive spermatogonia subpopulation may play a role in development of seminomas (Cardoso et al., 2014; Mauduit et al., 1999). Therefore, studying the biology of transit amplifying germ cells is also important to understand the etiology of seminomas.

Many studies have been conducted to understand the role of Kit in spermatogenesis, however, my study described below is the first to generate and analyze germ-cell specific mouse models of Kit alleles. Considering the role of Kit in many other crucial cell types such as hematopoietic stem cells and melanocytes, generating conditional mouse models was necessary to study the role of Kit in germ cell biology.

Results

Generation and validation of the conditional dominant gain-of-function allele Kit$^{D818V(L)}$

We generated a novel murine conditional allele, *Kit$^{D818V(L)}$*. to study the role of Kit in germ cell tumors. The Kit D818V (Asp→Val) amino acid substitution leads to constitutive Kit activity in the absence of ligand (KL), and exerts potent dominant gain-of-function effects (Chian et al., 2001; Lennartsson and Ronnstrand, 2012). Furthermore, it is the most common known *Kit* gain-of-function mutation in human germ cell tumors (Chian et al., 2001; Kemmer et al., 2004; Wang et al., 2014). The conditional (floxed) *Kit$^{D818V(L)}$* allele was designed to provide Kit function through a 3' cDNA cassette encoding exons 17-21. Cre-mediated recombination excises this cDNA cassette, permitting normal splicing of an exon 17 harboring the mutation, and thus expression of mutant D818V protein **(Fig.4.1)**. With respect to nomenclature for the four new *Kit* alleles described in this chapter, 1) genotypes signify somatic genotypes (per tail DNA genotyping) and 2) the floxed (i.e. latent) alleles end in "(*L*)". Whereas hemizygous *Kit* (a.k.a. *Dominant white spotting*) loss-of-function mutations produce abnormal coat pigmentation (Besmer et al., 1993) (see also below), mice harboring the *Kit $^{D818V(L)}$* allele were externally

normal with coat pigmentation similar to sibling controls, confirming that the floxed allele indeed provided Kit function **(Fig 4.2A)**. The *Kit* $^{D818V(L)}$ allele could be homozygosed, and such animals were also externally indistinguishable from littermate controls **(Fig. 4.2B).**

Constitutive Kit activation in transit-amplifying spermatogonia does not affect spermatogenesis

These mice were then bred to the germ cell-specific Cre driver, *Vasa-Cre* (a.k.a. *Ddx4-cre*$^{1Dcas/J}$) (abbreviated *VC*) to generate *VC*; *Kit*$^{D818V(L)}$/+ females. *VC* becomes active during late embryogenesis, around E15.5, and efficiently drives Cre-mediated recombination in all male and female germ cells (Gallardo et al., 2007a). Tail genotying and northern analysis from adult testes confirmed the presence of the floxed allele in the murine genome, and its stoichiometric expression was confirmed from cDNA and RNA levels **(Fig.4.2B and Fig.4.2D)**. To further validate the expression of the expected point mutation, testes and ovarian cDNAs were analyzed by RT-PCR, followed by Sanger sequencing. As expected, both testes and ovaries from experimental mice expressed mutant cDNA at levels close to wild-type as evidenced by electrophoretogram peaks, with the somewhat lower mutant allele peak intensities readily accounted by *Kit* expression from WT and somatic cells **(Fig.4.2E)**.

At 3 weeks of age the mutant testes sizes were about the same size as their sibling controls **(Fig.4.3A)**. To study whether Kit hyperactivity might lead to a phenotype in spermatogenesis or malignant transformation, I analyzed 3 different males from control and experimental siblings at a later time point, 16 weeks. To our surprise, the testes sizes and weights were not significantly different at 16 weeks (n=6 ; p=0.5134) **(Fig.4.3A)**. Histological analysis of

the testes and the epididymis sections also confirmed that the experimental males had normal spermatogenesis and normal testis histology; i.e. seminiferous tubules were of normal size and shape with robust spermatogenesis **(Fig.4.3B).** Kit immunohistochemistry confirmed the cell surface expression of Kit protein in the transit amplifying cells albeit at low levels **(Fig.4.3C).** Kit overexpression was not observed in the testes as a result of D818V mutation, suggesting that the mutant protein is being internalized. Kit activating mutations on exon 17 have been reported to affect the cellular localization of the protein from the plasma membrane in mast cells (Obata et al., 2014) . Downregulation of Kit in testicular germ cells might possibly explain the lack of phenotype in the mutant and suggest presence of a negative feed-back mechanism regulating constitutive Kit-hyperactivity. To analyze the effect of Kit hyperactivity on undifferentiated spermatogonia, we checked Foxo1 expression from experimental and control males by immunohistochemistry **(Fig. 4.3D).** Foxo1 is a marker for spermatogonia, which is controlled by the PI3K-Akt pathway and is predominantly nuclear (active) in adult testes, as shown by a previous graduate student in the Castrillon laboratory, Meredith Goertz (Goertz et al., 2011). Foxo1 labels the undifferentiated spermatogonia, while Kit labels the differentiated spermatogonia. Both the number of undifferentiated spermatogonia by Foxo1 counts, and the predominantly nuclear localization of Foxo1 were very similar to sibling controls in *VC; $Kit^{D818(V)L/+}$* males suggesting that Kit-hyperactivity was not affecting undifferentiated spermatogonia biology ($p=0.918$, $n=30$ tubules, for Foxo1 counts) **(Fig. 4.3D).** We also checked the Sertoli cell and germ cell histology from the experimental and control siblings by Gata1 (Sertoli cell marker) and GCNA (general germ cell nuclear antigen) immunostainings **(Fig. 4.4).** Location and the number of sertoli cells and germ cells were essentially identical in control and experimental testes. Proliferation markers such as Ki67 and proliferating cell nuclear antigen

(PCNA) also were not altered with in KitD818V males, which led us to conclude that D818V mutation do not affect germ cell proliferation in adult males. Lack of Akt hyper-phosphorylation in the experimental males with no distinctive effect on spermatogenesis also suggested the presence of a negative feedback loop controlling constitutive Kit hyperactivity in males **(Fig. 4.4)**. Degradation of Kit by a specific ubiquitin ligase, Cbl, has been reported in other systems (Zeng et al., 2005). We also checked whether Cbl is expressed in the experimental Kit-positive cells. Cbl is expressed in Kit-positive spermatogonia and its function remains to be elucidated but its expression on the undifferentiated spermatogonia might explain the lack of phenotype seen in males **(Fig. 4.4)**. For example, SCF stimulation induces phospohorylation of Cbl proteins, which in turn acts as E3 ligases to degragate Kit by ubiqutionation in mast cells (Zeng et al., 2005) Interestingly, in rats, Cbl deficient males have been reported to have fertility defects due to a disruption in germ cell organization in differentiated germ cells (i.e post meiotic cells) (El Chami et al., 2005). Considering the cytoplasmic localization of the mutant Kit protein in mouse spermatogonia, it is highly probable that constitutive Kit hyperactivity would phospohorylate Cbl proteins and would lead to its degradation as a negative feedback mechanism. Further experiments such as ubiqutionation and assays; analysis of Cbl and phosphorylated Cbl proteins; co-localisation experiments of Cbl and Kit in different timepoints and conditions are required to make a definitive conclusion of our results about Kit downregulation.

KitD818V mutation is embryonic lethal in the hemizygous state and hyperactive Kit might cause defective germ-cell migration in males

VC;Kit$^{D818V(L)/+}$ males had normal spermatogenesis and they were fertile, despite carrying the most common oncogenic mutation present in seminomas (the most potent gain-of-function activating Kit mutation known) in their germline **(Fig.4.3 and 4)**. When the *VC;Kit*$^{D818V(L)/+}$ males were bred to WT females, they transmitted the knock-in D818V mutation to half of their progeny in a Mendelian fashion as expected, demonstrating that the mutant allele did not affect spermatogenesis or result in a meiotic drive phenotype **(Fig.4.5A**) (Buckler et al., 1999) The mutant progeny would express hyperactive Kit from one allele in all the cells in their body. The nomenclature for whole body knock-in Kit mutation is *Kit*$^{D818V/+}$ as the floxed allele was not transmitted to the mutant embryos due to the action of *Vasa-Cre* in the germline. *D818V* mutations were embryonic lethal **(Fig.4.5A).** Considering the role of Kit in development of other cell types, such as hematopoietic stem cells, mast cells, interstitial cells of Cajal, this embryonic lethality phenotype was perhaps not surprising. The embryos were dead at E13.5 but they remained viable at E12.5 albeit with dilated blood vessels evident externally **(Fig.4.4B).** *Kit*$^{D818V/+}$ embryos had necrotic livers and abnormal white-blood cell clusters in their dilated blood vessels at E13.5, which was observed in their skin and placenta **(Fig.4.5D).**

In order to study the effect of Kit hyperactivity in germ cell migration and malignant transformation, I conducted embryonic dissections to analyze the germ cell migration pattern from Kit-hyperactive males at E12.5 **(Fig.4.5B and 4.5C)**. The germ cell migration from precursors in the embryonic yolk sac to the developing gonad is completed at around E10.5, and any aberrant or excessive germ cell proliferation due to a defect in germ cell migration would be predicted to be detectable at E12.5. To our surprise, germ cells were migrated to the cords

normally despite expressoin of a constituvely-active allele of Kit; however, some of the mutant germ cells appeared to be larger and exhibited different chromatin patterns seen from the hematoxylin and eosin-stained tissue sections **(Fig.4.5C)**. To further analyze the germ cells in the mutant embryos, I then stained sagittal embryonal sections with a germ cell marker, Sall4 **(Fig.4.6A)**. Sall4 is a germ cell marker for every stage of spermatogonia, including primordial germ cells. The mutant germ cells were normally Sall4 positive and the germ cell numbers were significantly less in the mutant cords compared to WT sibling controls ($n \geq 2$ per embryo; $p \leq 0.0001$) **(Fig.4.6A).** Whole embryonal sagittal-sections, stained with Sall4, were also analyzed for possible germ cell migration defects or possible-presence of hyper-proliferative germ cell clusters in the whole-body. No abnormal germ-cell clusters were found in the embryos by Sall4 staining and the germ cells in the cords were not hyperproliferative depending on the cell counts in the experimental gonads **(Fig.4.6A).**

Kit might be down-regulated in D818V embryos

Analysis of Kit immunohistochemistry showed that Kit protein appeared to be down-regulated and exhibited a cytoplasmic staining-pattern unlike the membrane-bound staining-pattern in the control embryonic testes **(Fig.4.6B)**. The observed cytoplasmic and patchy staining pattern of Kit in the mutant germ cells might be explained through a negative feedback loop mechanism degrading Kit, such as a specific ubiquitin-ligase, possibly Cbl, as reviewed earlier. Additionally, Foxo1, which is inactivated and exported to cytoplasm by Akt-pathway and co-expressed with Kit during embryonal-development in male germ-cells, was predominantly nuclear in the experimental embryos **(Fig.4.6B)** ($n \geq 2$ per embryo; $p = 0.0023$). These data

support the idea of Kit down-regulation controlling nuclear localization of Foxo1 by PI3K-Akt pathway, which might explain the lack of phenotype seen in experimental embryos.

Blimp-1-cre; Kit $^{D818V(L)/+}$ mice are embryonic lethal

Vasa-cre is active in all germ cells starting from E15.5. Thus, our *VC;Kit*$^{D818V(L)/+}$ mouse model has normal Kit expression during germ-cell migration. Considering the unexpected germ-cell migration and embryonic lethality phenotype seen in whole-body knock-in embryos at E12.5 **(Fig.4.5 and Fig.4.6)**, I decided to generate a mouse model of germ-cell specific Kit hyperactivity which might let us to study Kit hyperactivity during germ-cell migration. I thus bred the *Kit*$^{D818V(L)/+}$ females with *Blimp1-cre (BC)* males; *Blimp1* is expressed in germ cells as early as day 7.5 and it is active in 62% of germ cells (Ohinata et al., 2005) **(Fig 4.6A)**. However, *BC;Kit*$^{D818V(L)/+}$ embryos were also embryonic lethal. The embryos were viable up to E18.5 with larger livers and dilated blood vessels clearly visible in their limbs and placentas **(Fig 4.6B)**. The embryonic lethality must be due to Blimp1 expression in other cells types such as hematopoietic stem cells **(Fig.4.6B)**. For example, Blimp1 has been shown to be expressed in B cell and macrophage progenitors (Chang et al., 2002). Abnormal white blood cell clusters in *BC; Kit*$^{D818V/(L)/+}$ embryos were very similar to the phenotype observed in whole-body knock-in embryos at E12.5 instead of E18.5. As a result of this data, *BC; Kit*$^{D818V/(L)/+}$ was unfortunately not a good model for us to track germ-cell development as it was embryonic lethal due to a hematopoietic defect **(Fig.4.6)**.

Some of the VC;Kit$^{D818V(L)/+}$ males get Kit overexpressing tumors by one year of age

In order to see if aging would affect malignant transformation of germ cells in *VC;Kit$^{D818V(L)/+}$* males, we aged the experimental males and sibling controls up to 1 year. To our surprise, the germ-cell specific oncogenic mutation did not affect spermatogenesis at one year of age **(Fig.4.7C, Fig. 4.7D)**. Experimental testes weights were very similar to their sibling controls and experimental males also had normal spermatogenesis compared to WT siblings as determined by histological analysis **(Fig. 4.7C)**. However, two of five the *VC; Kit$^{D818V(L)/+}$* males had kitexpressining non-germ cell related tumors (i.e. in parts of the body other than the testis) **(Fig.4.7A, B, C).** One mouse had soft-tissue like tumors all over the abdominal cavity as well as on the diaphragm **(Fig.4.7A).** The other one year old *VC;Kit$^{D818V/L}$* male had a mass on his elbow and a separate mass visible on his spleen **(Fig.4.7B)**. These tumor cells were also Kit positive and had non-germ-cell origin **(Fig 4.7C).** Although the tumors were not fully worked up, the histological analyses were consistent with mastocytomas (i.e. malignant tumors of mast cell origin). This finding is consistent with the fact that 1) the KitD816V mutation is the most common mutation in human mastocytomas, and 2) normal mast cells and human mastocytomas express very high levels of Kit (Zhao et al., 2007)We speculate that very low levels of expression of Vasa-Cre in mast cells, or perhaps non-Cre mediated recombination occuring at very low levels rationalizes the occurrence of these tumors with long latency.

A radiation dosing regimen does not lead to malignant transformation of germ cells from VC; KitD818V(L)/+ males but does lead to lymphomas in control as well as experimental animals.

In all likelihood, the absence of malignant germ cell tumors in *VC; Kit*$^{D818V(L)/+}$ can be accounted for the need for multiple genetic "hits"; i.e. cooperating genetic mutations inactiviating multiple cell growth pathways (Hanahan and Weinberg, 2000; Parada et al., 1984) In order to test if DNA-damage induced by high-energy radiation might cause any second-hit mutations that can promote malignant transformation of *VC; Kit*$^{D818V(L)/+}$ male germ cells, a cohort of control and experimental adult males were exposed to whole-body irradiation **(Fig.4.8A).** It has been shown that radiation kills the transit amplifying Kit positive cells in testes, however, those transit amplifying germ-cells are capable of regenerating themselves as a rare population in spermatogonial stem cells are resistant to radiation (Aloisio et al., 2014; van der Meer et al., 1993). The dose and the fractionation of radiation were determined so that the highest mutation rate which can still lead to recovery of Kit positive germ-cells would still be possible (Aloisio et al., 2014; van der Meer et al., 1993). The fractionation interval was set as 24 hours such that the administration interval would be long enough to cause the most number of mutations, with a low dose, (2 Gray, fractionated in two doses) **(Fig.4.9A)**. Two *WT*, 1 *+/D818V(L),* and 2 *VC; D818V(L)* males died during the 6-month interval after radiation. Autopsy did not reveal any abnormalities in the testes sizes but these mice had larger spleens with tumors consistent with disseminated lymphomas (data not shown) independent of the genotypes. Other mice were then sacrificed; testes histology and weights were analyzed 6-8 months after the irradiation experiment **(Fig.4.9A).** The testes of *VC;Kit*$^{D818V(L)/+}$ mice were

significantly smaller compared to sibling controls after radiation ($n \geq 14$ per testes; $n \geq 7$ per genotype; $p<0.0001$) **(Fig. 4.9B)**. H&E analysis showed that some of the transit amplifying cells were depleted in a few tubules in the experimental males **(Fig. 4.9C)**. This effect might be due to a DNA-damage response mechanism or a defect in germ-cell recovery in *VC;Kit*$^{D818V(L)/+}$ males, however spermatogenesis was normal and there was no sign of malignant transformation in the experimental testes after radiation **(Fig. 4.9B and C).** This result showed us that radiation with the dosing regimen we used was not sufficient to generate a second hit in *VC;Kit*$^{D818V(L)/+}$ males. The mutation frequencies may not be sufficiently high to give rise to malignant germ cell tumors; also, the relatively short lifespan of mice might limit the opportunities for tumorigenesis.

Generation and validation of conditional floxed allele Kit^{L}

To expand upon our genetic analyses of *Kit* in malignant transformation of germ cells, we designed a new allele where exon 17, which encodes the kinase domain (Lennartsson and Ronnstrand, 2012), was floxed **(Fig.4.10)**. *Kit* is an essential locus due to its requirement for hematopoiesis, necessitating conditional genetic analysis. For germ cell specific *Kit* inactivation, *VC*;*Kit* $^{L/+}$ fathers were bred to *Kit* ^{L}*/Kit* ^{L} females **(Fig.4.11A).** *VC* activity in the father's germline converts any paternally transmitted *Kit* ^{L} allele to *Kit* $^{-}$ and thus, *VC* fathers can transmit a wild-type (*Kit* $^{+}$) or null *Kit* $^{-}$allele but not a *Kit* ^{L} allele (Gallardo et al., 2007a). The floxed allele *Kit* ^{L} could be homozygosed, and *Kit* ^{L}*/Kit* ^{L} animals were born at expected Mendelian ratios **(Fig.4.12B)**. Experimental females of the *VC*; *Kit* $^{L/-}$ genotype (per tail DNA) thus harbor homozygous *Kit* $^{-}$ loss-of-function mutations in their germline. RT-PCR of ovaries **(Fig.4.11C)** and Sanger sequencing of cDNAs **(Fig.4.11D)** confirmed *VC*-dependent deletion of exon 17. Whereas control mice harboring the floxed allele exhibited no pigmentation or other external

abnormalities, *VC*; *Kit* $^{L/-}$ mice showed striking midline hypopigmentation, consistent with hemizygous somatic loss of Kit activity **(Fig.4.11E).**

Kit inactivation leads to infertility due to a defect in transit amplifying spermatogonia

It has been earlier reported that Kit plays a role in early stages of spermatogenesis (Schrans-Stassen et al., 1999). We analyzed the testes from Kit$^{+/L}$ and VC; *Kit*$^{+/L}$ testes at 6 weeks of age. The testes of the experimental male were significantly smaller (n=2 testes per genotype, $p<0.0001$) **(Fig. 4.12A).** H&E analysis of the epididymis showed that the experimental males had no epididymal sperm **(Fig.4.12C)**. Histology of the testes showed that the lack of sperm phenotype was due to lack of the transit amplifying spermatogonia (Kit positive spermatogonia) **(Fig. 4.12B and D).** Immunohistochemistry confirmed that Kit expression in the leydig cells were normal; however, germ cells no longer contained a subpopulation of Kit positive spermatogonia **(Fig. 4.12D).** Tissue sections were then stained with Foxo1, a marker for the undifferentiated spermatogonia (Goertz et al., 2011). The overall number of Foxo1 positive cells per tubule was very similar among experimental and control mice, confirming that undifferentiated (Kit-negative) spermatogonia were still present in the Kit inactivated testes **(Fig.4.12D)**. These data are consistent with extensive prior data including previous genetic studies demonstrating that Kit is essential for meiosis and for the formation of Kit-positive differentiating spermatogonia (Schrans-Stassen et al., 1999).

VC; KitD818V$^{(L)/-}$ do not have a malignant phenotype but do have a severe defect in spermatogenesis

To analyze the role of Kit hyperactivity in malignant transformation of germ cells, we generated experimental males harboring the Kit hyperactivity mutation *(D818V)* from one allele, and Kit inactivity mutation from the other allele *(L)* in a germ-cell specific manner (**Fig.4.13A).** These mice differ from those previously described above in that they contain only the hyperactive form of Kit; the other allele is null. This experiment was of interest because in the previous experiments, residual normal Kit protein could serve to dampen any biological effects, and consequently, any biological phenotypes. Dominant Kit hyperactivity in the absence of normal Kit activity from a wild-type allele would therefore allow us to study the impact of Kit hyperactivation in spermatogenesis. We analyzed the experimental and control males at 6, 16 and 32 weeks. To our surprise, *Kit $^{-/D818V(L)}$* and *VC; Kit$^{-/D818V(L)}$* testes were significantly smaller than sibling controls at all the time-points analyzed **(Fig.4.12B)**. *VC;Kit$^{-/D818V(L)}$* testes were larger compared to *Kit $^{-/D818V(L)}$* testes and intratubular hyperplasia was seen in some of the experimental tubules at 16 weeks of age **(Fig.4.12C)**. The experimental germ cells were positive in Ki67 and the germ cell marker Vasa but negative for Kit and Sall4 suggesting that the surviving population was transit amplifying germ cells but surprisingly, they were Kit negative at 16 weeks of age **(Fig.4.12D).** Additionally, the surviving transit-amplifying germ cells of the experimental testes disappeared at later time points (16 weeks and 32 weeks) **(Fig.4.12E)** suggesting that Kit hyperactivity from one allele was not affecting malignant transformation or Kit overexpression of the germ cells **(Fig.4.12D and E)**.

KitD818V(L) homozygous males are infertile and they may harbor non-germ cell related tumors at later ages

Due to our allele design and the need for a targeting construct less than 20 kb (the upper range of bacterial plasmid size), the *D818V(L)* allele harbor a shorter 3'UTR; furthermore, the UTR used was the human sequence (to eliminate the possibility of homologous recombination during targeting, which would have led to undesired rearrangements). While the heterozygous males were completely normal in spermatogenesis, the homozygous males were infertile. The testes were significantly smaller and the males lack no epididymal sperm at 6 weeks of age **(Fig 4.14A).** Kit positive, transit-amplifying germ cells were depleted due to homozygous $Kit^{D818V(L)}$ allele **(Fig.4.14B).** Very similar to the Kit inactivation phenotype, undifferentiated spermatogonia counts were not significantly different compared to sibling controls **(Fig 4.14B)**. As the effect of the shorter 3' UTR was not cell specific but global, the homozygous *KitD818V(L)* mice form random tumors (or masses) by one years of age, some of the mice had loss of hair on their head at random ages (**Fig 4.14C**, data not shown). H&E analysis of the masses showed that the tumors were not carcinoma or sarcoma, however, the aberrant masses were resembling macrophages or B cells **(Fig.4.14D).** One of the experimental testes was hemorrhagic at one years of age **(Fig.4.14D).** The testes were vascular and it was dilated with blood vessels but the phenotype was due the spermatogenesis defect phenotype seen in earlier ages, no sign of malignant transformation was observed in the homozygous KitD818V(L) testes at one years of age **(Fig.4.14D).**

Discussion

Our aim was to develop a mouse model of seminoma by recapitulating the most common oncogenic mutation seen in human seminomas. Considering the role of Kit in normal spermatogenesis and previous data from diverse sources, it was seemed highly likely that dominant gain-of-function Kit hyperactivity; i.e. of such a vital germ cell factor controlling crucial germ cell growth pathways would lead to a defect in normal spermatogenesis and malignant transformation, or at least a premalignant lesion such as intratubular germ cell neoplasia (ITGCN), REF seminoma reviews. Our study showed that D818V mutation was not sufficient to drive malignant transformation in murine germ cells. Carcinogenesis typically requires at least two hits: Class I mutations in oncogenes typically RTKs; and Class II mutations in tumor suppressor genes, typically controlling cell cycle control (Hanahan and Weinberg, 2000; Knudson, 1971)**.** Lack of malignant transformation in germ-cell specific D818V mice was perhaps not a surprising result given this need for multiple hits. A second mutation (or more mutations) may be re required to generate a mouse model for seminomas in our system. On the other hand, one might have expected such hits to arise spontaneously with low frequency, resulting in germ cell cancers of precancers in at least some animals.

Radiation exposure has been well characterized as a mutagen leading to carcinogenesis as a result of DNA damage. Mouse models of myeloid leukemia or thymic lymphoma have been generated with ionizing radiation experiments (Rivina and Schiestl, 2013). Furthermore, chemical mutagenesis or radiation has been a common strategy to induce tumors in otherwise normal or tumor-prone mice, such as genetically-engineered mouse models. The aim of our radiation experiment was to generate a second hit mutation that would lead to the malignant transformation of germ cells. If germ cell tumors had arisen, then our plan was to perform studies

such as whole-genome sequencing to identify the responsible second hits. To our surprise, however *VC;Kit*$^{D818V(L)/+}$ males had normal spermatogenesis and normal testes histology 6 months after ionizing radiation. This result might be explained by the unique characteristics of germ cells. Indeed, low dose of radiation is sufficient to arrest spermatogenesis by killing mitotically active spermatogonia, which are reported to be Kit positive (Aloisio et al., 2014; van der Meer et al., 1993). Surviving spermatogonial stem cells that can regenerate spermatogenesis after radiation damage, might be over-protected against DNA damage. Interestingly, radiation exposed testes were smaller in D818V males. This phenotype might be due to 1) dying of the mutated cells as a result of a protection mechanism 2) a defect in recovery of spermatogenesis as a result of Kit down-regulation. Possible downregulation of Kit due to Kit hyperactivity may also be affecting entry to the meiosis, therefore the efficiency of recovery in the mutant males. The possible scenarios require further experiments to make any conclusions.

ENU, an alkylating reagent, has been well characterized as a powerful mutagen in the germline as it induces random point mutations (Cheon and Orsulic, 2011). It has been used as a powerful reagent to characterize and study specific point mutations, and generate mouse models of cancer (Cheon and Orsulic, 2011). Considering the lack of phenotype result with DNA damage in *VC;Kit*$^{D818V(L)/+}$ males, ENU mutagenesis might be a powerful tool to generate and characterize other mutations to study the malignant transformation of germ cells. Also, other potential candidate genes, which have been reported to be mutually exclusive with Kit mutations, such as p53 or Cbl can be analyzed and used to generate a double mutant mouse models to further characterize Kit mutations in germ-cell tumors (Wang et al., 2014).

That *VC;Kit*$^{D818V(L)/+}$ males had normal spermatogenesis and were fertile was an unexpected result in our research. Considering the essential role of Kit in germ cell proliferation,

we would have expected to see a defect in undifferentiated spermatogonia in response to Kit hyperactivity. However, this negative result led us to generate whole body D818V mutated progeny and potentially study its effect on other cell types. Our results showed that D818V mutation is embryonic lethal due to a defect in the hematopoietic system. Surprisingly, *BC;Kit*$^{D818V(L)/+}$ embryos were also embryonic lethal due to a similar phenotype, dilated blood vessels and aberrant white blood cell clusters. In addition to germ cell development, Blimp-1 has also been shown to be expressed and regulate B cell and macrophage development (Chang et al., 2002). Absence of Kit signaling has been reported not to affect fetal B cell development, and that was the reason we thought we might be able to generate *Blimp1-cre;Kit*$^{D818V(L)/+}$ mice and track the role of Kit-hyperactivity in germ cell migration (Takeda et al., 1997). However, the mice were embryonic lethal and thus did not prove a good experimental system for us to study germ cell migration. Our results showed that constitutive Kit activity might be leading to early differentiation of B cells and affecting their proliferation. The abnormal white blood cell clusters were Kit and Ki67 positive (data not shown). Analysis of early B cell markers such as Cd19 and Cd20 is required to make further conclusions about the embryonic lethal phenotype in *BC;Kit*$^{D818V(L)/+}$ mice. However, our preliminary results are suggestive that our *D818V(L)* mouse model would be novel and useful to study the role of Kit-hyperactivity in hematopoietic development.

Activation of Kit through gain of function mutations are well characterized in mastocytosis/acute myeloid leukemia, seminomas and gastrointestinal tumors (Miettinen and Lasota, 2005) Some of the *VC;Kit*$^{D818V(L)}$ mice formed Kit overexpressing tumors potentially resembling mast cell tumors at later ages. Considering the specific abundance of D816V mutation (D818V in mice) in mast cell tumors and its high association with mast cell disorders,

our data is highly suggestive that *Vasa* leakage from a few mast cells may be the cause of the Kit-amplifying tumors seen in *VC;Kit*$^{D818V(L)}$ males (Jara-Acevedo et al., 2015; Zhao et al., 2007). D818V mutation in a few or perhaps even just one mast cell may be sufficient to derive mast cell hyperplasia and neoplasia. Our results need further confirmation with characterization of the tumors we observed such as mast cell tryptase or CD117 immunostaining, or by flow cytometric analysis. (Zhao et al., 2007). However, *Kit*$^{D818V(L)}$ allele might be an important model to study malignant transformation of mast cells as even one mutation might potentially be sufficient to derive mast cell abnormalities.

The Kit gene in both mouse and human has a very long 3'UTR structure, which is highly suggestive that its translation might be controlled by many different mechanisms. The 3'UTR of a gene has many regulatory functions such as mRNA translation, protein stability and export. miRNAs are regulatory elements that can degrade mRNAs by binding to specific complementary sites on the gene's 3'UTR. Based on bioinformatics predictions, 12 different miRNAs have been suggested to bind to the 3'UTR of Kit (Igoucheva and Alexeev, 2009)**.** Among those, mir221/222 has been reported to directly interact with Kit 3'UTR in melanoma cell lines (Igoucheva and Alexeev, 2009). Yang et al. showed the restricted expression of miR-221/222 in mouse spermatogonia and they reported that miR-221/222 represses Kit mRNA stability and protein translation in spermatogonia cultures (Yang et al., 2013). The novel floxed Kit allele we generated has a shorter 3'UTR due to its specific design. Heterozygous males had normal spermatogenesis; however, homozygous fluxed males were infertile with a novel phenotype. Germ-cells in *Kit*$^{D818V(L)/D818V(L)}$ males maintained their undifferentiated state but did not differentiate. The males are infertile due to lack of mature sperm. Interestingly, Leydig cells in *Kit*$^{D818V(L)/D818V(L)}$ males overexpress Kit. This is an important finding as previous data shows that

Kit signaling plays a role in driving the differentiated state of spermatogonia (Schrans-Stassen et al., 1999; Yang et al., 2013). However, Kit-positive, undifferentiated spermatogonia were not present in $Kit^{D818V(L)/D818V(L)}$ males. This might be explained by 1) overexpression of Kit due to lack of functional miRNAs; its toxicity to the differentiating spermatogonia, therefore causing a differentiation arrest phenotype, which is very similar to Kit deficiency phenotype. 2) overexpression of Kit in Leydig cells interfering with the function of Kit ligand, therefore causing inactivation of Kit signaling.

We aimed to understand the effect of Kit hyperactivity on male germ cells by generating a trans-heterozygous mutant where one allele was globally Kit inactivated, the other allele was Kit hyperactivated in a germ cell specific manner ($VC;Kit^{-/D818V(L)}$). Interestingly, both *VC; Kit* $^{-/D818V(L)}$ and *Kit* $^{-/D818V(L)}$ males had similar phenotypes: smaller testes with no undifferentiated spermatogonia and complete lack of spermatogenesis. *D818V(L)* allele harbors Kit with a shorter 3'UTR globally. Even though it did not affect Kit expression when it was heterozygous, shorter 3'UTR affected Kit expression levels when the other allele was Kit inactivated. Kit was overexpressed from the Leydig cells in both of the models ($VC;Kit^{-/D818V(L)}$ and . *Kit* $^{-/D818V(L)}$). Therefore, it is hard to conclude if the phenotype is due to the shorter 3'UTR, or Kit hyperactivity. However, our results further shows that both germ cell specific Kit hyperactivity, and Kit overexpression due to shorter 3'UTR, cause infertility by affecting the undifferentiating spermatogonia population; and leading to their cell death with an unknown mechanism.

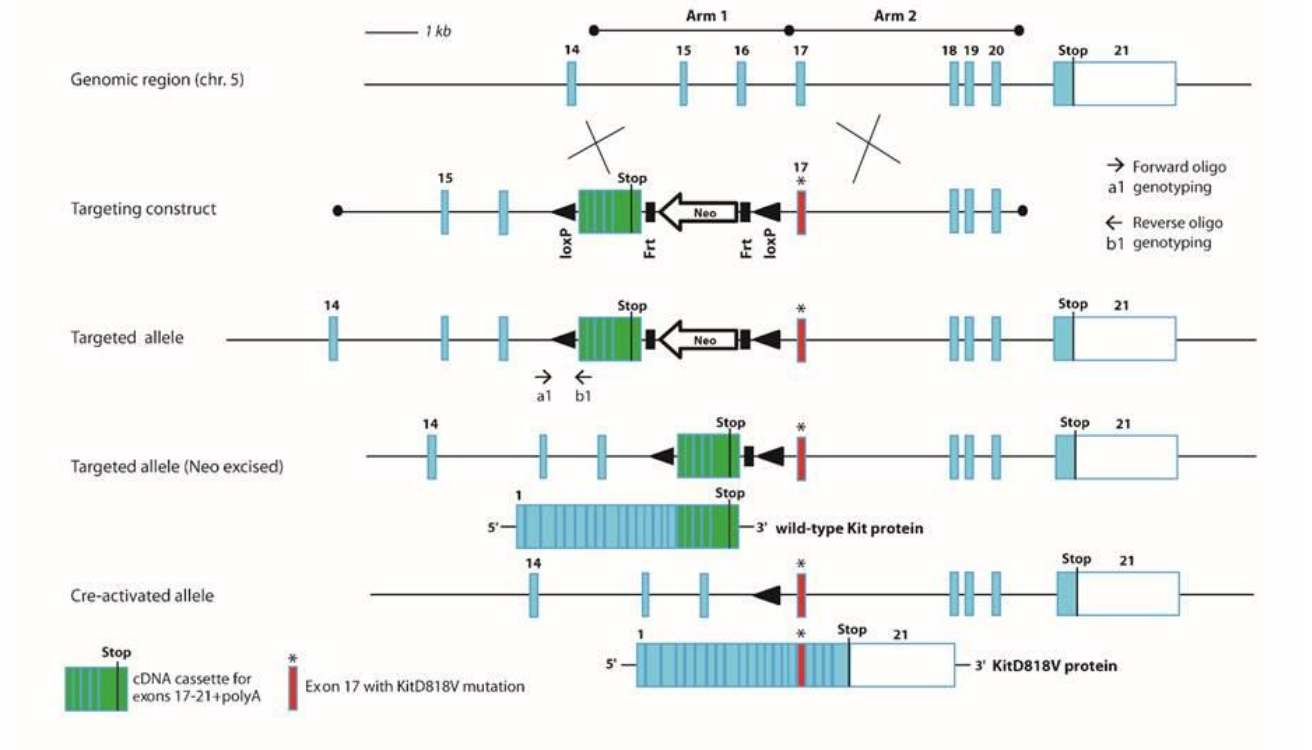

Figure 4.1. Map of the Kit$^{D818V(L)}$ allele. Maps of Kit locus (exons 14-21) and targeting construct. The modified exon 17 is shown in red and the D818V point mutation is indicated with an asterisk. Unmodified exons are represented in blue, the 3' cDNA cassette encoding exons 17-21 and polyA sequence in green. Genotyping primers are shown by small arrows (a1 and b1).**(Figure courtesy of Dr. Cuevas)**

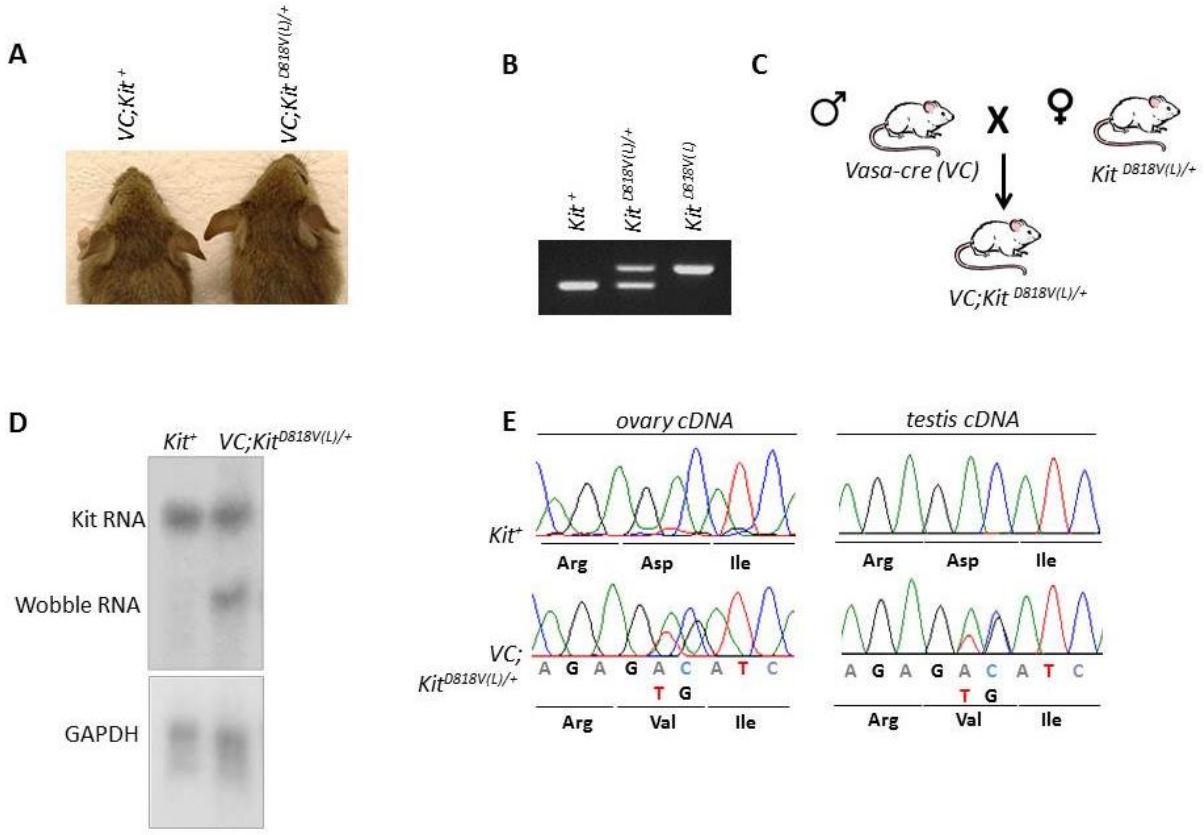

Figure 4.2. Generation of germline specific *Kit^{D818V}* mutation (A) Vasa-cre (VC) males were bred to Kit$^{D818V(L)}$ females to generate germ-line specific Kit hyperactivity. **(B)** Normal pigmentation in *Kit$^{D818V(L)}$*/+ and +/+ mice. Picture was taken at 4 weeks of age **(C)** PCR genotyping of WT, *Kit$^{D818V(L)}$*/+ heterozygous and *Kit$^{D818V(L)}$* homozygous mice. **(D)** Northern analysis of WT and VC; KitD818V(L)/+ mice. RNA was isolated from 8 weeks old WT and experimental testes. The blot was probed with cDNA fragments spanning exon 5 and 11 and then re-probed with GAPDH as a loading control. The **longer band** represents the *WT* and *VC; KitD818V(L)/+* RNA which are at the same size, while the shorter band represents the *Kit$^{D818V(L)}$* allele, which is designed to have a shorter 3'UTR. **(E)** cDNA expression analysis of mutant allele. Total RNA was isolated from PD7 ovaries and adult testis from experimental and sibling controls. Both ovaries and testes are analyzed by Sanger sequencing following RT-PCR. The expected two base-pair substition resulting in an Asp→Val substitution was observed.

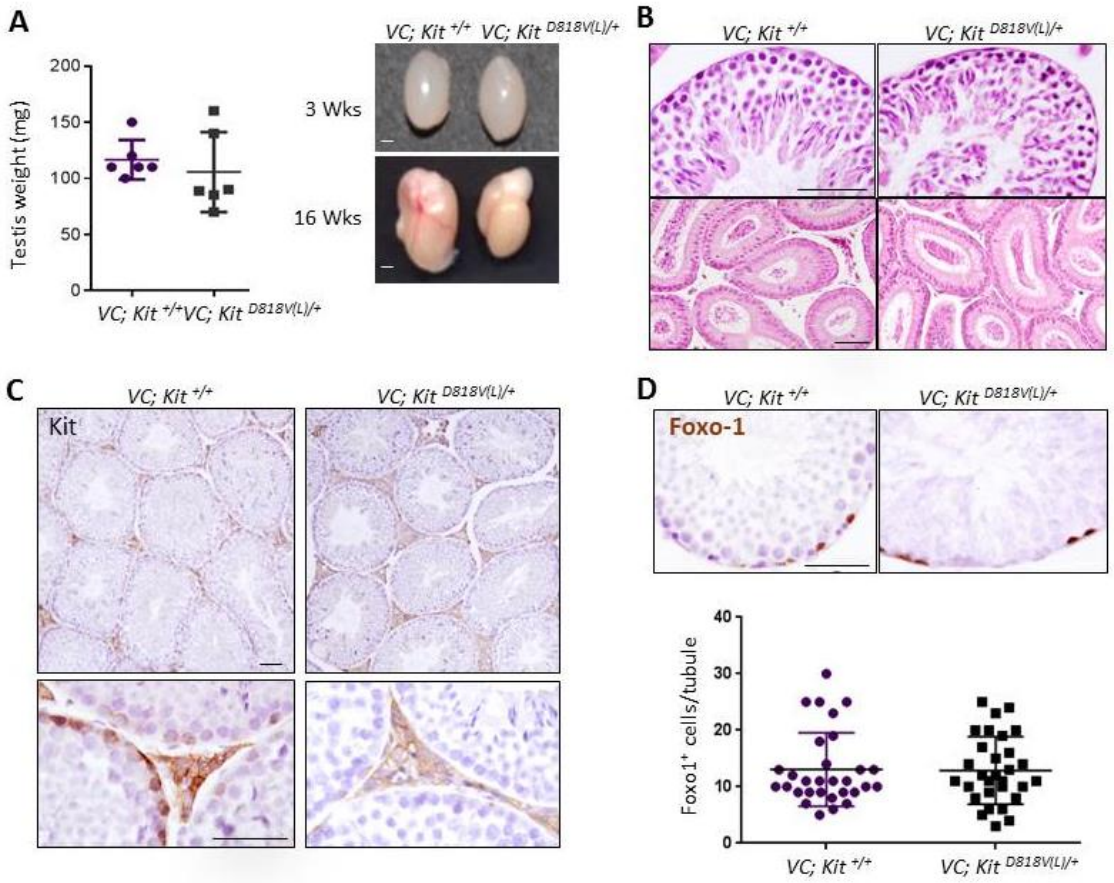

Figure 4.3. Germ-line specific KitD818V mutation does not affect spermatogenesis. (A) Testes weights and pictures from control and experimental males. Testes weights were not significantly different. (n=6 per testes; from 3 different mice; p= 0.5134). The gross pictures are at 3 weeks and 16 weeks from the experimental and sibling controls. Scale bars are 1 mm **(B)** H&Es of testes and epididymis from experimental and control males at 16 weeks of age. The scale bars are 50 µM, same for the experimental and the sibling control **(C)** Kit immunohistochemistry on experimental and control testes at 16 weeks of age. The slights were counterstained with hematoxylin. The scale bars are 50 µM, same for the experimental and the sibling control **(D)** Foxo1 immunohistochemistry on experimental and control testes. The slights were counterstained with hematoxylin. The graph shows the number of Foxo1 positive cells from 30 different tubules of *VC;+/+* and *VC; D818V(L)/+* males. The difference of Foxo1 positive cell counts were not significantly different in experimental and control testes (n=30 tubules, p=0.918).

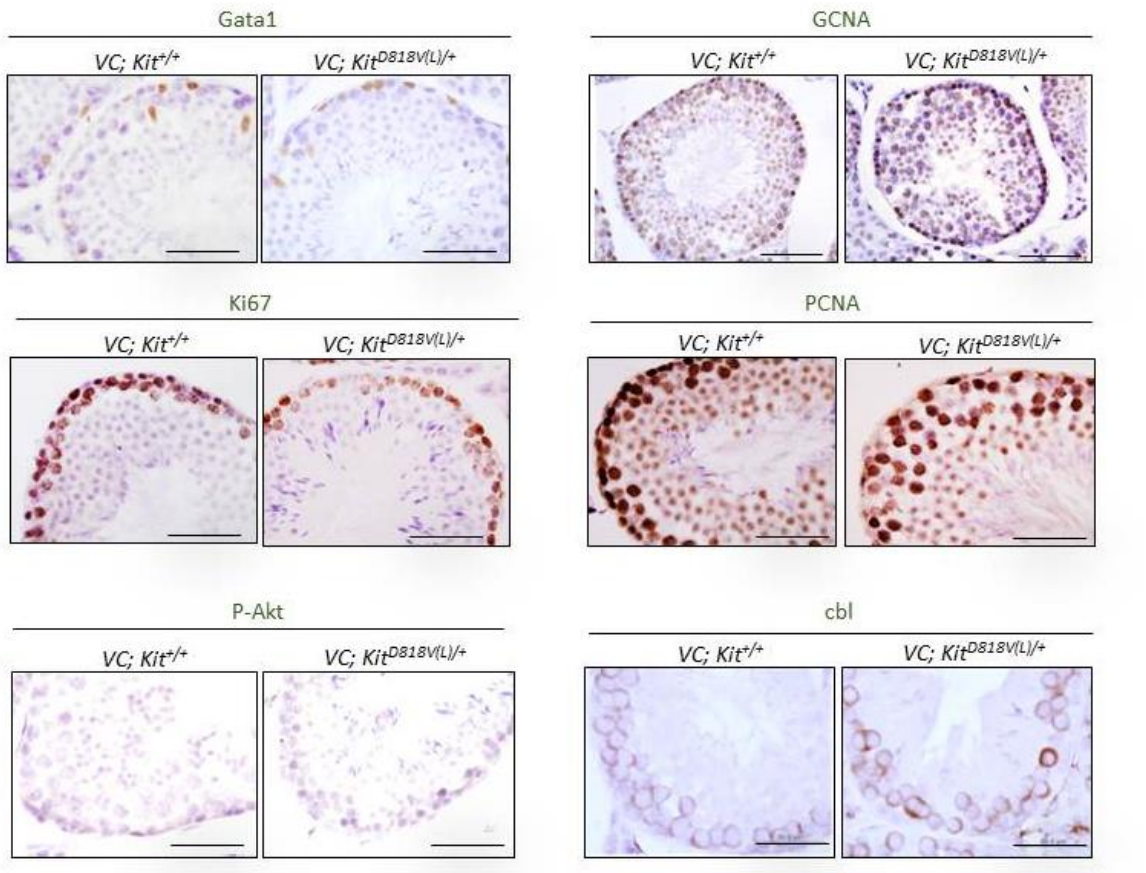

Figure 4.4. Marker analysis of control and *VC;Kit*$^{D818V(L)/+}$ testes. The sections were stained with Gata1, GCNA, Ki67, PCNA, P-Akt and Cbl from 16 weeks old control and experimental testes. The slights were counterstained with hematoxylin. The scale bars are 50µM, same for all. There wasn't any significant difference between experimental and control testes among the markers analyzed.

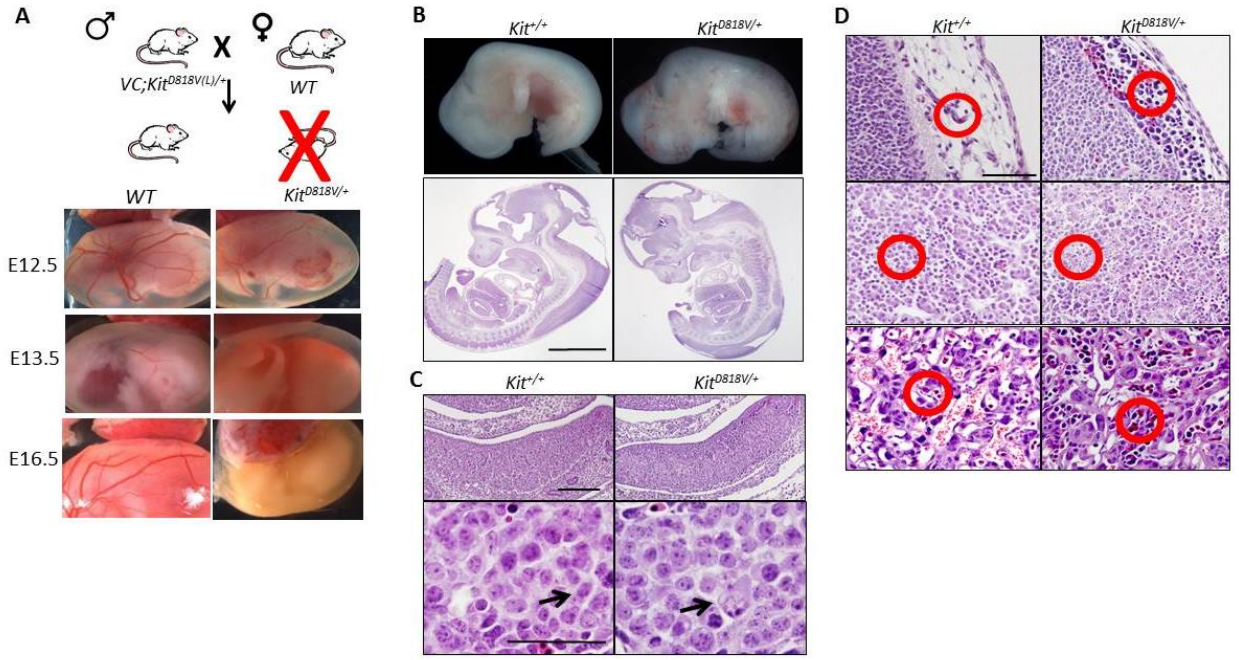

Figure 4.5. ***KitD818V/+* embryos are embryonic lethal and they have congested blood vessels with abnormal white-blood cell clusters. (A)** Generating whole-body *KitD818V* mutation. *VC; Kit* $^{D818V(L)/+}$ males were bred to *WT* females. The progeny was *WT* or heterozygous whole-body Kit knock-in (*Kit* $^{D818V/+}$). *D818V* mutation was embryonic lethal at E16.5 and E13.5. However, the mice were viable at E12.5. **(B)** Gross pictures of WT and *D818V/+* embryos and H&Es from sagittal sections. Note the hemorrhagic experimental embryo at E12.5**.** Scale bar for embryo H&Es are: 2 mm, same for both. **(C)** Embryonic testes at E12.5 from WT and experimental testes. Note the presence of normal and aberrant germ cells denoted by black arrows from gonadal sections. Some of the mutant germ cells have different chromatin patterns and larger cytoplasm Scale bars are 20 µM for gonad sections and 50 µM for amplified gonad pictures; same for both, for all. **(D)** 100X pictures from the H&Es of sagittal embryonal sections at E16.5. Shown are skin (top) and liver (middle); as well as placenta (bottom). Note the presence of aberrant white blood cell clusters and congested blood vessels only in the experimental organs, donated in red circles. Scale bar is 50 µM for all.

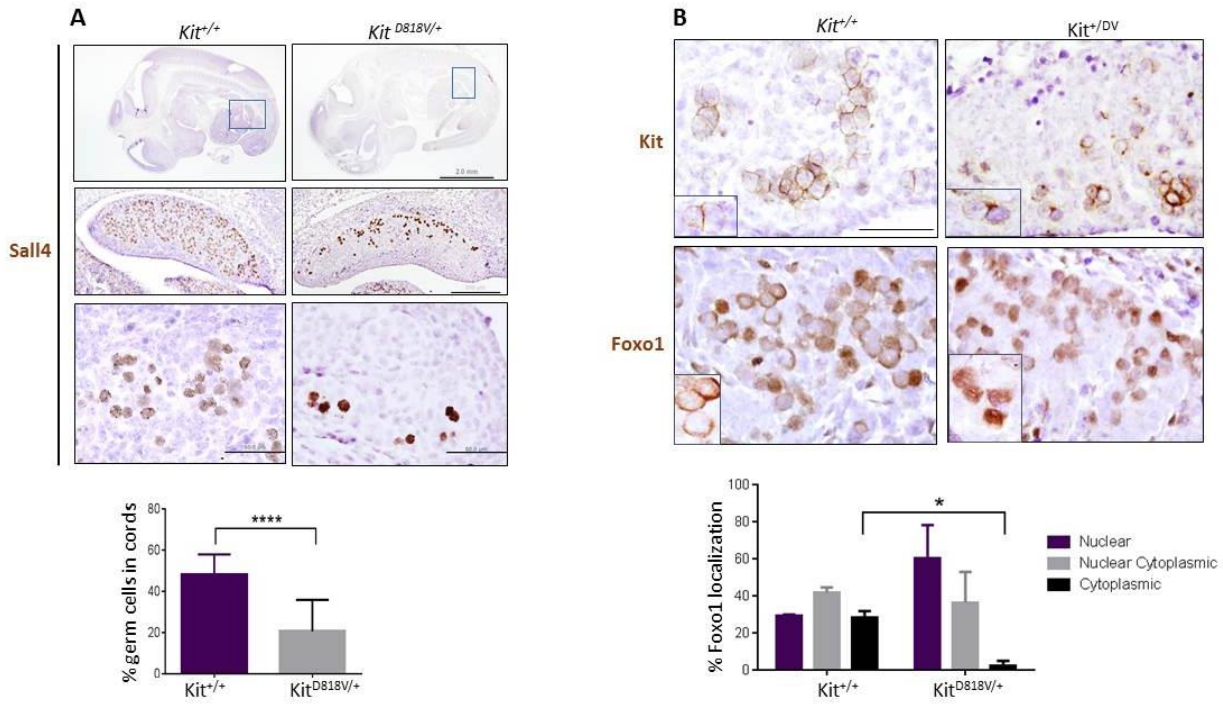

Figure 4.6. ***KitD818V*** **mutation leads to less number of germ cells migrated to the cords with down-regulated Kit expression and predominantly nuclear Foxo1. KitD818V mutation leads to fewer germ cells migrated into the primitive cords with down-regulated Kit expression and predominantly nuclear Foxo1 (A)** Less number of germ cells are migrated to the cords in the *Kit* $^{D818V/+}$ embryos. Sagittal embryonal sections that span the male gonads were stained with the germ-cell marker Sall4.The slights were counter-stained with hematoxylin. Scale bars are 2 mm for embryo pictures, 20 µM for gonads and 50 µM for the testicular cords; same for the control and the experimental sections. Blue rectangles are amplified in the next section. Note the presence of less Sall4 positive cells in the experimental embryos. All the cells in the cords were count from 2 different WT, and 3 different experimental embryo sections. Sall4 positive cells were also count and the percentage of Sall4 positive cells were calculated for each cord. The graph represents the average of Sall4-positive cell-percentage per cord. ($n \geq 2$ per embryo; ****$p<0.0001$). The slights were counter-stained with hematoxylin. **(B)** Kit is down-regulated and Foxo1 is predominantly nuclear in *KitD818V/+* embryos**.** Sagittal embryonal sections that span the male gonads were stained with Kit and Foxo1. Two different WT and 3 different experimental embryos were analyzed for Kit and Foxo1 expression. Note the cytoplasmic expression pattern of Kit in the experimental germ cells unlike the membrane-bound pattern in the WT germ cells. Total number of cytoplasmic, nuclear-cytoplasmic and nuclear Foxo1 cells were count and quantified. The experimental germ-cells have significantly less number of cytoplasmic Foxo1 ($n \geq 2$ per embryo; $p = 0.0023$).

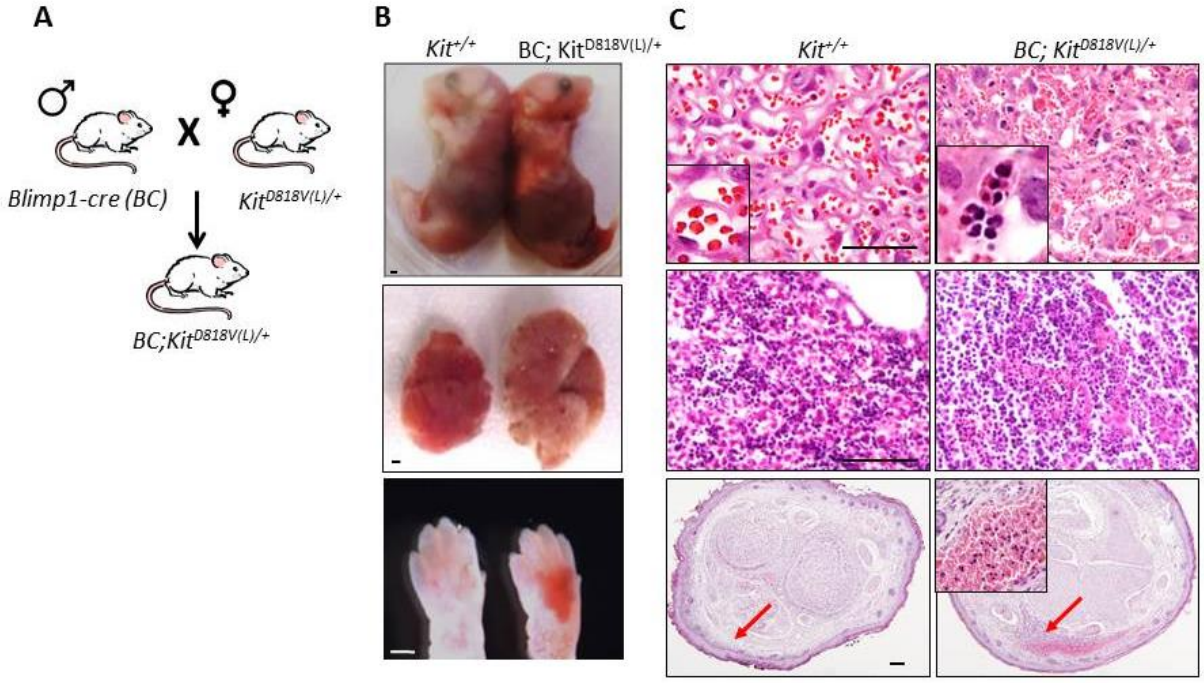

Figure 4.7.. ***Blimp1-cre (BC);Kit$^{D818V(L)/+}$*** **embryos are lethal. (A)** *BC* males were bred to *D818V(L)/+* females to generates germline-specific Kit hyperactivity starting from primordial germ cell stage (E7.5). **(B)** E18.5 embryos were viable with larger livers and dilated blood vessels visible from their limb. Scale bars are 1 mm for all. **(C)** H&Es from *WT* and experimental placenta, liver, and limb sections. Note the dilated blood vessels denoted by red arrows from the limb cross section. Note the aberrant white blood cell clusters from the placenta and the limb of the experimental tissues, amplified in small rectangles. The *BC;Kit $^{D818(V)/+}$* liver section had more necrotic cells compared to the control. The scale bars are 50 µM and same for the experimental and control sections.

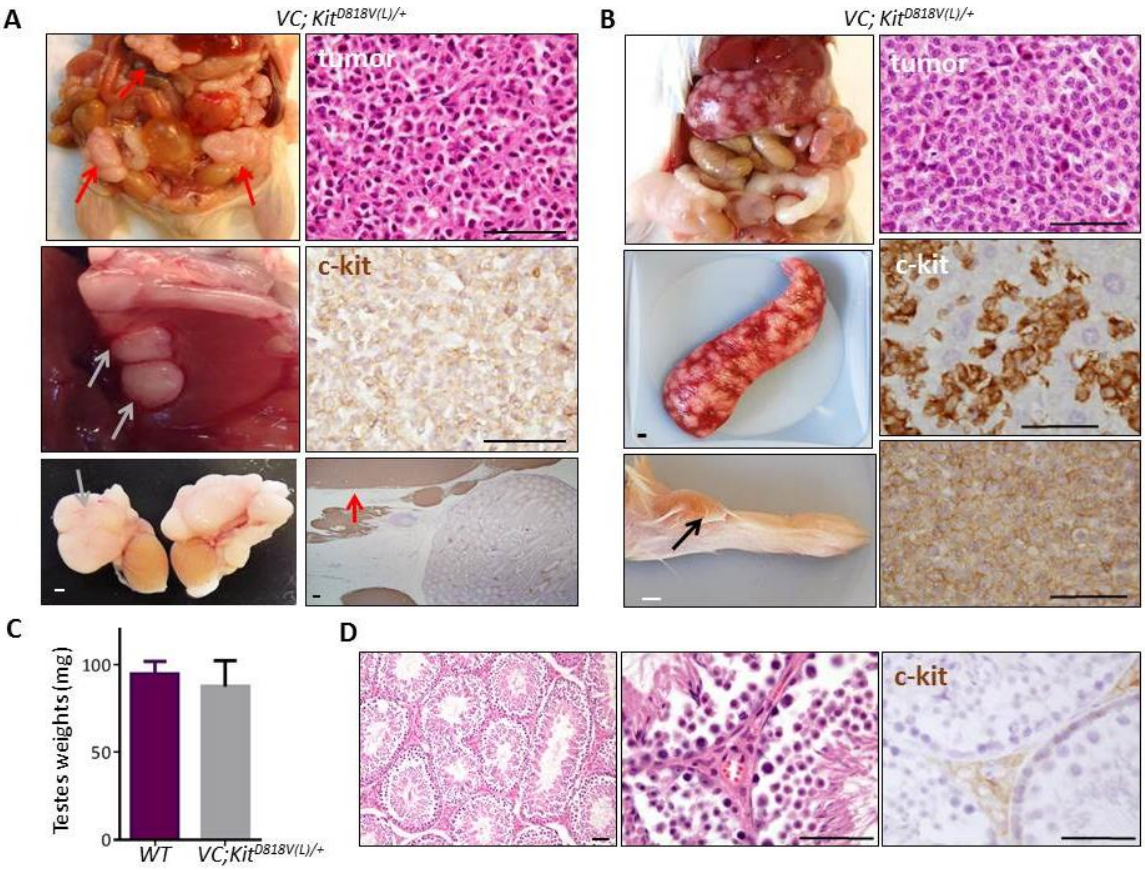

Figure 4.8. Spermatogenesis is normal but Kit expressing tumors can occur in *VC; Kit*$^{D8181V(L)/+}$ mice (A) Wide-spread nodules were present all over the body in one of the *VC; Kit*$^{D818V(L)/+}$ males analyzed. Red and gray arrows demarcate the nodules on/next to the abdomen, diaphragm and epididymis. Scale bar is 1 mm for the gross picture of the testes. Note that the testes sizes were normal at one years of age. The tumor sections were analyzed by H&Es and kit IHC. Note that the tumor cells are highly kit positive (shown by a red arrow), unlike the testes. Scale bars are 50µM. **(B)** Splenic tumors, and a nodule in limb were seen from a 1 year old *VC; Kit* $^{D818V(L)/+}$ mouse. Only the tumor cells were kit positive shown by IHC from the spleen section and the tumor on the limb. From top to the bottom, H&E section from the tumor on the limb, Kit staining on the spleen section and tumor section are shown, The scale bars are 50 µM, same for all. **(C)** Testes weights from *WT* and *VC; Kit* $^{D818V(L)/+}$ males (n=2 testes from one mouse for WT; n=6, from 3 mice for the experimental). The testes weights were not significantly different (p=0.555; n=2 testes from from *WT* males; n=6 testes from *VC; Kit* $^{D818V(L)/+}$ males at one years of age.**(D)** H&E analysis and Kit IHC of the testes from 1 year old *VC; Kit* $^{D818V(L)/+}$ males. The scale bars are 50 µM. Kit IHCs are counterstained with hematoxylin.

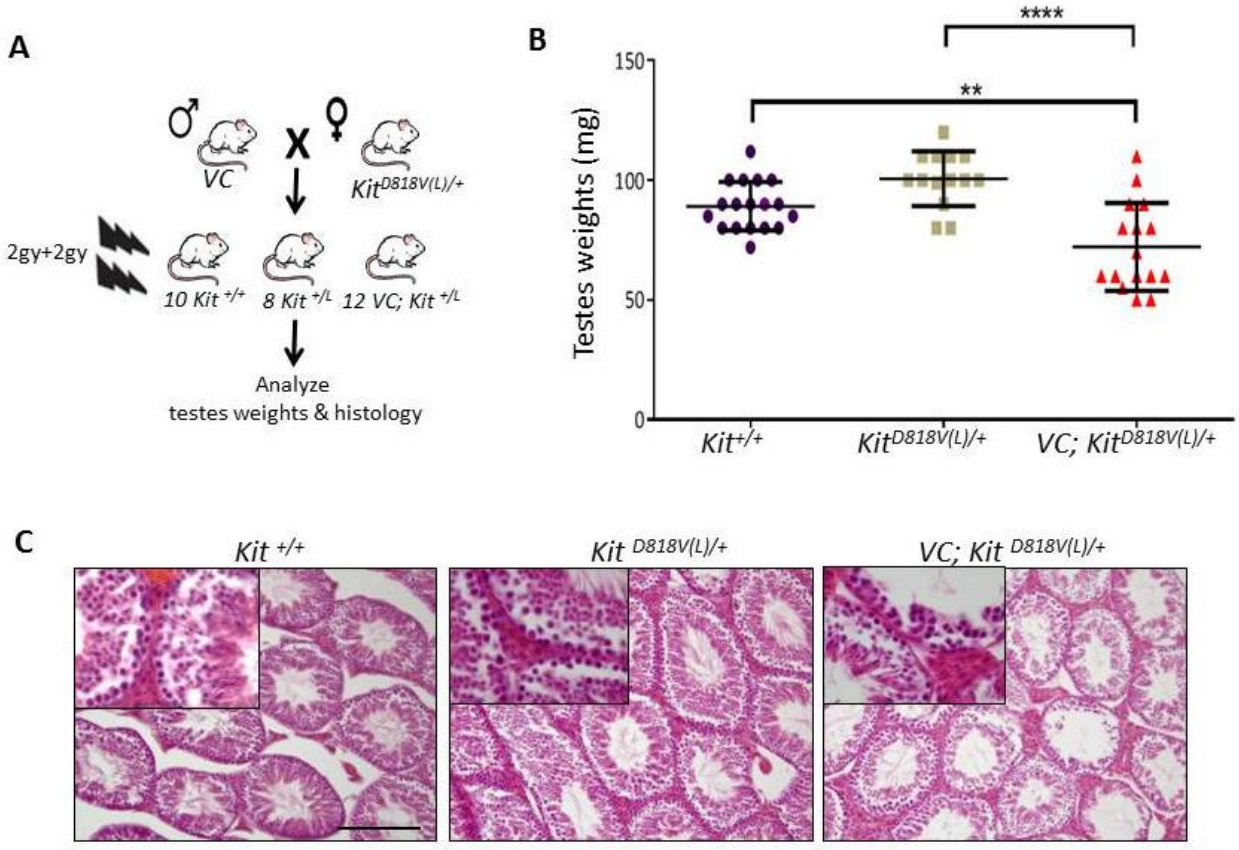

Fig 4.9. *VC; KitD818V(L)/+* testes are smaller 6 months after low-dose radiation. (A) Adult males (4-8 months of age) harboring the germ-cell specific *KitD818V* mutation were generated. Adult males were exposed to fractionated low dose radiation (2gy+2gy). **(B)** Testes weights were measured 6 to 9 months after radiation exposure from experimental and sibling controls. ($n \geq 14$ per testes; $n \geq 7$ per genotype.****$p<0.0001$; **$p<0.01$). VC; KitD818V(L)/+ testes were significantly smaller compared to WT and +/D818V(L) sibling controls after radiation treatment. **(C)** H&E analysis of the testes 6 to 8 months after radiation exposure. Scale bar is 20 µM and same for all sections. Little squares show the magnified testicular tubules and germ cells from each genotype. Sperm is present and testes histology is normal in the experimental tubules. However, note the presence of less number of spermatids in the experimental sections, shown by black arrows, which might explain the significantly different testes weights from the experimental males.

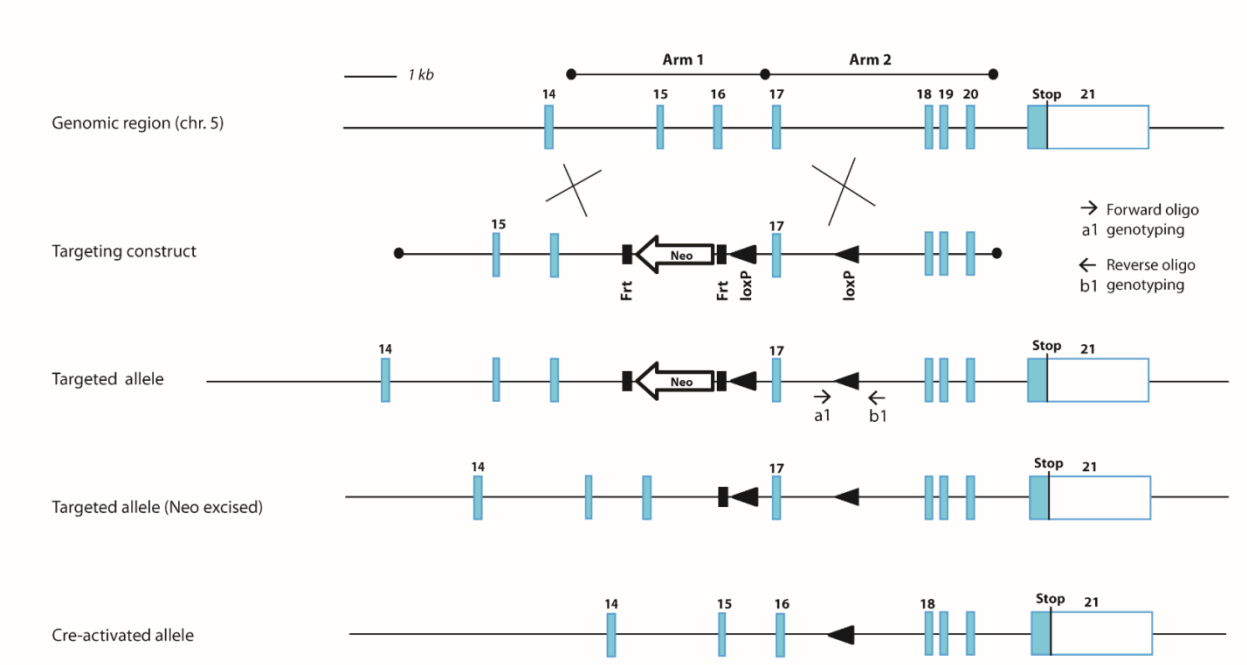

Figure 4.10. Maps of *Kit* locus (exons 14-21) and targeting construct. Exon 17 is fluxed. Genotyping primers are indicated by small arrows (a1 and b1). Exon 17 is deleted upon cre-activation. **(Figure courtesy of Dr. Cuevas)**

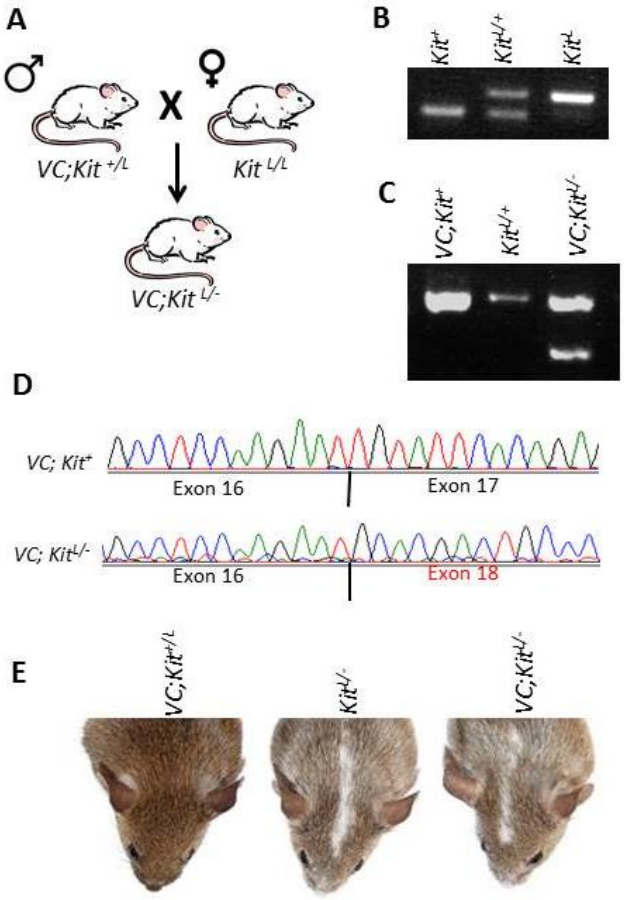

Figure. 4.11. Generation of *Kit*^{L} allele (exon 17 floxed). (A) Males harboring the Kit inactivating mutation in their germ-line were bred to *Kit* $^{L/L}$ females to generate homozygous Kit inactivation in a germ cell specific manner. **(B)** PCR genotyping of wild-type, *Kit* $^{L/+}$ and *Kit* $^{L/L}$ mouse tails. The 174 bp (upper) product was gel-purified; Sanger sequencing showed expected sequences spanning the 3' loxP site of the *Kit* ^{L} allele. The 126 bp (lower) represents the wild-type *Kit* allele. **(C)** cDNA expression analysis of mutant allele. Total RNA was isolated from PD3 wild-type and *VC; Kit* $^{L/-}$ ovaries and analyzed by RT-PCR. The smaller product (382 bp) in *VC*; *Kit* $^{L/-}$ ovaries indicates deletion of exon 17. **(D)** Sanger sequencing of cDNA from *VC*; *Kit* $^{L/-}$ and control ovaries confirms exon 17 deletion

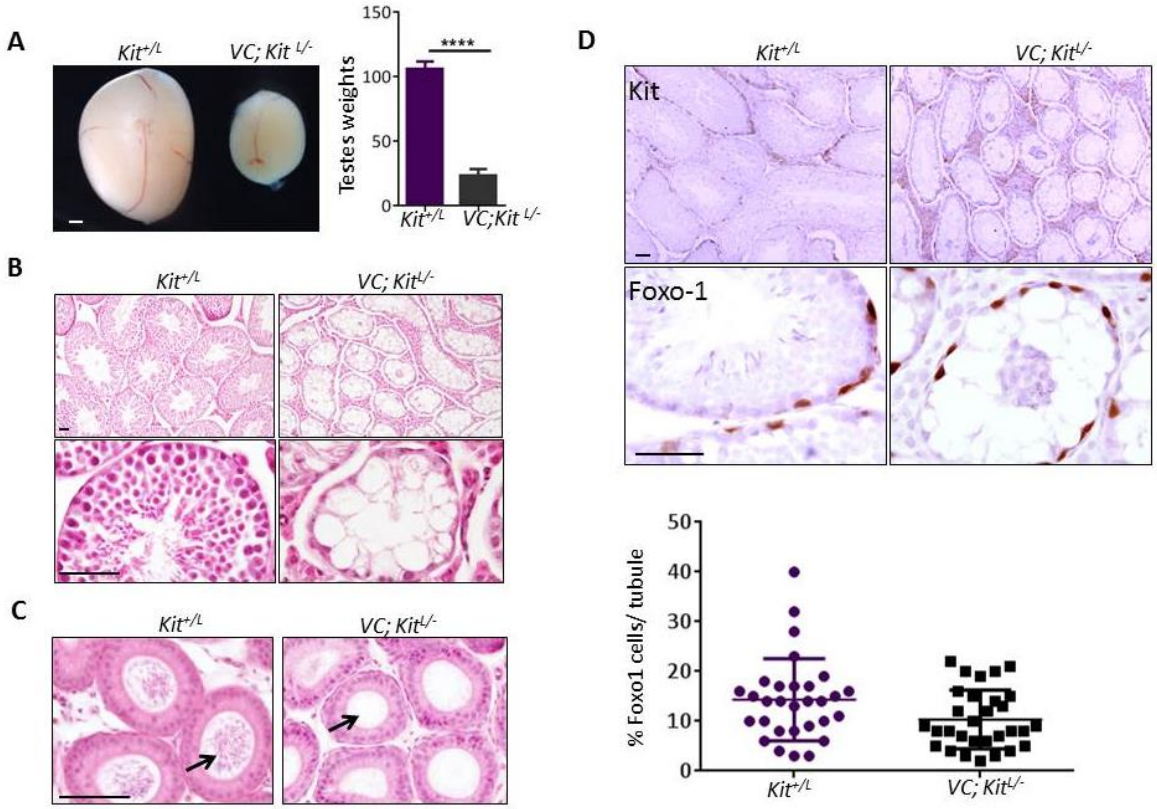

Figure 4.12. Infertility due to Kit loss of function mutation in males. (A). Testes were significantly smaller in *VC; Kit* $^{L/-}$ males compared to sibling controls at 6 weeks of age (n=2 per testes; n=1 per animal.****p<0.0001). **(B)** H&E analysis of control and Kit deficient testes at 6 weeks of age. Note that the experimental tubules lack sperm. Kit loss of function mutation leads to infertility in males, due to depletion of the transit amplifying germ cells. Scale bars are 50 µM and same for both sections **(C)** H&E analysis of control and Kit deficient epididymis at 6 weeks of age. The black arrows show the epididymal sperm. Note the absence of mature sperm in Kit deficient epididymis**. (D)** Expression pattern of Kit and Foxo1 in control and *VC; Kit* $^{L/-}$ testes at 6 weeks of age. The slights are counterstained with hematoxylin. Scale bars are 50 µM and same for both sections. The graph shows the number of Foxo1 positive cells for tubule (n=25 per tubule per one section). Number of Foxo1 positive cells are significantly less in Kit deficient testes.

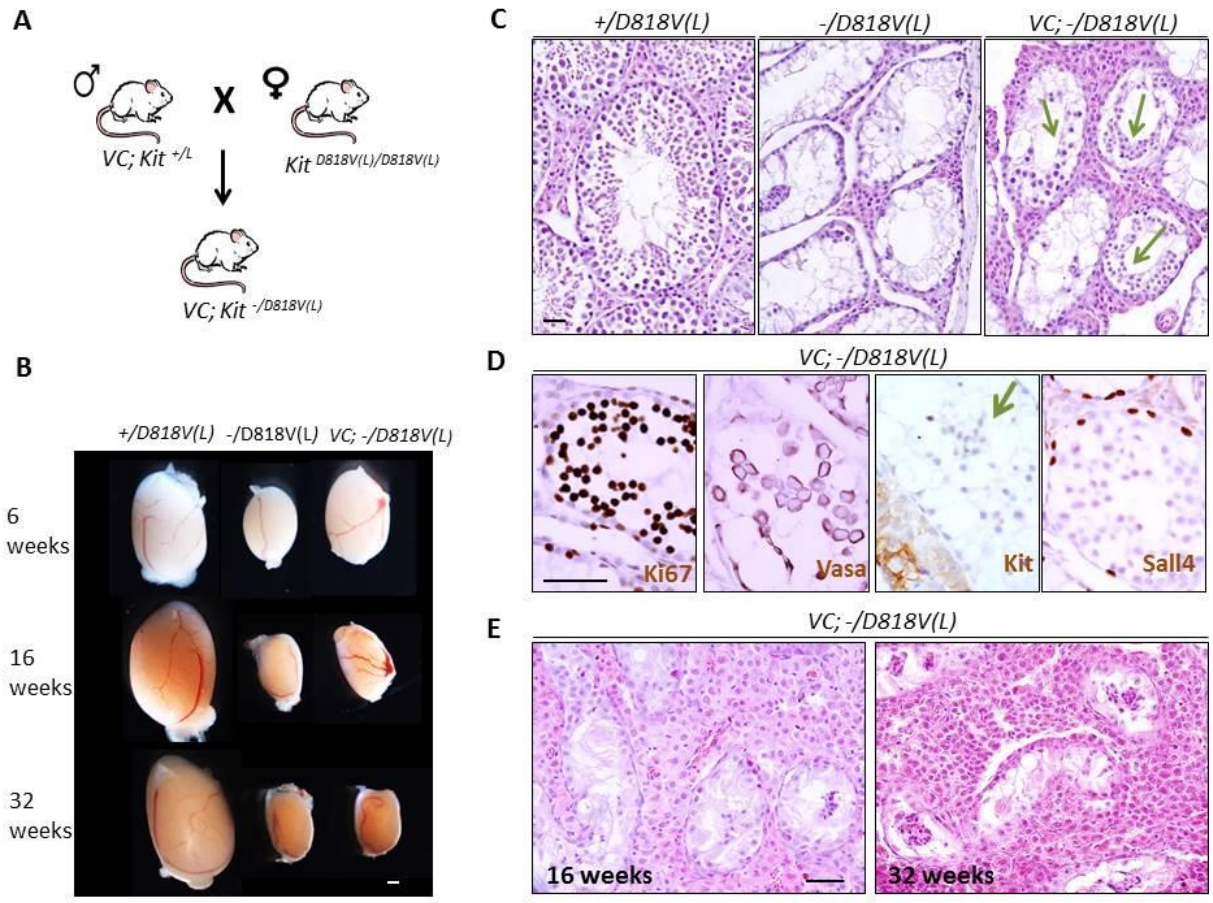

Figure 4.13. Germ-cell specific *Kit* $^{D818V/-}$ mice have smaller testes and lack undifferentiated spermatogonia. (A) *VC; Kit* $^{+/L}$ males were bred to homozygous *Kit*$^{D818V(L)}$ females to generate males harboring the *D818V* mutation from one allele, and Kit inactivating mutation from the other allele (*VC; Kit* $^{-/D818V(L)}$). **(B)** Gross pictures of *+/D818V(L)*, *-/D818V(L)*, and *VC; D818V(L)* testes. Note that the *-/D818V(L)* and *VC; D818V(L)* testes were both significantly smaller compared to the sibling controls. The testes pictures are placed on a black background with the same scale. Scale bar=1 mm. **(C)** H&E analysis of control and experimental testes from 6 weeks of age. Note the presence of proliferative and aberrant looking undifferentiated spermatogonia clusters in the experimental testes demarcated by green arrows. The scale bar is 50 µM and same for all the sections. **(D)** Ki67, Vasa, Kit, and Sall4 staining on the experimental testes at 6 weeks of age. Slights are counterstained with hematoxylin. Scale bars are 50 µM and same for both sections. Green arrow shows the germ cell clusters that are Kit negative. **(E)** H&E analysis of experimental testes at later ages (16 weeks and 32 weeks). Note that the aberrant germ cell clusters die at later ages. Scale bar is 50 µM and same for both.

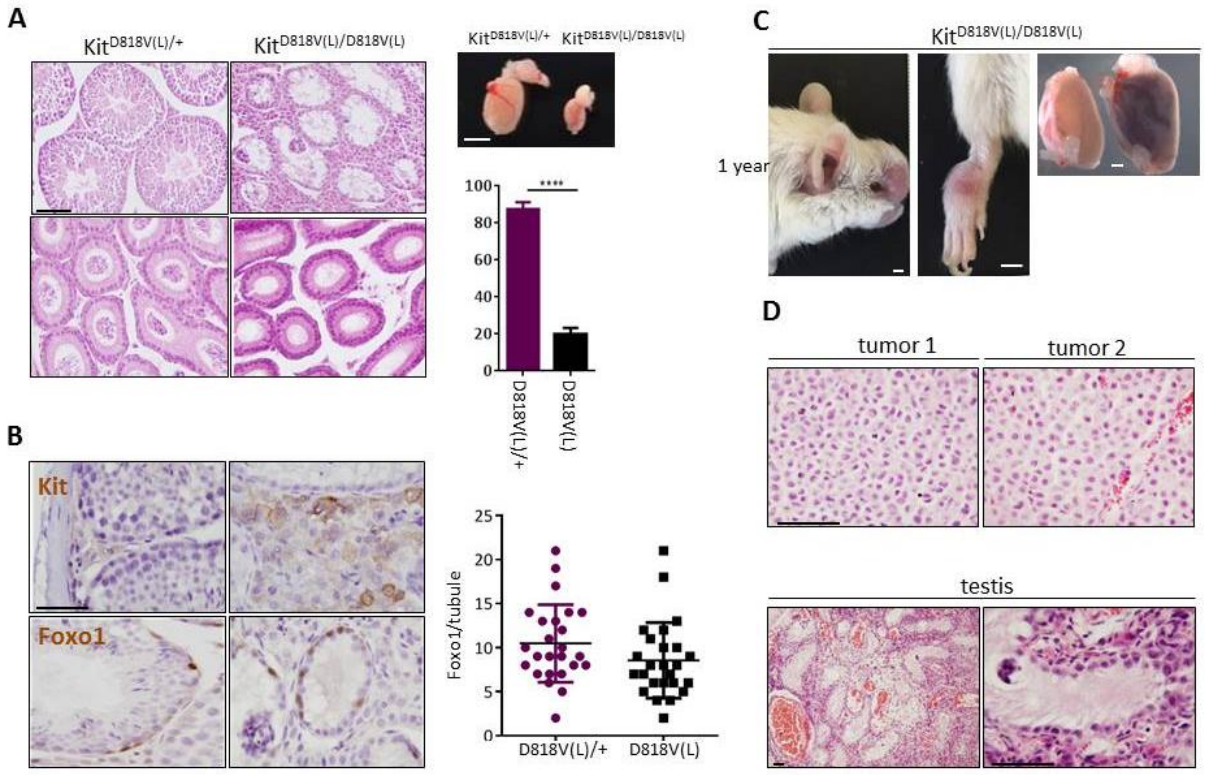

Figure 4.14. **Heterozygous *KitD818V(L)* mice are normal but homozygous *KitD818V(L)* males are infertile and they form tumors by 1 years of age. (A)** H&E analysis, weights and gross pictures of heterozygous and homozygous *D818V(L)* testes at 6 weeks of age**.** Homozygous fluxed allele has significantly smaller testes. They are depleted of mature sperm. Scale bar is 50 µM, same for all. **(B)** Kit and Foxo1 IHC from control and *D818V(L)/ D818V(L)* testes. Slights are counterstained with hematoxylin. The graph shows the number of Foxo1 positive cells in the tubules. The undifferentiated spermatogonia numbers were not significantly different than control at 6 weeks of age. **(C)** Homozygous fluxed males form tumors at one years of age. Noise, limb and testes pictures are shown from the experimental male. The scale bars are 3 mm, same for all gross pictures. Note that one of the testes is hemorrhagic. **(D)**. H&E analysis of the tumors and the testes from the experimental mice at one years of age, tumor 1 formed on the noise, tumor 2 formed on the limb. Scale bar is 50 µM, same for both. No that there is no malignant transformation but an azopermia phenotype in the testes. Scale bars are 50 µM for the testis H&Es.

CHAPTER 5

Results

CONTROL OF PRIMORDIAL OOCYTE REAWAKENING BY KIT

Introduction

Primordial follicles are the reserve precursor pool for maturing follicles throughout reproductive life (Zhang et al., 2014a). Primordial follicles are reawakened via an ovarian-intrinsic (gonadotropin independent) process whereby they are selected from the quiescent reserve into the growing follicle pool (McGee and Hsueh, 2000; Sullivan and Castrillon, 2011). The morphologic hallmark of reawakening is oocyte growth, and this is followed by a transition of the surrounding granulosa cells from a flattened to a cuboidal shape (Lintern-Moore and Moore, 1979). Reawakening is irreversible, in that follicles that have initiated growth undergo atresia if not selected for subsequent stages of maturation. Primordial follicle numbers decrease with advancing age due to oocyte reawakening or apoptosis; following follicle depletion, ovulation ceases and reproductive senescence ensues. Reawakening must therefore be metered throughout reproductive life to ensure that some growing follicles are available during each estrus cycle, but at the same time, limit the number of growing follicles to forestall depletion of primordial follicles (see **Chapter 1** for summary schematic of follicle maturation). Characterization of the molecular mechanisms underlying reawakening remains an important challenge in reproductive biology (Adhikari and Liu, 2009; Matzuk et al., 2002; Skinner, 2005; Tingen et al., 2009).

The forkhead transcription factor Foxo3 is a critical regulator and suppressor of oocyte reawakening. Foxo3 serves as an active molecular switch whose activity, localization within the

oocyte (cytoplasmic vs. nuclear) is under the control of PI3K-AKT signalling within the oocyte. However, the identity of the presumptive upstream signalling factor(s) controlling this process and the PI3K-AKT-Foxo3 axis has been controversial. Because follicle reawakening cannot be faithfully modeled *in vitro*, genetic approaches are needed to formally establish the identity of these putative upstream factors.

Results

Kit activation in primordial oocytes results in a global primordial follicle reawakening phenotype

Kit is an RTK that acts via PI3K-AKT, and is expressed within primordial oocytes (Lennartsson and Ronnstrand, 2012; Manova et al., 1990). To study the role of Kit in the reawakening of primordial follicles, $Kit^{D818V(L)}$/+ females were bred to the germ cell-specific Cre driver, Vasa-Cre (a.k.a. Ddx4-$cre^{1Dcas/J}$) (abbreviated VC) to generate VC; $Kit^{D818V(L)}$/+ females. Ovaries were harvested at postnatal day (PD) 7 and ovarian cDNA was analyzed by RT-PCR, followed by Sanger sequencing **(Chapter 4, Figure 4.1).** As expected, ovaries from experimental females expressed mutant cDNA at levels close to wild-type as evidenced by electrophoretogram peaks, with the somewhat lower mutant allele peak intensities readily accounted by *Kit* expression from ovarian somatic cells and the wild-type allele **(Chapter 4, Fig. 4.2A).** By PD7, *VC*; $Kit^{D818V(L)}$/+ ovaries were consistently larger than ovaries from sibling controls. By PD14, these size differences were even more marked, but from PD28 onward (up to 16 weeks of age), ovaries were of equal size or somewhat smaller **(Fig.5.1A)**. To understand the cellular basis of this increase in ovarian size (and subsequent decrease), tissue sections were analyzed. At PD7, there was an obvious increase in oocyte diameters in follicles that otherwise resembled primordial follicles (i.e., follicles without granulosa cell growth or change to cuboidal shape) **(Fig.5.1A;**

5.2B). Interestingly, whereas Kit protein is predominantly membranous in controls, Kit protein underwent a general redistribution to the cytoplasm in *VC*; $Kit^{D818V(L)}$/+ oocytes **(Fig 5.3A; 5.4A-C)** with overall Kit protein levels comparable to $Kit^{D818V(L)}$/+ controls **(Fig.5.4D)**. This is consistent with prior data demonstrating that Kit protein normally undergoes ligand-dependent internalization, and that constitutively active mutant variants are internalized more efficiently than the wild-type protein (Gommerman et al., 1997; Jahn et al., 2002).

Of note, these morphological alterations were global, occurring in all primordial follicles. *VC*; $Kit^{D818V(L)}$/+ oocytes grew in size up to PD28, resulting in aberrant follicles with dramatically enlarged oocytes **(Fig. 5.1B, 5.6B).** Some morphologically normal follicles up to the corpora lutea stage were also present, indicating that some of the reawakened follicles progressed normally to more advanced states of follicle maturation **(Fig. 5.1B).** Concordantly, most markers of primordial or primary follicles including periodic acid-Schiff (PAS) stain (labels the zona pellucida (Zp)), Zp1, Inhibin, growth differentiation factor 9 (Gdf9), Sohlh1, Nobox, and Sall4 retained their typical patterns of expression in oocytes or granulosa cells, consistent with normal differentiation despite global reawakening **(Fig. 5.5; 5.6A).** However, in some reawakened follicles, granulosa cells remained flattened and were negative for Anti-Müllerian Hormone (AMH), which is normally induced at the primary follicle stage **(Fig. 5.6A).** A similar spectrum of abnormalities has been documented in other global reawakening mutants such as *Foxo3* and *Pten* (Castrillon et al., 2003; John et al., 2008; Reddy et al., 2008).

By 16 weeks, however, oocyte atresia occurred, resulting in morphologically abnormal, "empty" follicles depleted of oocytes (note also the absence of more advanced follicles such as corpora lutea) **(Fig. 5.1B).** No teratomas or other ovarian tumors were identified **(Fig. 5.1B).** Thus, constitutive Kit activation in the female germline resulted in a classic, global primordial

follicle reawakening phenotype identical to that described for *Foxo3* and *Pten* (Castrillon et al., 2003; John et al., 2008; Reddy et al., 2008). Global reawakening occurred in all *VC*; $Kit^{D818V(L)}$/+ primordial oocytes, which ultimately underwent atresia resulting in loss of all oocytes with premature ovarian failure. Serum follicle stimulating hormone (FSH) and luteinizing hormone (LH) levels at 5 months of age were elevated in adult mutant females, consistent with hypergonadotropic hypogonadic premature ovarian failure ($P<0.003$ and $P<0.02$ respectively) **(Fig.5.6B).** These results strongly implicate Kit as the upstream RTK regulating primordial oocyte reawakening.

At birth to PD7, oocyte numbers were unaltered in *VC*; $Kit^{D818V(L)}$/+ ovaries, indicating a normal initial endowment of oocytes (Sullivan and Castrillon, 2011). Oocytes were markedly depleted by PD28, and totally absent by 6 weeks of age ($P<0.02$ and $P<0.0004$, respectively) **(Fig.5.2A).** Measurements of oocyte diameters confirmed that average oocyte sizes were significantly increased by PD7, and the difference was even more marked at PD14 ($P<0.0001$ for both PD7 and PD14). Oocytes continued to grow through PD28, although by this timepoint, relatively few oocytes remained **(Figs.5.2A-B and 5.6A).** Sections from experimental and control ovaries embedded in plastic confirmed the absence of oocytes by 6 weeks of age as well as the presence of atretic oocytes and zona pellucida remnants (the "ghosts" of oocytes that underwent reawakening and subsequent atresia) in *VC*; $Kit^{D818V(L)}$/+ females **(Fig.5.6C)**.

Kit activation results in global primordial oocyte reawakening via AKT-Foxo3

Next, various markers were analyzed by immunohistochemistry at PD*7* to further characterize potential abnormalities in downstream effectors such as Foxo3. All oocytes were strongly Vasa-positive, indicating preservation of germline identity following Kit activation. Kit protein was present at high levels within oocytes, although some redistribution to the cytoplasm

was evident in the mutant as was the case by immunofluorescence **(Fig.5.3A).** Activated early oocytes exhibited increased phosphorylated AKT (P-AKT) on their cell membranes as compared to control primordial and primary follicles, which did not contain detectable P-AKT **(Fig.5.3A).** This is consistent with the known role of PI3K-AKT as the key signaling pathway mediating oocyte reawakening (John et al., 2008), and argues strongly that Kit controls reawakening via this pathway. Importantly, AKT hyperphosphorylation drove translocation of Foxo3 protein from the nucleus to the cytoplasm in all *VC*; $Kit^{D818V(L)}$/+ oocytes **(Fig.5.3A).** Confocal microscopy, which allows for higher resolution than immunohistochemistry, confirmed these results; i.e. Foxo3 was predominantly nuclear in controls, but cytoplasmic in the mutant oocytes **(Fig. 5.3B).**

Analysis of conditional floxed allele Kit^{L} in females

The above results provide the strongest genetic evidence to date implicating Kit as the upstream RTK controlling oocyte reawakening via the PI3K-AKT-Foxo3 axis. However, phenotypes associated with gain-of-function mutations should generally be interpreted with caution, as even a single amino acid substitution could have multiple, distinct, and potentially unexpected effects on protein function and thus, phenotypes. To expand upon our genetic analyses of *Kit* in oocyte reawakening with a complementary genetic approach, *VC*; $Kit^{L/+}$ fathers were bred to Kit^{L}/Kit^{L} females **(Chapter 4, Fig.11A)** Experimental females of the *VC*; $Kit^{L/-}$ genotype (per tail DNA) thus harbor homozygous Kit^{-} loss-of-function mutations in their germline. RT-PCR of ovaries **(Chapter 4, Fig.11B)** and Sanger sequencing of cloned cDNAs **(Chapter 4, Fig. 11D)** confirmed *VC*-dependent deletion of exon 17 in ovaries, which encodes for the kinase domain of Kit.

Conditional inactivation of Kit within primordial oocytes results in a complete failure of oocyte reawakening with persistence of quiescent primordial follicles

At PD7, *VC*; $Kit^{L/-}$ovaries were minute, and their small size persisted at all mouse ages analyzed, up to 12 weeks of age **(Fig.5.7A).** Histological analyses revealed a striking and complete failure of oocyte reawakening. Follicles remained small and no growing oocytes were present, although granulosa cells became cuboidal **(Fig.5.7B, Fig.5.8B)** In these follicles, oocytes typically assumed an eccentric location **(Fig.5.7B, 5.9B)**. Electron microscopy (EM) confirmed the viability of these oocytes and their lack of physical growth **(Fig.5.9B)** . Granulosa cells exhibited some mitotic activity in the mutant follicles per Ki67 immunohistochemistry (whereas normal primordial follicles are mitotically inactive) **(Fig.5.9D)**, consistent with increased granulosa cell numbers in the aberrant follicles of *VC*; $Kit^{L/-}$ovaries. Interestingly, EM also revealed abundant lipid droplets in the granulosa cells, which could contribute to their change in shape **(Fig.5.9B)**.The significance of these lipid droplets is uncertain. One interpretation is that granulosa cells "sense" the lack of oocyte growth (due to known, if poorly understood, bidirectional oocyte/granulosa cell communication), and respond in some manner to promote reawakening (Eppig et al., 2002; Matzuk et al., 2002). Alternatively, an abnormal hormonal milieu associated with ovarian failure could also indirectly contribute to the observed changes in granulosa cells. In any case, ZP1, which is expressed in growing oocytes, was not expressed in any *VC*; $Kit^{L/-}$ oocytes, consistent with a constitutional inability to reawaken/initiate growth despite the granulosa cell changes **(Fig.5.9C)**.

Oocyte numbers were unaltered in *VC*; $Kit^{L/-}$ovaries at PD7, demonstrating that the minute ovaries were due to a complete lack of oocyte growth, and not a diminished initial endowment of primordial follicles **(Fig. 5.8A).** Measurements of oocyte diameters confirmed the

lack of oocyte growth **(Fig. 5.8B-C).** These quantitative and morphometric data thus revealed a complete failure of oocyte reawakening in *Kit*-deficient oocytes. Somewhat unexpectedly given prior studies implicating Kit in germ cell and primordial oocyte survival, $Kit^{-/-}$ oocytes did not undergo rapid apoptosis (John et al., 2009; Saga, 2008). To the contrary, *VC*; $Kit^{L/-}$ primary/primordial oocyte counts showed only a minor (statistically not significant) decrease even at 12 weeks of age, consistent with a remarkably specific role for Kit in oocyte reawakening **(Fig. 5.8A).** However, by 6 months of age, the ovaries were entirely depleted of follicles and oocytes and contained only luteinized stroma **(Fig 5.10A-C)**, demonstrating that Kit is required for the long-term maintenance of oocytes, in keeping with prior studies implicating Kit as an oocyte survival factor (Carlsson et al., 2006; John et al., 2009).

At birth, oocytes are syncytial and interconnected by intercellular bridges, which are broken down by PD3 to give rise to individualized primordial follicles. Follicle individualization (also known as assembly) occurred normally in *VC*; $Kit^{L/-}$ovaries (e.g., no follicles contained more than one oocyte), demonstrating that Kit is not essential for individualization despite its abundant expression within oocytes at PD1-3 when individualization takes place **(Fig. 5.8B).** Additional marker studies at 6 weeks of age showed that all oocytes retained germline identity, with normal expression of primordial oocyte markers such as Vasa, p63 (an oocyte survival factor), Foxo3, Sohlh1, and Nobox **(Fig.5.11A).** Granulosa cells continued to express inhibin and AMH (markers of female gonadal somatic cell differentiation) but did not express the Sertoli cell marker Gata-1 **(Figs.5 11C,D)**, evidence against a sex-reversal phenotype, a possibility entertained because of the morphologic resemblance of the aberrant follicles—particularly those with eccentric oocytes—to primitive male sex cords. These results are consistent with a specific role of Kit in oocyte reawakening. Additionally, Foxo3 was constitutively nuclear and P-AKT

was undetectable in *Kit*-deficient oocytes **(Fig. 5 11A,B)** further supporting a critical role of the Kit signaling pathway in regulating oocyte awakening via P-AKT/Foxo3.

Discussion

Primary ovarian insufficiency (POI), also known as premature ovarian failure, is a form of hypergonadotropic hypogonadic ovarian failure that causes early menopause and infertility in 1% of women before the age of 40, in addition to other important health consequences due to estrogen deficiency (Nelson, 2009). POI is associated with the accelerated depletion of primordial follicles, arguing that abnormalities in primordial follicle maintenance are the unifying pathophysiologic basis of POI. However, the identification and further study of key factors regulating primordial follicle maintenance and reawakening has proven difficult with human subjects; for example, ovaries are not biopsied in the clinical workup of POI, limiting available human ovarian tissue for direct analyses. Genome-wide studies have implicated several loci, but further and more detailed genome-wide investigations are needed to more fully define the genetic basis of POI (AlAsiri et al., 2015; Bilgin and Kovanci, 2015; Laven, 2015; McGuire et al., 2011). Numerous factors have been proposed as regulators of reawakening, such as the AMH type 2 receptor (AMHR2), a member of the transforming growth factor β superfamily of growth and differentiation factors (Braem et al., 2013). *AMHR2* female mice are fertile with no overt defects in follicle maturation, however, arguing against an essential role in reawakening (Mishina et al., 1996). Similarly, while AMH has also been proposed as a regulator of oocyte utilization and reawakening, AMH-null females are fertile, suggesting that AMH plays at most a secondary role in regulating reawakening. Other factors must therefore participate in this process (Durlinger et al., 1999).

Phenotypic analysis of Kit^{Y719F} homozygous female mice have provided intriguing genetic evidence implicating Kit in reawakening (John et al., 2009). Kit activates PI3K through a direct interaction with an SH2 domain on the p85 regulatory subunit of PI3K. This interaction is dependent on Kit tyrosine residue 719, which undergoes autophosphorylation following ligand binding. Mutation of this tyrosine residue prevents binding of Kit to p85, and thus abrogates Kit signaling via PI3K (Serve et al., 1994). Mice engineered with this Kit^{Y719F} mutation (via a "knockin" approach) have permitted genetic dissection of the contribution of PI3K signaling to diverse Kit-dependent biological processes (Blume-Jensen et al., 2000; Kissel et al., 2000). Homozygous Kit^{Y719F} males are sterile with severe defects in spermatogenesis. Kit^{Y719F} females, however, are fertile at 16 weeks of age, suggesting that Kit might not play an essential role in reawakening (although severe defects in early follicle maturation including an arrest at the primary/secondary follicle stage were documented) (John et al., 2009). Subsequent analyses of this allele have been interpreted as supportive of a role of Kit in reawakening, rationalizing its use in studies to genetically dissect reawakening. For example, genetic inactivation of *Tsc1* within primordial follicle granulosa cells leads to global reawakening via Foxo3 cytoplasmic relocalization, and this was found to occur through enhancement of Kit ligand production in primordial follicle granulosa cells. Kit^{Y719F} homozygosity suppressed this *Tsc1*-null reawakening phenotype, arguing that the observed increase in Kit ligand was responsible for reawakening (Zhang et al., 2014b).

Foxo3 relocalization to the cytoplasm occurs normally after the primordial-primary transition, and cytoplasmic Foxo3 relocalization has been well-documented in mutants undergoing global reawakening (John et al., 2008; Reddy et al., 2008; Ren et al., 2015; Zhang et al., 2014b). However, for reasons that are not well understood, Foxo3 relocalization as visualized

by IHC/IF does not anticipate reawakening; i.e., early growing follicles appear to have nuclear Foxo3 (John et al., 2008). Thus, in practice, the most useful, sensitive, and earliest indicators of reawakening (i.e., for scoring mutant phenotypes) are morphologic. As emphasized in this study, oocyte diameter is the earliest and most sensitive endpoint for reawakening. In diverse investigations of mutants with global reawakening (e.g., *Pten* and *Foxo3* mutants, also in the Kit^{D818V} mutant described here), granulosa cells remain flattened and unilayered in many follicles with massively enlarged oocytes that have clearly undergone reawakening; indeed, such oocytes can continue to grow unabated for several weeks despite the persistence of "primordial follicle-like" granulosa cell morphology (Adhikari et al., 2009; Adhikari et al., 2010; Castrillon et al., 2003; John et al., 2008; Ren et al., 2015). Furthermore, we have here documented in $VC;Kit^{L/-}$ ovaries a transition in granulosa cell morphology to a cuboidal shape and mitotic activity resulting in a few layers even in follicles where oocytes were constitutionally unable (due to Kit inactivation) to grow/reawaken. Thus, while granulosa cells normally undergo significant changes in morphology and arrangement during reawakening, these do not always correlate with oocyte status in individual follicles and are not as useful as morphological indicators in mutants with strong reawakening phenotypes. Thus, we stress that abnormal oocyte diameters should be considered the *sine qua non* for scoring oocyte reawakening phenotypes and that careful measurements of oocyte diameters (e.g., in tissue sections) should represent the gold standard in such analyses until earlier molecular markers of reawakening are identified.

That the Kit^{Y719F} mutation did not lead to a complete oocyte dormancy phenotype, as documented in earlier studies (females were fertile up to at least 16 weeks of age) can be explained by the hypomorphic nature of this mutation (John et al., 2009). For example, residual Kit signalling via PI3K or other surrogate signalling pathways could feed back to PI3K, resulting

in some PI3K tonic activity. Finally, some hypomorphic alleles of KL (a.k.a. *Steel*^{panda}) also accumulate follicles with cuboidal granulosa cells (albeit with growth-arrested oocytes), consistent with a role of KL in reawakening, although these ovaries contain very few follicles, obscuring interpretation of phenotypes (Bedell et al., 1995; John et al., 2009). The role of KL in reawakening should be further explored in future studies; i.e., through conditional genetic analysis of KL in granulosa cells. KL appears to be constitutively expressed in granulosa cells in primordial follicles (Huang et al., 1993), and although KL is elevated in the *Tsc1* reawakening mutant, the nature of the signals and inter/intra-follicular communication triggering reawakening via Kit-PI3K-Foxo3 in individual primordial follicles remains uncertain. More recently, conditional deficiency of the Lim homeodomain protein Lhx8 was found to promote global reawakening, with a synergistic effect of Lhx8 and Pten on Foxo3 nucleocytoplasmic translocation. These effects were mediated by Lin28a, an RNA binding protein and regulator of the let-7 microRNAs, a finding of particular interest given studies implicating the Lin28/let-7 axis in the control of PI3K-mTOR signalling (Ren et al., 2015; Zhu et al., 2011). Clearly, more work is needed to fully dissect the interactions of the diverse members of the PI3K and mTOR pathways and how these function together to trigger reawakening of individual primordial follicles.

One notable aspect of this study is that we have now documented global oocyte reawakening and dormancy phenotypes with our *Kit*^{D818V} and *Kit*^{L} alleles, respectively. Such complementary and contrasting phenotypes with alleles that have opposite effects on Kit activity (i.e., gain- vs. complete loss-of-function alleles) represent compelling genetic evidence incriminating Kit as the critical receptor upstream of PI3K-Foxo3 in the control of reawakening. The phenotype we describe for the oocyte conditional *Kit* knockout represents the first report of

a pure global dormancy mutant; i.e., where female sterility was associated with minute ovaries containing a numerically normal complement of primordial follicles but where a complete failure of oocyte reawakening left oocytes incapable of growth/reawakening. Conversely, Kit serves essential roles in other aspects of follicle formation, development, and survival (John et al., 2009; Jones and Pepling, 2013; Sullivan and Castrillon, 2011).

Our genetic studies do not exclude a contribution from other cell surface receptors in reawakening, but help establish Kit as the principal upstream factor regulating reawakening, and also demonstrate a remarkably specific role for Kit in reawakening. It is surprising that Kit played such a modest role in oocyte survival, with normal oocyte counts up to 12 weeks of age, a result suggesting that other factors regulate oocyte survival and prevent apoptosis (Reddy et al., 2009). Oocyte conditional ablation (*Vasa-Cre*) of other genes encoding cell surface receptors acting through PI3K and known to be expressed on the oocyte, such as *Igf1r*, *Insr*, *Ret*, *Pdgfr* had no effect on fertility or follicle maturation (unpublished data), further stressing the uniqueness of the *Kit* reawakening phenotypes.

POI is a form of hypergonadotropic hypogonadism that causes infertility in 1% of women before the age of 40 and has important health consequences. POI is due to accelerated depletion of primordial follicles (Board et al., 1979; Russell et al., 1982; Starup and Sele, 1973; Zarate et al., 1970), arguing that abnormalities in primordial follicle maintenance are the unifying pathophysiologic basis of POI. However, the molecular mechanisms that cause follicle depletion in POI are poorly understood. Elucidating these mechanisms is needed to develop better treatment strategies and assays predictive of POI. Our results should help focus further investigations on Kit and, by extension, Kit ligand, as keystone regulators of primordial oocyte maintenance and hence, female reproductive aging. Pharmacologic manipulation of this pathway

may someday prove useful in fertility preservation by increasing the pool of actively growing follicles (Li et al., 2010). This is further underscored by the fact that PI3K-Foxo3 signaling regulates the egg supply throughout life (John et al., 2009). For example, transient treatment of mouse or human oocytes with either a Pten inhibitor or a PI3K activating peptide results in activation of dormant primordial follicles. Pharmacologic control of this pathway either at the level of PI3K-AKT or Kit-KL may thus prove useful in fertility preservation by increasing the pool of growing follicles (Cheng et al., 2015; Hsueh et al., 2015; Li et al., 2010).

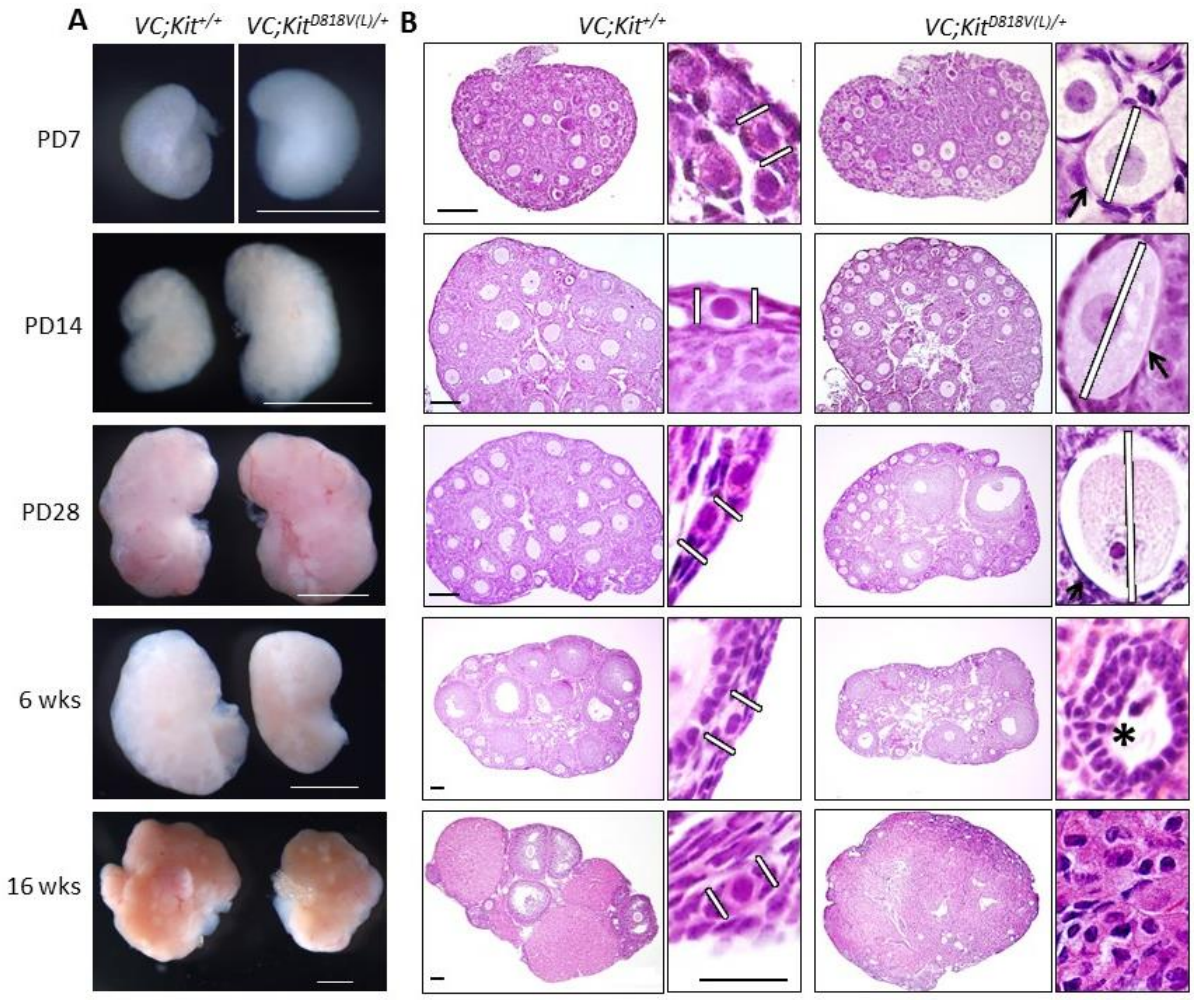

Figure.5.1. Global oocyte reawakening phenotype following conditional Kit activation within oocytes. **(A)** *VC*; *Kit*$^{D818V(L)}$/+ ovaries were larger than sibling controls up to PD28; scale bars=1 mm. **(B)** Histological analyses (H&E-stained sections) revealed significant oocyte enlargement (white lines) and flattened granulosa cells (arrows) in many of the activated follicles (PD7-28). Numerous preantral and early antral follicles are present at PD28. By 6 weeks there was some oocyte death, follicle atresia and empty follicles (asterisk); by 16 weeks there was a complete absence of follicles with the ovary consisting of a luteinized stroma. These features indicate a classic global reawakening phenotype. Scale bars=100 μm in large panels (same for control and experimental sections); 25 μm for small panels (all at the same magnification). Pictures are representative of at least three animals analyzed per genotype/time-point.

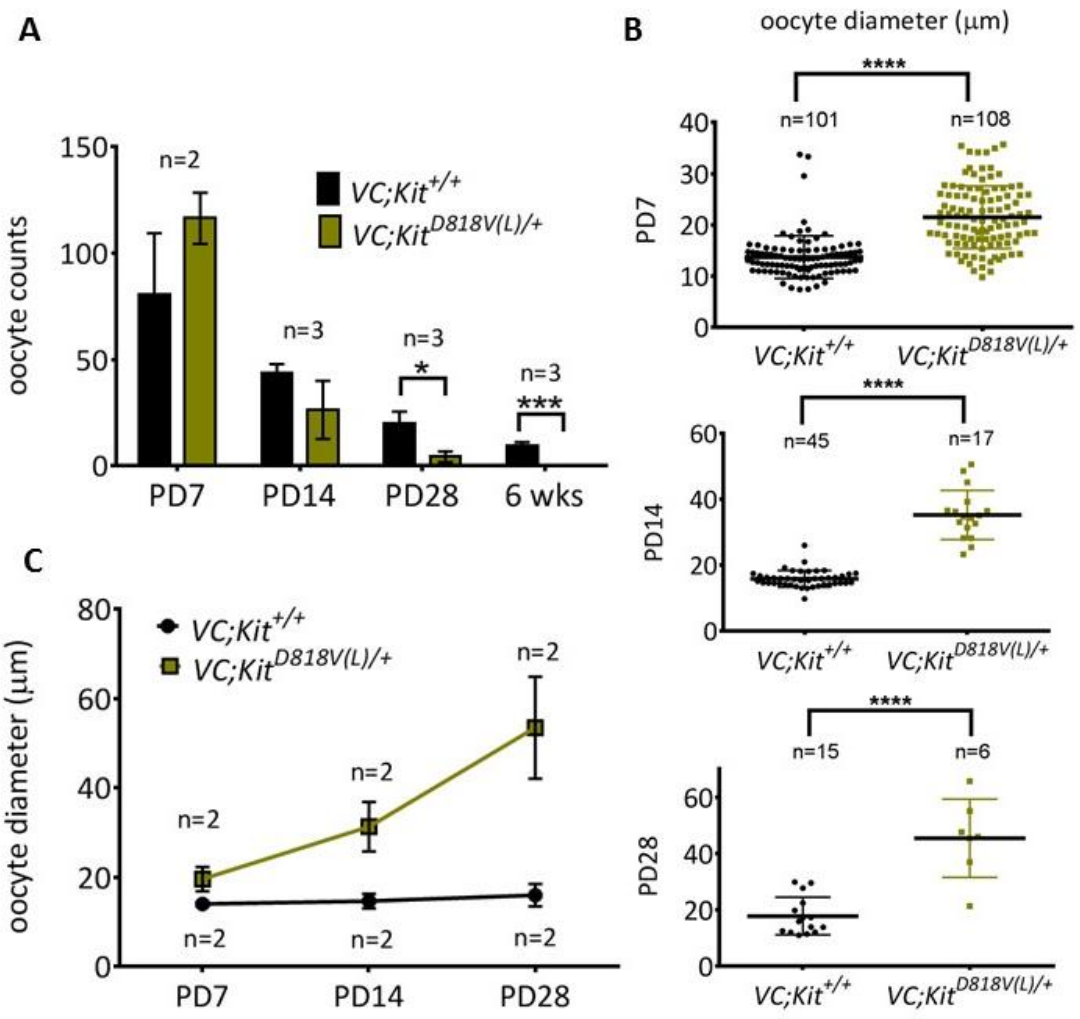

Figure 5.2. Quantitative analyses of oocyte phenotypes following conditional Kit activation within oocytes. (A) Primordial/primary oocyte numbers of *VC*; $Kit^{D818V(L)}$/+ and control ovaries (n≥2 animals per genotype per timepoint; *p<0.05; ***p<0.001, unpaired student t test, error bars=S.E.M. **(B)** Oocyte diameters (micrometers) of early oocytes in *VC;* $Kit^{D818V(L)}$/+ and *VC;* +/+ mice; ****p<0.0001, n≥6 unpaired student t test. Error bars are S.E.M. **(C)** Average primordial/primary oocyte diameters in *VC;* $Kit^{D818V(L)}$/+ and *VC;* +/+ ovaries; at least 6 oocytes were measured from two different animals per genotype/time-point.

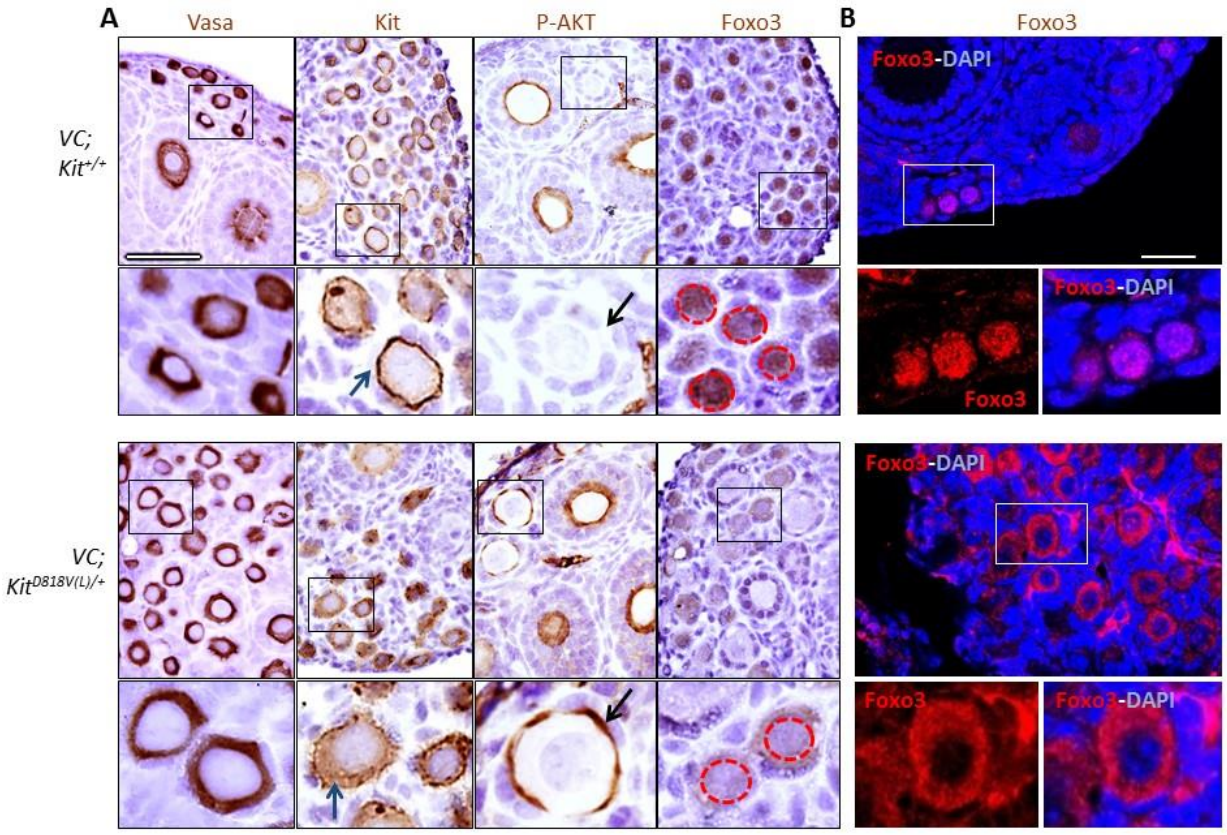

Figure 5.3. Kit activation promotes oocyte reawakening through AKT-Foxo3 axis. (A) Immunohistochemistry for markers as shown; slides counterstained with hematoxylin. Lower panels are higher magnifications of areas shown in black rectangles. Blue arrows, Kit localization in experimental and control oocytes. Note membrane-bound staining in the control vs. greater cytoplasmic staining in *VC; Kit*$^{D818V(L)}$/+ oocytes. Black arrows, oocyte membrane of primordial/primary follicles in control vs. mutant; only mutant oocytes were positive for P-AKT. Red dashed circles in Foxo3 panels demarcate nuclei to highlight nuclear to cytoplasmic export in the mutant. Scale bar=25 μm, all panels at same magnification. **(B)** Foxo3 localization by confocal microscopy/immunofluorescence of control and experimental ovaries at PD14. Scale bar=33 μm for both large panels. Lower panels are higher magnifications of areas in white rectangles.

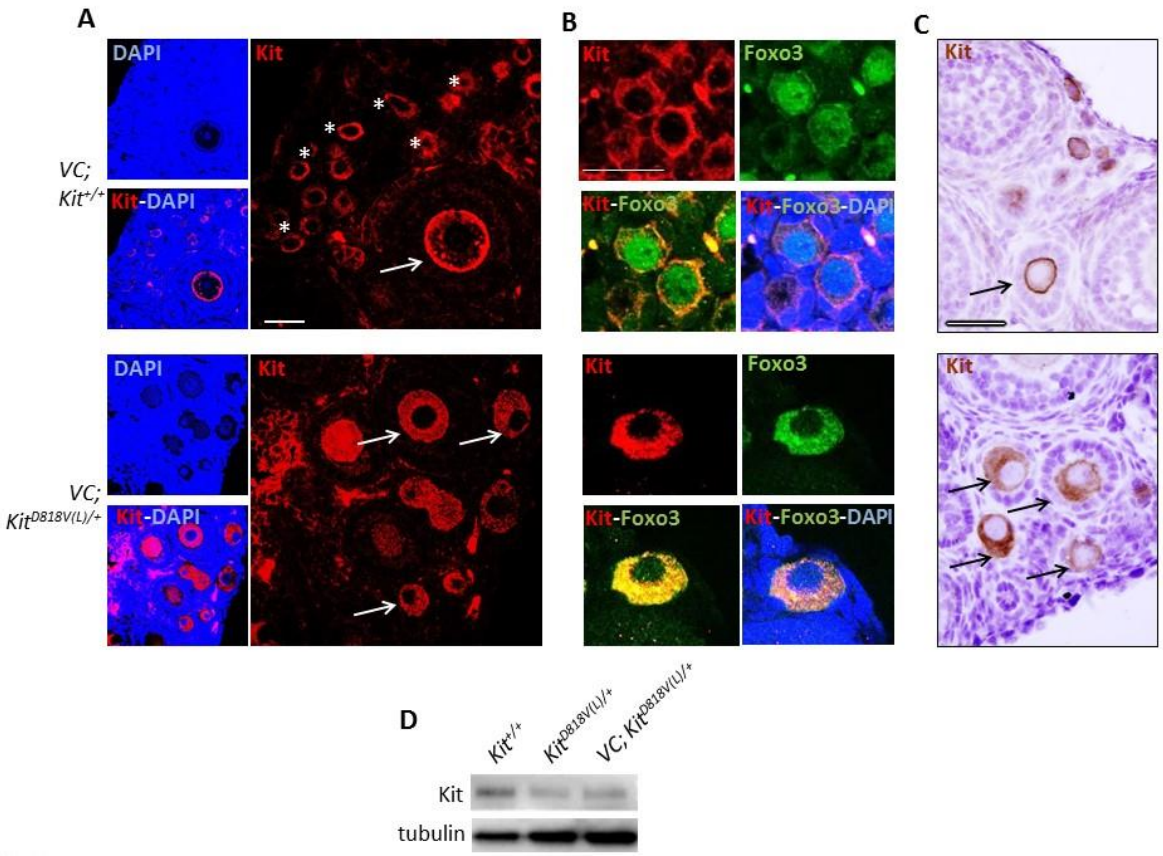

Figure 5.4 Analysis of Kit expression in *VC; Kit$^{D818V(L)/+}$* ovaries. (A) Kit immunohistochemistry at PD14. White asterisks indicate normal primordial follicles; white arrows point to growing follicles. Scale bar=33 μm; both large panels are at same magnification. **(B)** Kit and Foxo3 double-labeling at PD14. Foxo3 is nuclear and cytoplasmic in control oocytes but exclusively cytoplasmic in experimental oocytes. Scale bar=33 μm; all panels are at the same magnification. **(C)** Kit immunohistochemistry at PD14; slides are counterstained with hematoxylin. Scale bar=25 μm; both panels at same magnification. **(D)** Western analysis of PD7 ovaries.

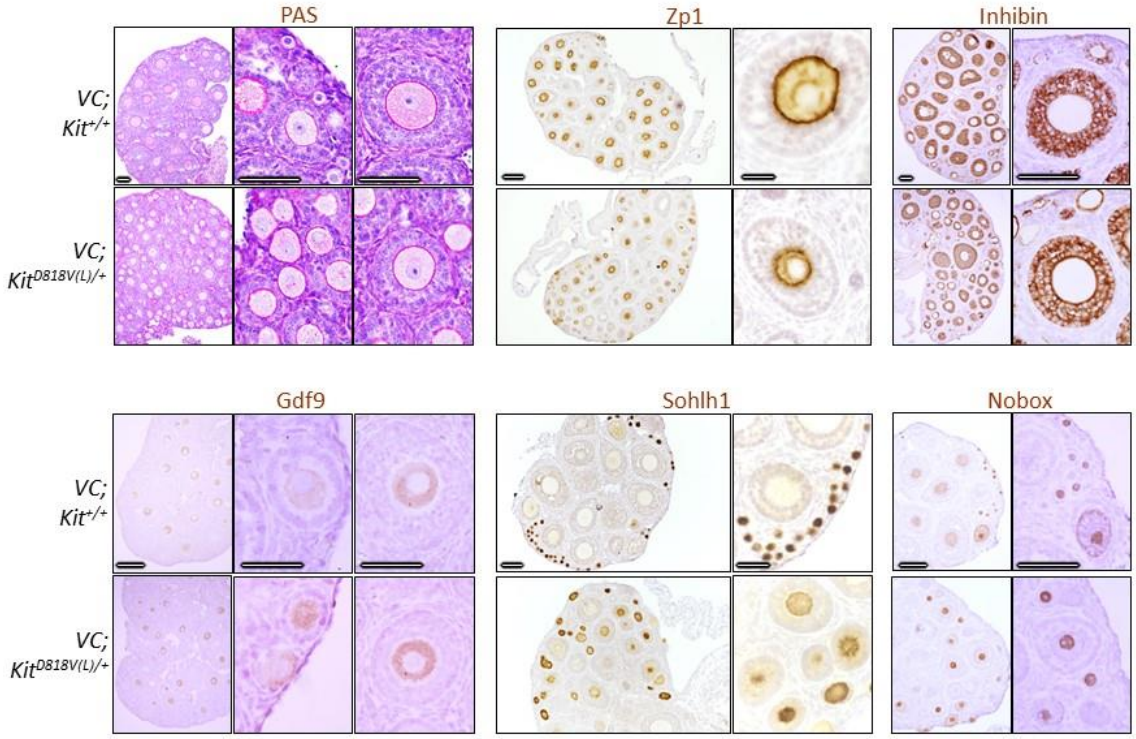

Figure 5.5. Reawakened oocytes differentiate normally in *VC; Kit$^{D818V(L)/+}$* ovaries (PD14). Tissue sections stained with periodic acid-Schiff (PAS) or analyzed by immunohistochemistry and counterstained with hematoxylin. PAS and Zp1 staining indicate development of zona pellucida. Granulosa cells express the differentiation marker, inhibin, and oocytes express Gdf9, Sohlh1 and Nobox. Insets show higher magnification. Scale bars=25 μm; top and bottom panels at same magnification.

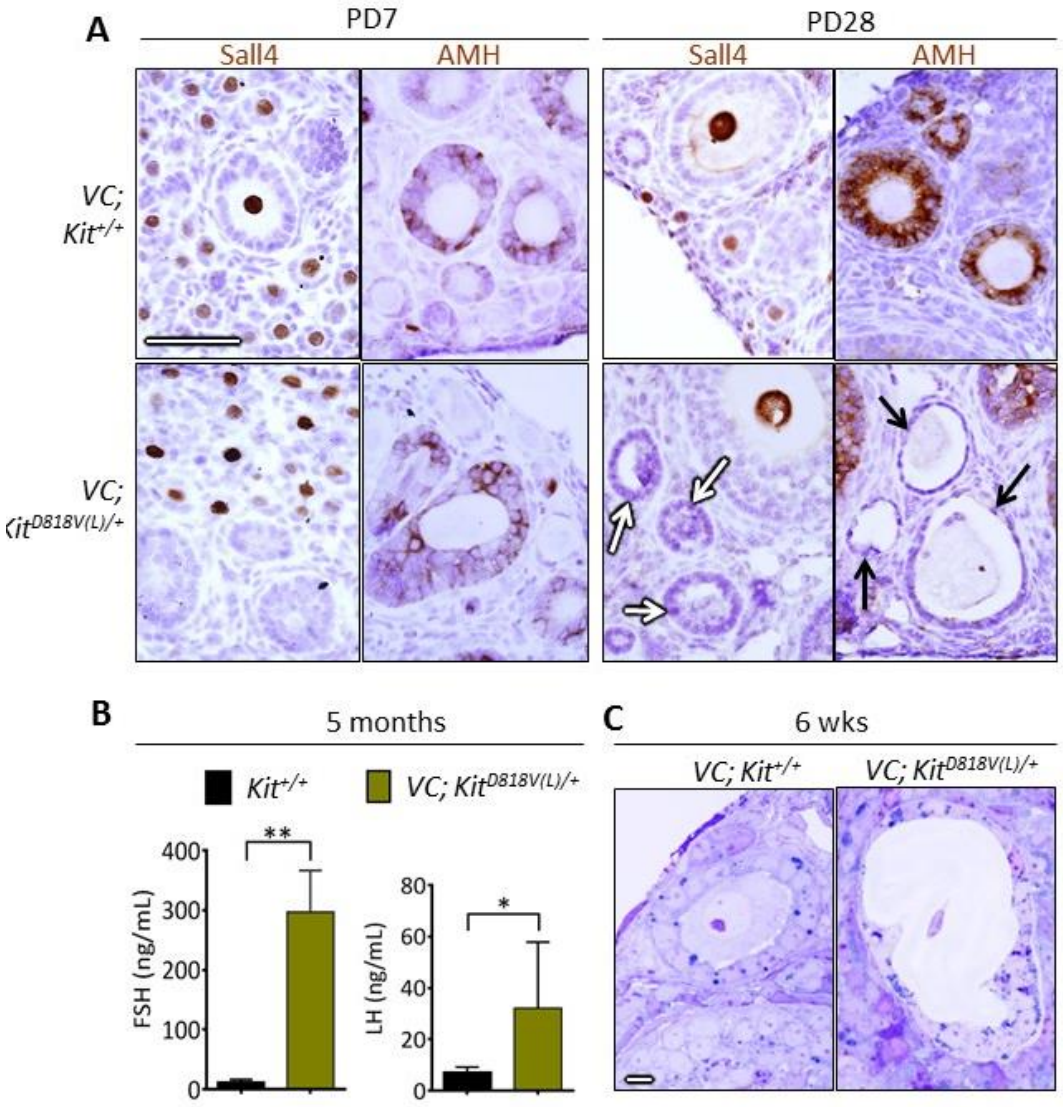

Figure 5.6. Loss of the primordial follicle pool due to oocyte reawakening. (A) Oocyte reawakening phenotype at PD7 and PD28. Immunohistochemistry for markers as shown; slides counterstained with hematoxylin. White arrows indicate follicles with atretic (Sall4-negative) oocytes; black arrows indicate AMH-negative granulosa cells. Scale bar=25 μm; all panels at same magnification. **(B)** Serum FSH and LH levels of *VC*; *Kit*$^{D818V(L)}$/+ and control females at five months of age. *p<0.05, **p<0.01; unpaired student t test; n=3 animals per genotype. **(C)** Toluidine-blue stained sections of plastic-embedded ovaries from experimental and sibling controls at 6 weeks of age; scale bar=10 μm, both panels at same magnification. The follicle shown on the right does not contain a viable oocyte.

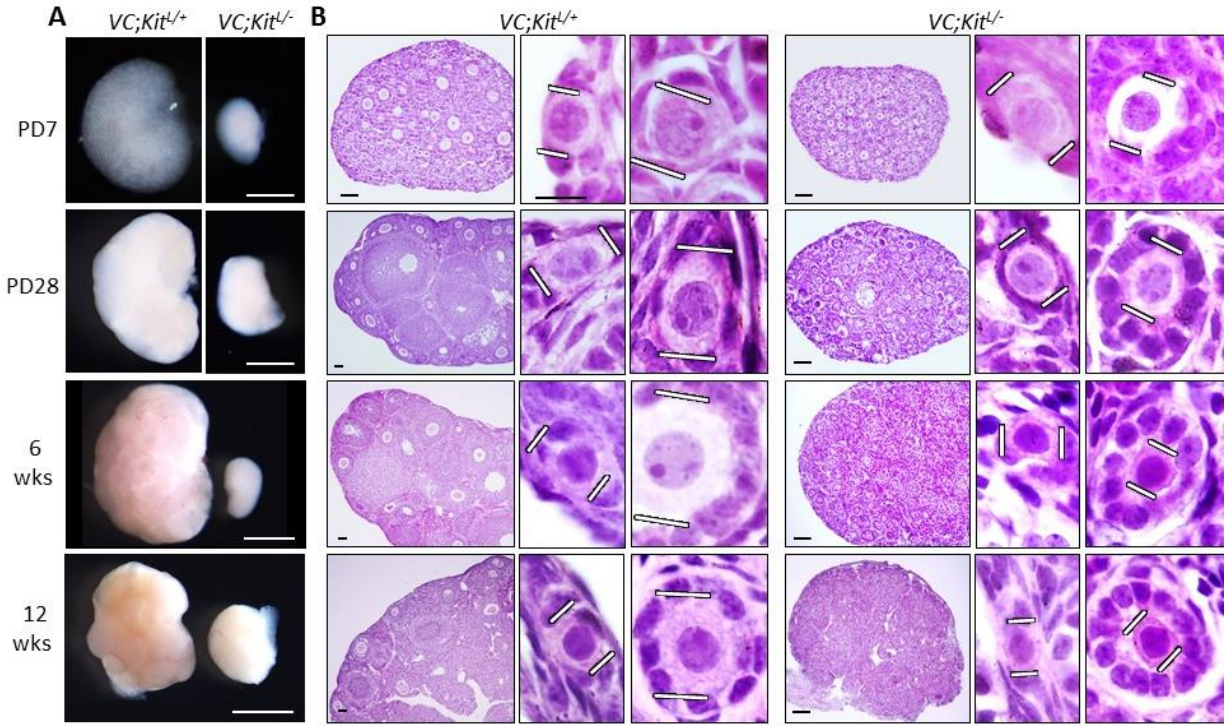

Figure 5.7. Primordial follicle arrest phenotype following Kit inactivation in oocytes. (A) *VC*; *Kit*$^{L/-}$ ovaries were minute relative to *VC; Kit*^{L}/+ sibling controls at all timepoints analyzed; scale bar=1 mm. **(B)** Histological analyses (H&E-stained sections) revealed abundant primordial follicles with a complete failure of oocyte growth and absence of advanced follicles in *VC*; *Kit*$^{L/-}$ ovaries. White lines demarcate oocyte diameters. Scale bars=50 μm (large panels) or 10 μm (small panels). Pictures are representative of ≥4 ovaries from ≥2 different animals per timepoint.

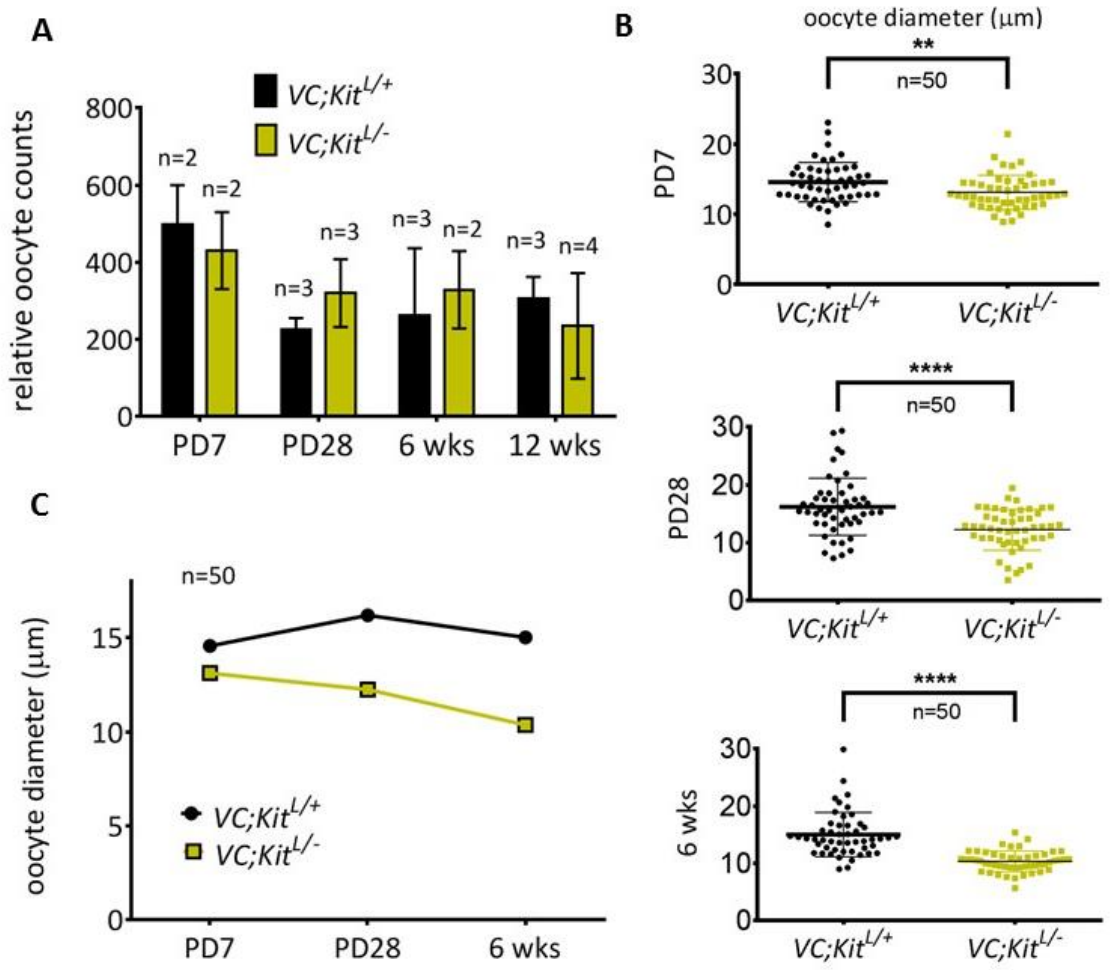

Figure 5.8 Quantitative analyses of oocyte phenotypes following Kit inactivation in oocytes. **(A)** Relative oocyte numbers at PD7 to 12 wks; n=3 animals per genotype per timepoint except PD7 and 6 weeks experimental (n=2 animals, total of 4 ovaries analyzed per genotype), error bars=S.E.M. Note that there is no significant oocyte loss up to 12 weeks (p=0.4475 at 12 weeks, unpaired student t-test). **(B)** Oocyte diameters (micrometers) of early (primordial/primary) oocytes; **p<0.01, ****p<0.0001; unpaired student t test; n=50 per genotype. **(C)** Average oocyte diameters, n=50 oocytes per genotype per timepoint.

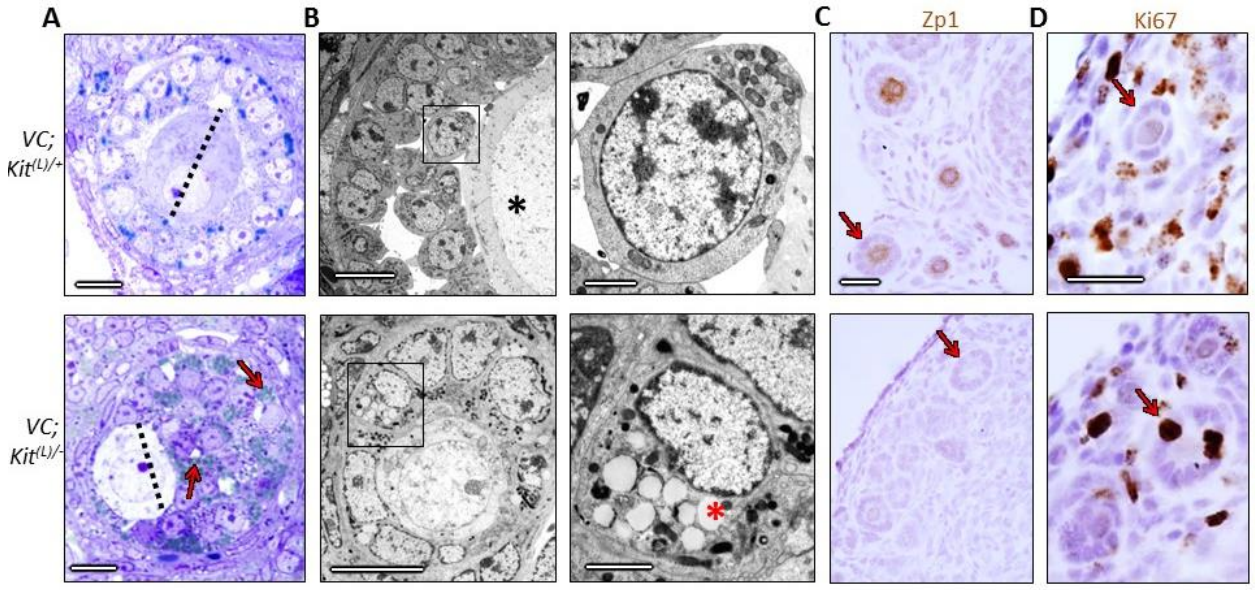

Fig. 5.9. Ultrastructural analysis and absence of zona pellucida in *VC*; *Kit*$^{L/-}$ follicles. (A) Toluidine-blue stained sections highlight presence of viable but small oocytes that were often eccentrically located within follicles in *VC; Kit*$^{L/-}$ ovaries. Note lipid droplets in granulosa cells shown by red arrows. Dashed lines demarcate oocyte diameters (30 µm for control, 21 µm for mutant). Scale bars=10 µm. **(B)** Transmission electron microscopy of control (top) and *VC*; *Kit*$^{L/-}$ ovaries. Note presence of zona pellucida (black asterisk) surrounding a large oocyte in control (left panel). Right panels show high-magnification views of single granulosa cells (indicated by black boxes). In the mutant, note the small, eccentrically-located oocyte and complete absence of a zona pellucida. Higher magnification views of granulosa cells confirm lipid droplets in the mutant (red asterisk). Scale bars=10 µm for follicle images, 2 µm for granulosa cells. **(C)** Zp1 immunohistochemistry at 6 weeks of age; slides counterstained with hematoxylin. Red arrows point to small follicles; Zp1 is readily detected in control oocytes. Scale bars=25 µm, same for both panels. **(D)** Ki67 immunohistochemistry at 4 weeks of age; slides counterstained with hematoxylin. Red arrows indicate granulosa cells. Scale bars=25 µm, same for both panels.

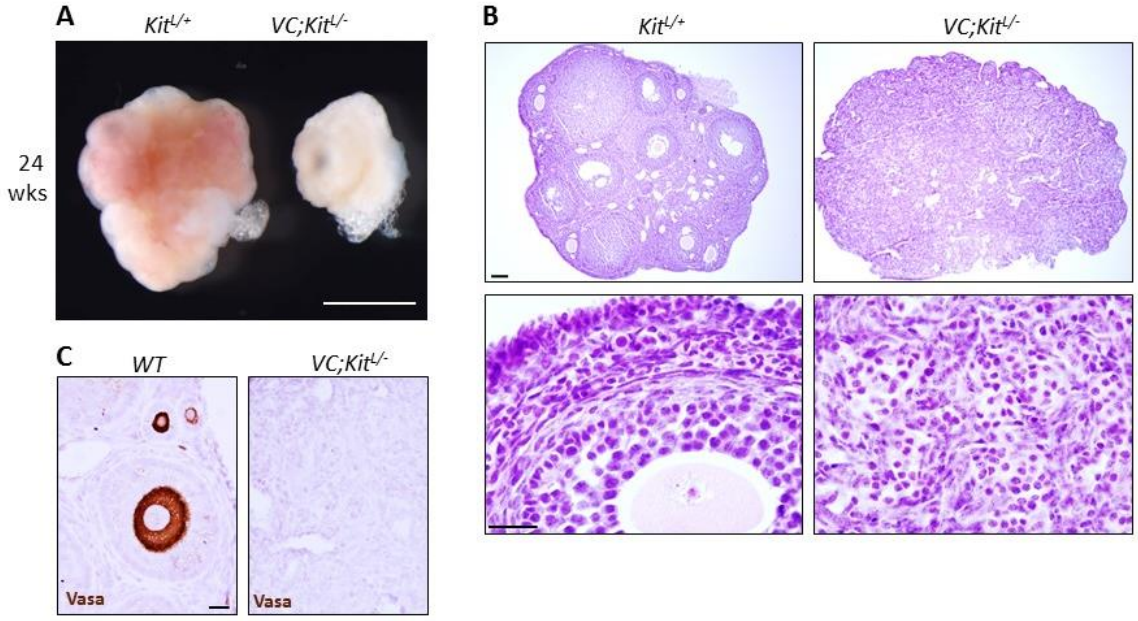

Figure. 5.10. ***VC; Kit$^{L/-}$*** **oocytes die by 6 months of age. (A)** Gross pictures of ovaries from control and *VC; Kit$^{L/-}$* females. Scale bar=1 mm. **(B)** Histological analyses (H&E-stained sections) reveal complete absence of follicles in *VC; Kit$^{L/-}$* females. Scale bars=25 μm for all panels. **(C)** Loss of oocytes by 6 months of age analyzed Vasa immunohistochemistry. Scale bars=25 μm, same for all panels.

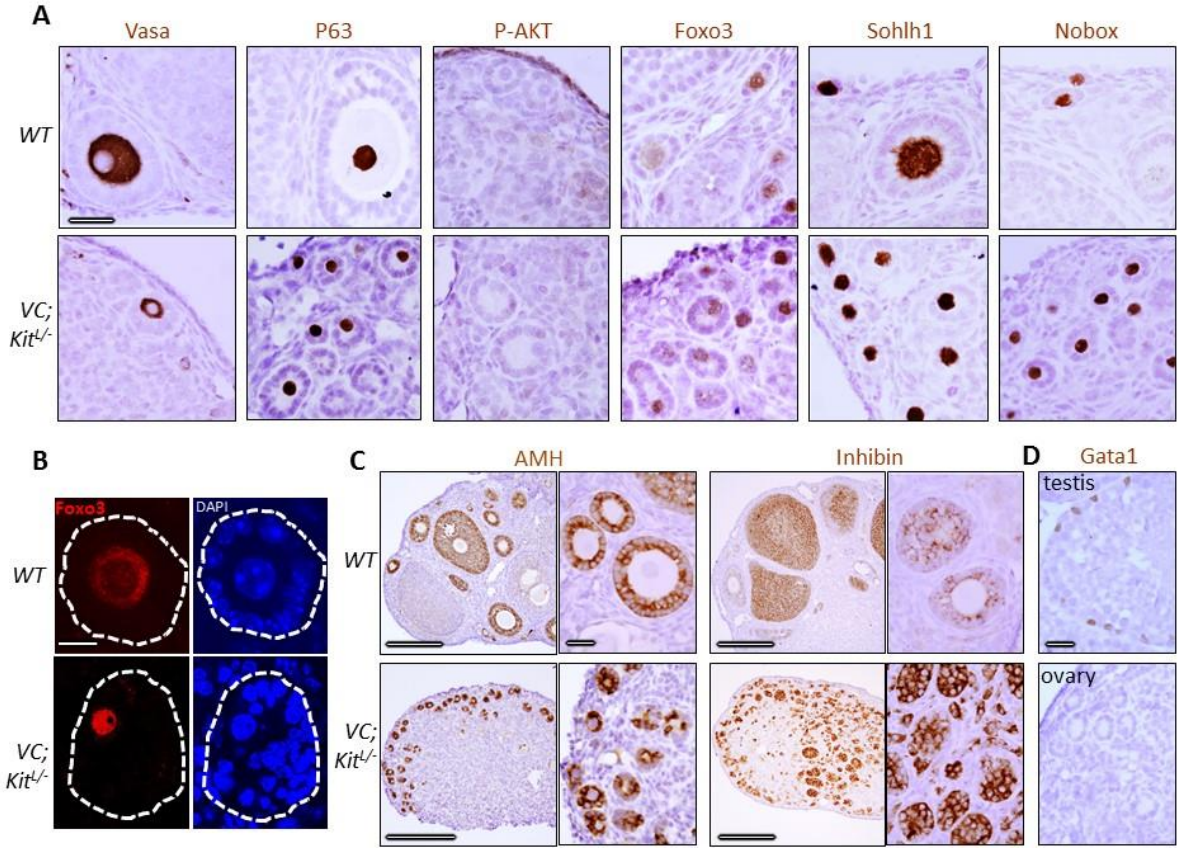

Figure. 5.11. Marker studies of Kit-deficient oocytes are consistent with specific defect in oocyte reawakening via Foxo3. (A) Immunohistochemistry for markers as shown at 6 weeks of age; slides counterstained with hematoxylin. Note absence of P-AKT (in contrast to D818V mutant) and constitutively nuclear localization of Foxo3. Scale bars=25 μm; all panels at same magnification. **(B)** Immunofluorescence detection of Foxo3 protein; slides counterstained with DAPI. Foxo3 undergoes nuclear to cytoplasmic export in wild-type primary follicles but is constitutively nuclear in the mutant. Scale bar=10 μm, same for all panels. **(C)** Analysis of granulosa cells in wild-type and *VC; Kit$^{L/-}$* ovaries. Immunohistochemistry for markers as shown at 6 wks of age; slides counterstained with hematoxylin. Scale bars=200 μm in large panels, or 25 μm in small panels; all small panels at same magnification. **(D)** Absence of Gata1-positive cells in aberrant follicles in *VC; Kit$^{L/-}$* ovaries. Wild-type testis is shown as a positive control (Gata1 is expressed in Sertoli cells). Scale bar=25 μm; both panels at same magnification.

REFERENCES

Abid, S.N., Richardson, T.E., Powell, H.M., Jaichander, P., Chaudhary, J., Chapman, K.M., and Hamra, F.K. (2014). A-single spermatogonia heterogeneity and cell cycles synchronize with rat seminiferous epithelium stages VIII-IX. Biology of reproduction *90*, 32.

Adhikari, D., Flohr, G., Gorre, N., Shen, Y., Yang, H., Lundin, E., Lan, Z., Gambello, M.J., and Liu, K. (2009). Disruption of Tsc2 in oocytes leads to overactivation of the entire pool of primordial follicles. Mol Hum Reprod *15*, 765-770.

Adhikari, D., and Liu, K. (2009). Molecular mechanisms underlying the activation of mammalian primordial follicles. Endocr Rev *30*, 438-464.

Adhikari, D., Zheng, W., Shen, Y., Gorre, N., Hamalainen, T., Cooney, A.J., Huhtaniemi, I., Lan, Z.J., and Liu, K. (2010). Tsc/mTORC1 signaling in oocytes governs the quiescence and activation of primordial follicles. Human molecular genetics *19*, 397-410.

AlAsiri, S., Basit, S., Wood-Trageser, M.A., Yatsenko, S.A., Jeffries, E.P., Surti, U., Ketterer, D.M., Afzal, S., Ramzan, K., Faiyaz-Ul Haque, M., *et al.* (2015). Exome sequencing reveals MCM8 mutation underlies ovarian failure and chromosomal instability. The Journal of clinical investigation *125*, 258-262.

Aloisio, G. (2015). Pax7 defines germline stem cells in the adult testis. Thesis: Graduate School of Cancer Biology (UT Southwestern Medical Center).

Aloisio, G.M., Nakada, Y., Saatcioglu, H.D., Pena, C.G., Baker, M.D., Tarnawa, E.D., Mukherjee, J., Manjunath, H., Bugde, A., Sengupta, A.L., *et al.* (2014). PAX7 expression defines germline stem cells in the adult testis. The Journal of clinical investigation *124*, 3929-3944.

Ashman, L.K. (1999). The biology of stem cell factor and its receptor C-kit. The international journal of biochemistry & cell biology *31*, 1037-1051.

Bedell, M.A., Brannan, C.I., Evans, E.P., Copeland, N.G., Jenkins, N.A., and Donovan, P.J. (1995). DNA rearrangements located over 100 kb 5' of the Steel (Sl)-coding region in Steel-panda and Steel-contrasted mice deregulate Sl expression and cause female sterility by disrupting ovarian follicle development. Genes & development *9*, 455-470.

Besmer, P., Manova, K., Duttlinger, R., Huang, E.J., Packer, A., Gyssler, C., and Bachvarova, R.F. (1993). The kit-ligand (steel factor) and its receptor c-kit/W: pleiotropic roles in gametogenesis and melanogenesis. Dev Suppl, 125-137.

Bilgin, E.M., and Kovanci, E. (2015). Genetics of premature ovarian failure. Current opinion in obstetrics & gynecology *27*, 167-174.

Blume-Jensen, P., Jiang, G., Hyman, R., Lee, K.F., O'Gorman, S., and Hunter, T. (2000). Kit/stem cell factor receptor-induced activation of phosphatidylinositol 3'-kinase is essential for male fertility. Nature genetics *24*, 157-162.

Board, J.A., Redwine, F.O., Moncure, C.W., Frable, W.J., and Taylor, J.R. (1979). Identification of differing etiologies of clinically diagnosed premature menopause. American journal of obstetrics and gynecology *134*, 936-944.

Braem, M.G., Voorhuis, M., van der Schouw, Y.T., Peeters, P.H., Schouten, L.J., Eijkemans, M.J., Broekmans, F.J., and Onland-Moret, N.C. (2013). Interactions between genetic variants in AMH and AMHR2 may modify age at natural menopause. PloS one *8*, e59819.

Browne, C.M., Hime, G.R., Koopman, P., and Loveland, K.L. (2005). Genetic basis of human testicular germ cell cancer: insights from the fruitfly and mouse. Cell and tissue research *322*, 5-19.

Brunet, A., Bonni, A., Zigmond, M.J., Lin, M.Z., Juo, P., Hu, L.S., Anderson, M.J., Arden, K.C., Blenis, J., and Greenberg, M.E. (1999). Akt promotes cell survival by phosphorylating and inhibiting a Forkhead transcription factor. Cell *96*, 857-868.

Buckler, E.S.t., Phelps-Durr, T.L., Buckler, C.S., Dawe, R.K., Doebley, J.F., and Holtsford, T.P. (1999). Meiotic drive of chromosomal knobs reshaped the maize genome. Genetics *153*, 415-426.

Cardoso, H.J., Figueira, M.I., Correia, S., Vaz, C.V., and Socorro, S. (2014). The SCF/c-KIT system in the male: Survival strategies in fertility and cancer. Molecular reproduction and development *81*, 1064-1079.

Carlsson, I.B., Laitinen, M.P., Scott, J.E., Louhio, H., Velentzis, L., Tuuri, T., Aaltonen, J., Ritvos, O., Winston, R.M., and Hovatta, O. (2006). Kit ligand and c-Kit are expressed during early human ovarian follicular development and their interaction is required for the survival of follicles in long-term culture. Reproduction *131*, 641-649.

Castrillon, D.H., Miao, L., Kollipara, R., Horner, J.W., and DePinho, R.A. (2003). Suppression of ovarian follicle activation in mice by the transcription factor Foxo3a. Science *301*, 215-218.

Chabot, B., Stephenson, D.A., Chapman, V.M., Besmer, P., and Bernstein, A. (1988). The proto-oncogene c-kit encoding a transmembrane tyrosine kinase receptor maps to the mouse W locus. Nature *335*, 88-89.

Chan, F., Oatley, M.J., Kaucher, A.V., Yang, Q.E., Bieberich, C.J., Shashikant, C.S., and Oatley, J.M. (2014). Functional and molecular features of the Id4+ germline stem cell population in mouse testes. Genes & development *28*, 1351-1362.

Chang, D.H., Cattoretti, G., and Calame, K.L. (2002). The dynamic expression pattern of B lymphocyte induced maturation protein-1 (Blimp-1) during mouse embryonic development. Mechanisms of development *117*, 305-309.

Cheng, Y., Kim, J., Li, X.X., and Hsueh, A.J. (2015). Promotion of ovarian follicle growth following mTOR activation: synergistic effects of AKT stimulators. PloS one *10*, e0117769.

Cheon, D.J., and Orsulic, S. (2011). Mouse models of cancer. Annual review of pathology *6*, 95-119.

Chian, R., Young, S., Danilkovitch-Miagkova, A., Ronnstrand, L., Leonard, E., Ferrao, P., Ashman, L., and Linnekin, D. (2001). Phosphatidylinositol 3 kinase contributes to the transformation of hematopoietic cells by the D816V c-Kit mutant. Blood *98*, 1365-1373.

Da Silva-Buttkus, P., Marcelli, G., Franks, S., Stark, J., and Hardy, K. (2009). Inferring biological mechanisms from spatial analysis: prediction of a local inhibitor in the ovary. Proc Natl Acad Sci U S A *106*, 456-461.

Dankort, D., Filenova, E., Collado, M., Serrano, M., Jones, K., and McMahon, M. (2007). A new mouse model to explore the initiation, progression, and therapy of BRAFV600E-induced lung tumors. Genes & development *21*, 379-384.

Dann, C.T., Alvarado, A.L., Molyneux, L.A., Denard, B.S., Garbers, D.L., and Porteus, M.H. (2008). Spermatogonial stem cell self-renewal requires OCT4, a factor downregulated during retinoic acid-induced differentiation. Stem cells *26*, 2928-2937.

de Rooij, D.G. (2001). Proliferation and differentiation of spermatogonial stem cells. Reproduction *121*, 347-354.

Dexter, T.M., and Moore, M.A. (1977). In vitro duplication and "cure" of haemopoietic defects in genetically anaemic mice. Nature *269*, 412-414.

Durlinger, A.L., Kramer, P., Karels, B., de Jong, F.H., Uilenbroek, J.T., Grootegoed, J.A., and Themmen, A.P. (1999). Control of primordial follicle recruitment by anti-Mullerian hormone in the mouse ovary. Endocrinology *140*, 5789-5796.

Edson, M.A., Nagaraja, A.K., and Matzuk, M.M. (2009). The mammalian ovary from genesis to revelation. Endocrine reviews *30*, 624-712.

El Chami, N., Ikhlef, F., Kaszas, K., Yakoub, S., Tabone, E., Siddeek, B., Cunha, S., Beaudoin, C., Morel, L., Benahmed, M., *et al.* (2005). Androgen-dependent apoptosis in male germ cells is regulated through the proto-oncoprotein Cbl. The Journal of cell biology *171*, 651-661.

Eppig, J.J., Wigglesworth, K., and Pendola, F.L. (2002). The mammalian oocyte orchestrates the rate of ovarian follicular development. Proceedings of the National Academy of Sciences of the United States of America *99*, 2890-2894.

Ezzati, M.M., Baker, M.D., Saatcioglu, H.D., Aloisio, G.M., Pena, C.G., Nakada, Y., Cuevas, I., Carr, B.R., and Castrillon, D.H. (2015). Regulation of FOXO3 subcellular localization by Kit ligand in the neonatal mouse ovary. Journal of assisted reproduction and genetics.

Falciatori, I., Lillard-Wetherell, K., Wu, Z., Hamra, F.K., and Garbers, D.L. (2008). Deriving mouse spermatogonial stem cell lines. Methods in molecular biology *450*, 181-192.

Fortuno, C., and Labarta, E. (2014). Genetics of primary ovarian insufficiency: a review. Journal of assisted reproduction and genetics *31*, 1573-1585.

Gallardo, T., Shirley, L., John, G.B., and Castrillon, D.H. (2007a). Generation of a germ cell-specific mouse transgenic Cre line, Vasa-Cre. Genesis *45*, 413-417.

Gallardo, T.D., John, G.B., Shirley, L., Contreras, C.M., Akbay, E.A., Haynie, J.M., Ward, S.E., Shidler, M.J., and Castrillon, D.H. (2007b). Genomewide discovery and classification of candidate ovarian fertility genes in the mouse. Genetics *177*, 179-194.

Gassei, K., Valli, H., and Orwig, K.E. (2014). Whole-mount immunohistochemistry to study spermatogonial stem cells and spermatogenic lineage development in mice, monkeys, and humans. Methods in molecular biology *1210*, 193-202.

Geissler, E.N., Ryan, M.A., and Housman, D.E. (1988). The dominant-white spotting (W) locus of the mouse encodes the c-kit proto-oncogene. Cell *55*, 185-192.

Godshalk, S.E., Paranjape, T., Nallur, S., Speed, W., Chan, E., Molinaro, A.M., Bacchiocchi, A., Hoyt, K., Tworkoski, K., Stern, D.F., *et al.* (2011). A Variant in a MicroRNA complementary site in the 3' UTR of the KIT oncogene increases risk of acral melanoma. Oncogene *30*, 1542-1550.

Goertz, M.J., Wu, Z., Gallardo, T.D., Hamra, F.K., and Castrillon, D.H. (2011). Foxo1 is required in mouse spermatogonial stem cells for their maintenance and the initiation of spermatogenesis. The Journal of clinical investigation *121*, 3456-3466.

Gommerman, J.L., Rottapel, R., and Berger, S.A. (1997). Phosphatidylinositol 3-kinase and Ca2+ influx dependence for ligand-stimulated internalization of the c-Kit receptor. The Journal of biological chemistry *272*, 30519-30525.

Grive, K.J., and Freiman, R.N. (2015). The developmental origins of the mammalian ovarian reserve. Development *142*, 2554-2563.

Guan, K., Nayernia, K., Maier, L.S., Wagner, S., Dressel, R., Lee, J.H., Nolte, J., Wolf, F., Li, M., Engel, W., *et al.* (2006). Pluripotency of spermatogonial stem cells from adult mouse testis. Nature *440*, 1199-1203.

Guertin, D.A., and Sabatini, D.M. (2007). Defining the role of mTOR in cancer. Cancer cell *12*, 9-22.

Hamra, F.K., Chapman, K.M., Wu, Z., and Garbers, D.L. (2008). Isolating highly pure rat spermatogonial stem cells in culture. Methods in molecular biology *450*, 163-179.

Hanahan, D., and Weinberg, R.A. (2000). The hallmarks of cancer. Cell *100*, 57-70.

Hermann, B.P., Mutoji, K.N., Velte, E.K., Ko, D., Oatley, J.M., Geyer, C.B., and McCarrey, J.R. (2015). Transcriptional and translational heterogeneity among neonatal mouse spermatogonia. Biology of reproduction *92*, 54.

Hirsch, E., Katanaev, V.L., Garlanda, C., Azzolino, O., Pirola, L., Silengo, L., Sozzani, S., Mantovani, A., Altruda, F., and Wymann, M.P. (2000). Central role for G protein-coupled phosphoinositide 3-kinase gamma in inflammation. Science *287*, 1049-1053.

Hsueh, A.J., Kawamura, K., Cheng, Y., and Fauser, B.C. (2015). Intraovarian control of early folliculogenesis. Endocr Rev *36*, 1-24.

Huang, E.J., Manova, K., Packer, A.I., Sanchez, S., Bachvarova, R.F., and Besmer, P. (1993). The murine steel panda mutation affects kit ligand expression and growth of early ovarian follicles. Developmental biology *157*, 100-109.

Huang, E.J., Nocka, K.H., Buck, J., and Besmer, P. (1992). Differential expression and processing of two cell associated forms of the kit-ligand: KL-1 and KL-2. Molecular biology of the cell *3*, 349-362.

Huckins, C. (1971). The spermatogonial stem cell population in adult rats. I. Their morphology, proliferation and maturation. The Anatomical record *169*, 533-557.

Igoucheva, O., and Alexeev, V. (2009). MicroRNA-dependent regulation of cKit in cutaneous melanoma. Biochemical and biophysical research communications *379*, 790-794.

Jagarlamudi, K., and Rajkovic, A. (2012). Oogenesis: transcriptional regulators and mouse models. Mol Cell Endocrinol *356*, 31-39.

Jahn, T., Seipel, P., Coutinho, S., Urschel, S., Schwarz, K., Miething, C., Serve, H., Peschel, C., and Duyster, J. (2002). Analysing c-kit internalization using a functional c-kit-EGFP chimera containing the fluorochrome within the extracellular domain. Oncogene *21*, 4508-4520.

Jara-Acevedo, M., Teodosio, C., Sanchez-Munoz, L., Alvarez-Twose, I., Mayado, A., Caldas, C., Matito, A., Morgado, J.M., Munoz-Gonzalez, J.I., Escribano, L., *et al.* (2015). Detection of the KIT D816V mutation in peripheral blood of systemic mastocytosis: diagnostic implications. Modern pathology : an official journal of the United States and Canadian Academy of Pathology, Inc *28*, 1138-1149.

John, G.B., Gallardo, T.D., Shirley, L.J., and Castrillon, D.H. (2008). Foxo3 is a PI3K-dependent molecular switch controlling the initiation of oocyte growth. Developmental biology *321*, 197-204.

John, G.B., Shidler, M.J., Besmer, P., and Castrillon, D.H. (2009). Kit signaling via PI3K promotes ovarian follicle maturation but is dispensable for primordial follicle activation. Developmental biology *331*, 292-299.

John, G.B., Shirley, L.J., Gallardo, T.D., and Castrillon, D.H. (2007). Specificity of the requirement for Foxo3 in primordial follicle activation. Reproduction *133*, 855-863.

Jones, R.L., and Pepling, M.E. (2013). KIT signaling regulates primordial follicle formation in the neonatal mouse ovary. Developmental biology *382*, 186-197.

Kaipia, A., and Hsueh, A.J. (1997). Regulation of ovarian follicle atresia. Annual review of physiology *59*, 349-363.

Kanatsu-Shinohara, M., Ogonuki, N., Iwano, T., Lee, J., Kazuki, Y., Inoue, K., Miki, H., Takehashi, M., Toyokuni, S., Shinkai, Y., *et al.* (2005). Genetic and epigenetic properties of mouse male germline stem cells during long-term culture. Development *132*, 4155-4163.

Kanatsu-Shinohara, M., and Shinohara, T. (2013). Spermatogonial stem cell self-renewal and development. Annual review of cell and developmental biology *29*, 163-187.

Kemmer, K., Corless, C.L., Fletcher, J.A., McGreevey, L., Haley, A., Griffith, D., Cummings, O.W., Wait, C., Town, A., and Heinrich, M.C. (2004). KIT mutations are common in testicular seminomas. The American journal of pathology *164*, 305-313.

Kim, J.Y. (2012). Control of ovarian primordial follicle activation. Clinical and experimental reproductive medicine *39*, 10-14.

Kissel, H., Timokhina, I., Hardy, M.P., Rothschild, G., Tajima, Y., Soares, V., Angeles, M., Whitlow, S.R., Manova, K., and Besmer, P. (2000). Point mutation in kit receptor tyrosine kinase reveals essential roles for kit signaling in spermatogenesis and oogenesis without affecting other kit responses. The EMBO journal *19*, 1312-1326.

Knudson, A.G., Jr. (1971). Mutation and cancer: statistical study of retinoblastoma. Proceedings of the National Academy of Sciences of the United States of America *68*, 820-823.

Kosmider, O., Denis, N., Lacout, C., Vainchenker, W., Dubreuil, P., and Moreau-Gachelin, F. (2005). Kit-activating mutations cooperate with Spi-1/PU.1 overexpression to promote tumorigenic progression during erythroleukemia in mice. Cancer cell *8*, 467-478.

Kwiatkowski, D.J., Zhang, H., Bandura, J.L., Heiberger, K.M., Glogauer, M., el-Hashemite, N., and Onda, H. (2002). A mouse model of TSC1 reveals sex-dependent lethality from liver hemangiomas, and up-regulation of p70S6 kinase activity in Tsc1 null cells. Human molecular genetics *11*, 525-534.

Laven, J.S. (2015). Genetics of Early and Normal Menopause. Semin Reprod Med.

Lennartsson, J., and Ronnstrand, L. (2012). Stem cell factor receptor/c-Kit: from basic science to clinical implications. Physiological reviews *92*, 1619-1649.

Li, J., Kawamura, K., Cheng, Y., Liu, S., Klein, C., Duan, E.K., and Hsueh, A.J. (2010). Activation of dormant ovarian follicles to generate mature eggs. Proc Natl Acad Sci U S A *107*, 10280-10284.

Liang, J., Wu, Y.L., Chen, B.J., Zhang, W., Tanaka, Y., and Sugiyama, H. (2013). The C-kit receptor-mediated signal transduction and tumor-related diseases. International journal of biological sciences *9*, 435-443.

Lintern-Moore, S., and Moore, G.P. (1979). The initiation of follicle and oocyte growth in the mouse ovary. Biology of reproduction *20*, 773-778.

Liu, K., Rajareddy, S., Liu, L., Jagarlamudi, K., Boman, K., Selstam, G., and Reddy, P. (2006). Control of mammalian oocyte growth and early follicular development by the oocyte PI3 kinase pathway: new roles for an old timer. Developmental biology *299*, 1-11.

Luisi, S., Orlandini, C., Regini, C., Pizzo, A., Vellucci, F., and Petraglia, F. (2015). Premature ovarian insufficiency: from pathogenesis to clinical management. Journal of endocrinological investigation *38*, 597-603.

Manova, K., Nocka, K., Besmer, P., and Bachvarova, R.F. (1990). Gonadal expression of c-kit encoded at the W locus of the mouse. Development *110*, 1057-1069.

Martins, R., Lithgow, G.J., and Link, W. (2015). Long live FOXO: unraveling the role of FOXO proteins in aging and longevity. Aging Cell.

Matzuk, M.M., Burns, K.H., Viveiros, M.M., and Eppig, J.J. (2002). Intercellular communication in the mammalian ovary: oocytes carry the conversation. Science *296*, 2178-2180.

Mauduit, C., Hamamah, S., and Benahmed, M. (1999). Stem cell factor/c-kit system in spermatogenesis. Human reproduction update *5*, 535-545.

McGee, E.A., and Hsueh, A.J. (2000). Initial and cyclic recruitment of ovarian follicles. Endocr Rev *21*, 200-214.

McGuire, M.M., Bowden, W., Engel, N.J., Ahn, H.W., Kovanci, E., and Rajkovic, A. (2011). Genomic analysis using high-resolution single-nucleotide polymorphism arrays reveals novel microdeletions associated with premature ovarian failure. Fertility and sterility *95*, 1595-1600.

Miettinen, M., and Lasota, J. (2005). KIT (CD117): a review on expression in normal and neoplastic tissues, and mutations and their clinicopathologic correlation. Applied immunohistochemistry & molecular morphology : AIMM / official publication of the Society for Applied Immunohistochemistry *13*, 205-220.

Mishina, Y., Rey, R., Finegold, M.J., Matzuk, M.M., Josso, N., Cate, R.L., and Behringer, R.R. (1996). Genetic analysis of the Mullerian-inhibiting substance signal transduction pathway in mammalian sexual differentiation. Genes & development *10*, 2577-2587.

Mithraprabhu, S., and Loveland, K.L. (2009). Control of KIT signalling in male germ cells: what can we learn from other systems? Reproduction *138*, 743-757.

Miyazawa, K., Williams, D.A., Gotoh, A., Nishimaki, J., Broxmeyer, H.E., and Toyama, K. (1995). Membrane-bound Steel factor induces more persistent tyrosine kinase activation and longer life span of c-kit gene-encoded protein than its soluble form. Blood *85*, 641-649.

Nagano, M.C. (2003). Homing efficiency and proliferation kinetics of male germ line stem cells following transplantation in mice. Biology of reproduction *69*, 701-707.

Nakagawa, T., Sharma, M., Nabeshima, Y., Braun, R.E., and Yoshida, S. (2010). Functional hierarchy and reversibility within the murine spermatogenic stem cell compartment. Science *328*, 62-67.

Nelson, L.M. (2009). Clinical practice. Primary ovarian insufficiency. N Engl J Med *360*, 606-614.

Nikolaou, M., Valavanis, C., Aravantinos, G., Fountzilas, G., Tamvakis, N., Lekka, I., Arapantoni-Dadioti, P., Zizi, A., Ghiconti, I., Economopoulos, T., *et al.* (2007). Kit expression in male germ cell tumors. Anticancer research *27*, 1685-1688.

Nocka, K., Tan, J.C., Chiu, E., Chu, T.Y., Ray, P., Traktman, P., and Besmer, P. (1990). Molecular bases of dominant negative and loss of function mutations at the murine c-kit/white spotting locus: W37, Wv, W41 and W. The EMBO journal *9*, 1805-1813.

Oatley, J.M., Avarbock, M.R., Telaranta, A.I., Fearon, D.T., and Brinster, R.L. (2006). Identifying genes important for spermatogonial stem cell self-renewal and survival. Proceedings of the National Academy of Sciences of the United States of America *103*, 9524-9529.

Obata, Y., Toyoshima, S., Wakamatsu, E., Suzuki, S., Ogawa, S., Esumi, H., and Abe, R. (2014). Oncogenic Kit signals on endolysosomes and endoplasmic reticulum are essential for neoplastic mast cell proliferation. Nature communications *5*, 5715.

Ogawa, T., Dobrinski, I., Avarbock, M.R., and Brinster, R.L. (2000). Transplantation of male germ line stem cells restores fertility in infertile mice. Nature medicine *6*, 29-34.

Ohinata, Y., Payer, B., O'Carroll, D., Ancelin, K., Ono, Y., Sano, M., Barton, S.C., Obukhanych, T., Nussenzweig, M., Tarakhovsky, A., *et al.* (2005). Blimp1 is a critical determinant of the germ cell lineage in mice. Nature *436*, 207-213.

Ohta, H., Yomogida, K., Dohmae, K., and Nishimune, Y. (2000). Regulation of proliferation and differentiation in spermatogonial stem cells: the role of c-kit and its ligand SCF. Development *127*, 2125-2131.

Paik, J.H., Kollipara, R., Chu, G., Ji, H., Xiao, Y., Ding, Z., Miao, L., Tothova, Z., Horner, J.W., Carrasco, D.R., *et al.* (2007). FoxOs are lineage-restricted redundant tumor suppressors and regulate endothelial cell homeostasis. Cell *128*, 309-323.

Parada, L.F., Land, H., Weinberg, R.A., Wolf, D., and Rotter, V. (1984). Cooperation between gene encoding p53 tumour antigen and ras in cellular transformation. Nature *312*, 649-651.

Pelosi, E., Omari, S., Michel, M., Ding, J., Amano, T., Forabosco, A., Schlessinger, D., and Ottolenghi, C. (2013). Constitutively active Foxo3 in oocytes preserves ovarian reserve in mice. Nat Commun *4*, 1843.

Peters, H., Byskov, A.G., Lintern-Moore, S., Faber, M., and Andersen, M. (1973). The effect of gonadotrophin on follicle growth initiation in the neonatal mouse ovary. Journal of reproduction and fertility *35*, 139-141.

Reddy, P., Adhikari, D., Zheng, W., Liang, S., Hamalainen, T., Tohonen, V., Ogawa, W., Noda, T., Volarevic, S., Huhtaniemi, I., *et al.* (2009). PDK1 signaling in oocytes controls reproductive aging and lifespan by manipulating the survival of primordial follicles. Hum Mol Genet *18*, 2813-2824.

Reddy, P., Liu, L., Adhikari, D., Jagarlamudi, K., Rajareddy, S., Shen, Y., Du, C., Tang, W., Hamalainen, T., Peng, S.L., *et al.* (2008). Oocyte-specific deletion of Pten causes premature activation of the primordial follicle pool. Science *319*, 611-613.

Ren, Y., Suzuki, H., Jagarlamudi, K., Golnoski, K., McGuire, M., Lopes, R., Pachnis, V., and Rajkovic, A. (2015). Lhx8 regulates primordial follicle activation and postnatal folliculogenesis. BMC biology *13*, 39.

Rivina, L., and Schiestl, R. (2013). Mouse models of radiation-induced cancers. Advances in genetics *84*, 83-122.

Russell, P., Bannatyne, P., Shearman, R.P., Fraser, I.S., and Corbett, P. (1982). Premature hypergonadotropic ovarian failure: clinicopathological study of 19 cases. Int J Gynecol Pathol *1*, 185-201.

Ryu, B.Y., Kubota, H., Avarbock, M.R., and Brinster, R.L. (2005). Conservation of spermatogonial stem cell self-renewal signaling between mouse and rat. Proceedings of the National Academy of Sciences of the United States of America *102*, 14302-14307.

Saadatpour, A., Guo, G., Orkin, S.H., and Yuan, G.C. (2014). Characterizing heterogeneity in leukemic cells using single-cell gene expression analysis. Genome biology *15*, 525.

Saga, Y. (2008). Mouse germ cell development during embryogenesis. Curr Opin Genet Dev *18*, 337-341.

Sanchez, F., and Smitz, J. (2012). Molecular control of oogenesis. Biochimica et biophysica acta *1822*, 1896-1912.

Sandlow, J.I., Feng, H.L., Cohen, M.B., and Sandra, A. (1996). Expression of c-KIT and its ligand, stem cell factor, in normal and subfertile human testicular tissue. Journal of andrology *17*, 403-408.

Sarbassov, D.D., Ali, S.M., and Sabatini, D.M. (2005). Growing roles for the mTOR pathway. Current opinion in cell biology *17*, 596-603.

Schrans-Stassen, B.H., van de Kant, H.J., de Rooij, D.G., and van Pelt, A.M. (1999). Differential expression of c-kit in mouse undifferentiated and differentiating type A spermatogonia. Endocrinology *140*, 5894-5900.

Serve, H., Hsu, Y.C., and Besmer, P. (1994). Tyrosine residue 719 of the c-kit receptor is essential for binding of the P85 subunit of phosphatidylinositol (PI) 3-kinase and for c-kit-associated PI 3-kinase activity in COS-1 cells. J Biol Chem *269*, 6026-6030.

Singh, S.R., Burnicka-Turek, O., Chauhan, C., and Hou, S.X. (2011). Spermatogonial stem cells, infertility and testicular cancer. Journal of cellular and molecular medicine *15*, 468-483.

Skinner, M.K. (2005). Regulation of primordial follicle assembly and development. Hum Reprod Update *11*, 461-471.

Sorrentino, V., Giorgi, M., Geremia, R., Besmer, P., and Rossi, P. (1991). Expression of the c-kit proto-oncogene in the murine male germ cells. Oncogene *6*, 149-151.

Starup, J., and Sele, V. (1973). Premature Ovarian Failure. Acta Obstet Gynec Scand *52*, 259-268.

Sullivan, S.D., and Castrillon, D.H. (2011). Insights into Primary Ovarian Insufficiency through Genetically Engineered Mouse Models. Semin Reprod Med *29*, 283-298.

Sun, F., Xu, Q., Zhao, D., and Degui Chen, C. (2015). Id4 Marks Spermatogonial Stem Cells in the Mouse Testis. Scientific reports *5*, 17594.

Takeda, S., Shimizu, T., and Rodewald, H.R. (1997). Interactions between c-kit and stem cell factor are not required for B-cell development in vivo. Blood *89*, 518-525.

Tarnawa, E.D., Baker, M.D., Aloisio, G.M., Carr, B.R., and Castrillon, D.H. (2013). Gonadal expression of Foxo1, but not Foxo3, is conserved in diverse Mammalian species. Biology of reproduction *88*, 103.

Thomas, F.H., Ismail, R.S., Jiang, J.Y., and Vanderhyden, B.C. (2008). Kit ligand 2 promotes murine oocyte growth in vitro. Biology of reproduction *78*, 167-175.

Thomas, F.H., and Vanderhyden, B.C. (2006). Oocyte-granulosa cell interactions during mouse follicular development: regulation of kit ligand expression and its role in oocyte growth. Reprod Biol Endocrinol *4*, 19.

Tingen, C., Kim, A., and Woodruff, T.K. (2009). The primordial pool of follicles and nest breakdown in mammalian ovaries. Molecular human reproduction *15*, 795-803.

Tothova, Z., Kollipara, R., Huntly, B.J., Lee, B.H., Castrillon, D.H., Cullen, D.E., McDowell, E.P., Lazo-Kallanian, S., Williams, I.R., Sears, C., *et al.* (2007). FoxOs are critical mediators of hematopoietic stem cell resistance to physiologic oxidative stress. Cell *128*, 325-339.

Unni, S.K., Modi, D.N., Pathak, S.G., Dhabalia, J.V., and Bhartiya, D. (2009). Stage-specific localization and expression of c-kit in the adult human testis. The journal of histochemistry and cytochemistry : official journal of the Histochemistry Society *57*, 861-869.

van der Meer, Y., Huiskamp, R., Davids, J.A., and de Rooij, D.G. (1993). Differential effects of fractionated X irradiation on mouse spermatogonial stem cells. Radiation research *135*, 222-228.

Vanhaesebroeck, B., Guillermet-Guibert, J., Graupera, M., and Bilanges, B. (2010). The emerging mechanisms of isoform-specific PI3K signalling. Nat Rev Mol Cell Biol *11*, 329-341.

Waheeb, R., and Hofmann, M.C. (2011). Human spermatogonial stem cells: a possible origin for spermatocytic seminoma. International journal of andrology *34*, e296-305; discussion e305.

Wang, L., Yamaguchi, S., Burstein, M.D., Terashima, K., Chang, K., Ng, H.K., Nakamura, H., He, Z., Doddapaneni, H., Lewis, L., *et al.* (2014). Novel somatic and germline mutations in intracranial germ cell tumours. Nature *511*, 241-245.

Witte, O.N. (1990). Steel locus defines new multipotent growth factor. Cell *63*, 5-6.

Yang, Q.E., Racicot, K.E., Kaucher, A.V., Oatley, M.J., and Oatley, J.M. (2013). MicroRNAs 221 and 222 regulate the undifferentiated state in mammalian male germ cells. Development *140*, 280-290.

Yarden, Y., Kuang, W.J., Yang-Feng, T., Coussens, L., Munemitsu, S., Dull, T.J., Chen, E., Schlessinger, J., Francke, U., and Ullrich, A. (1987). Human proto-oncogene c-kit: a new cell surface receptor tyrosine kinase for an unidentified ligand. The EMBO journal *6*, 3341-3351.

Zarate, A., Karchmer, S., Gomez, E., and Castelazo-Ayala, L. (1970). Premature menopause. A clinical, histologic, and cytogenetic study. American journal of obstetrics and gynecology *106*, 110-114.

Zeng, S., Xu, Z., Lipkowitz, S., and Longley, J.B. (2005). Regulation of stem cell factor receptor signaling by Cbl family proteins (Cbl-b/c-Cbl). Blood *105*, 226-232.

Zhang, H., Liu, L., Li, X., Busayavalasa, K., Shen, Y., Hovatta, O., Gustafsson, J.A., and Liu, K. (2014a). Life-long in vivo cell-lineage tracing shows that no oogenesis originates from putative germline stem cells in adult mice. Proceedings of the National Academy of Sciences of the United States of America *111*, 17983-17988.

Zhang, H., Risal, S., Gorre, N., Busayavalasa, K., Li, X., Shen, Y., Bosbach, B., Brannstrom, M., and Liu, K. (2014b). Somatic cells initiate primordial follicle activation and govern the development of dormant oocytes in mice. Current biology : CB *24*, 2501-2508.

Zhao, W., Bueso-Ramos, C.E., Verstovsek, S., Barkoh, B.A., Khitamy, A.A., and Jones, D. (2007). Quantitative profiling of codon 816 KIT mutations can aid in the classification of systemic mast cell disease. Leukemia *21*, 1574-1576.

Zheng, W., Nagaraju, G., Liu, Z., and Liu, K. (2012). Functional roles of the phosphatidylinositol 3-kinases (PI3Ks) signaling in the mammalian ovary. Mol Cell Endocrinol *356*, 24-30.

Zhu, H., Shyh-Chang, N., Segre, A.V., Shinoda, G., Shah, S.P., Einhorn, W.S., Takeuchi, A., Engreitz, J.M., Hagan, J.P., Kharas, M.G., *et al.* (2011). The Lin28/let-7 axis regulates glucose metabolism. Cell *147*, 81-94.